Advanced Numerical and Experimental Transient Modelling of Water and Gas Pipeline Flows Incorporating Distributed and Local Effects

YOUNG IL KIM

Thesis for Doctor of Philosophy (PhD)
School of Civil, Environmental and Mining Engineering
July 2008

CHAPTER 1

INTRODUCTION

1.1 MOTIVATION

One of the best opportunities to reduce pipeline accidents and subsequent leaks comes from implementing better pipeline condition assessment. Current techniques of condition assessment for pipelines can be divided into two categories, hydraulic and non-hydraulic based methods. Most of the non-hydraulic based techniques detect leaking product outside the pipeline by traditional procedures, such as visual or audial inspection and sampling devices. These methods are frequently labour intensive, time consuming, expensive and only partially effective. In addition, these techniques cannot monitor a pipeline continuously. Many researchers have investigated hydraulic based techniques for detecting, locating, and sizing pipeline faults and for calibrating and monitoring pipeline systems. Hydraulic based methods, also known as computational pipeline monitoring or computational based methods, use instruments to monitor internal pipeline parameters such as pressure, flow and temperature. These parameters are used for input data to infer faults in a pipeline. Among hydraulic based methods, a transient model based system is a promising technique because pressure transients propagate through the entire system and interact with the pipes and devices and, as a result, embody a large amount of information about the physical characteristics of the system. The analysis of these features provides a potential tool for fault detection, system calibration, and real-time system monitoring.

The performance of the pipeline assessment system based on a transient model highly depends on the accuracy of a transient analysis model. Flow system components and/or

system abnormalities commonly encountered in pipelines, such as valves, orifices, leakages, blockages, accumulators, entrapped gas cavities, and changes of pipe thickness and material, create unique dynamic behaviours of pressure waves during transients. These behaviours result from the interaction between system components and pressure waves involving energy dissipation and dispersion, multiple superpositions of pressure waves, and nonlinear dynamic characteristics. These unique behaviours cause a major obstacle in the development of a precise transient analysis model. Understanding the unique unsteady characteristics caused by distributed and local energy loss elements is of great importance for dynamic calculation in system design and calibration. The development of an advanced transient model for analysing these unsteady characteristics is essential prerequisite for pipeline condition assessment.

To develop the advanced transient model, this research investigates the effects of distributed energy loss component (unsteady pipe wall friction) and local energy loss components (viscoelasticity of localised polymer pipe sections, leakages, entrapped air pockets, orifices, and blockages) that may affect the shape and phase of transient pressure waves. The dynamic characteristics of these system components are modelled based on the conservative solution scheme using the governing equations in their conservative forms to improve the accuracy and applicability of transient analysis in both liquid and gas pipelines. An experimental investigation has been carried out for the tank-pipeline-valve system with various flow system components. This research presents a number of experimental results of how distributed and local energy loss components affect pressure waves in a pipeline system during transients. The developed models are verified by comprehensive laboratory experiments.

1.2 OBJECTIVES

The ultimate goal of this research is the development of an appropriate and accurate transient analysis model for various system components to improve the performance of pipeline condition assessment. This model would be able to be used directly for characterising pipeline systems and applied to the inverse transient analysis for pipeline fault detection as an advanced forward solver. To achieve this goal, the following work has been conducted in this research.

1) To overcome the limitations of traditional transient analysis models and to improve the accuracy and applicability of transient analysis, by developing a conservative solution scheme to analyse hydraulic transients in both liquid and gas pipelines based on the governing equations in their conservative form.
2) To understand unsteady wall resistance in pipeline systems during transient events, by developing various unsteady friction models based on convolution weighting functions that have been incorporated and modified into the conservative solution scheme.
3) To overcome the difficulties of transient analysis in real pipeline systems with various pipeline system components and/or abnormalities, by investigating the dynamic characteristics of system components, such as leakages, orifices, blockages (axial-extended orifice), entrapped gas cavities, and local polymer pipe, that affect the shape and phase of transient pressure waves due to energy dissipation and dispersion, and developing mathematical models based on a conservative solution scheme to simulate their unsteady behaviour.
4) To validate the proposed conservative solution scheme, unsteady friction models, and unsteady local loss models, by carrying out comprehensive laboratory experiments in water and gas pipelines to observe the interaction between transient pressure waves and unsteady energy loss components, and to verify the proposed models.

1.3 OUTLINE OF THE THESIS

The scope of each chapter is described below. Chapter 5 to 9 contain their own literature reviews focussing on the topic of each chapter. Finally, the conclusions of the research presented in this thesis are given in Chapter 10.

Chapter 2 contains a review of current condition assessment techniques, such as risk assessment and fault detection, and unsteady flow analysis in liquid and gas pipelines. The techniques for pipeline condition assessment are introduced by the divided two categories, hydraulic and non-hydraulic based methods. The literature review for transient analysis models mainly focuses on one-dimensional models. This review presents the basic equations for unsteady flow analysis, their numerical solutions, and underlying assumptions.

Chapter 3 presents the proposed conservative solution scheme for unsteady flow analysis in liquid and gas pipelines. The advantage of this scheme is the flexibility in dealing with a large variety of non-pipe elements and unsteady friction. Also, the model can simulate gas transient flows by slightly modifying the liquid transient model. The conservative scheme solves for (pressure, fluid density, pipe cross-sectional area, and flow velocity) or five dependent variables including temperature rather than two in the standard unsteady pipe flow approach (pressure and velocity). The model can simulate one-dimensional fluid transient problems with heat transfer from the pipe wall to the external environment and the conversion of frictional work into thermal energy.

Chapter 4 introduces the pipeline apparatus used for experimental investigations. The experimental apparatus is comprised of a pipeline system, pressure control system, and data acquisition system. The pipeline is rigidly fixed to foundation plates with a special steel construction to prevent structural vibration during transient events and connects two electronically controlled pressurised tanks. The pressure waves are recorded by high-resolution pressure transducers and transferred by triggering via amplifiers and 16-bit analogue/digital (A/D) converter card to personal computer with data acquisition interface based on LabVIEW software.

Chapter 5 shows unsteady friction effects in water and gas pipelines and the application of unsteady friction models in the conservative solution scheme. Understanding the unsteady hydraulic resistance behaviour caused by boundary shear stresses is of great importance for the longer period dynamic calculation in system design and condition assessment. Steady friction models cannot accurately describe the real physical phenomena of rapid transient events. Various unsteady friction models (for both laminar and turbulent flow, and for both smooth and rough pipe flow) based on convolution weighting functions are incorporated and modified into the conservative solution scheme to simulate transient water and gas pipe flows.

Chapter 6 presents the effect of leakage on transient pipe flows. Leakage is a common fault in pipeline systems and generates additional damping of transient pressure waves. Leakages are simulated at nodal points using an orifice equation in the case of water

transients and frictionless adiabatic flow theory (isentropic flow) for simulating leak behaviour of gas transients.

Chapter 7 introduces the effect of an entrapped air pocket on transient pipe flows. Gas cavities can develop in a liquid pipeline by bubble entrainment through the action of pump suction, air release during low-pressure transients, cavitation and/or column separation. The presence of the gas cavities has a significant effect on the character of transients in the pipeline. Gas cavities compensate for pressure fluctuations or increase the maximum pressure in the pipe. A mathematical model for simulating the effect of entrapped air pocket on transient pipe flows is presented by using air accumulator (small air chamber) model that yields practical results. Incorporating mathematical model for entrapped air pocket into the conservative solution scheme leads to the discrete gas cavity analysis model for single or multiple isolated cavities. Although the study particularly focuses on relatively small-entrapped pockets of air within pressurised systems, a range of applicability is various for differing proportions of air to liquid systems, discrete vapour cavities, or homogenous gas-liquid mixtures.

Chapter 8 shows the effect of orifice and blockage on transient pipe flows. The dynamic flow behaviour through a pipe restriction is represented by three different energy loss factors, which include the irreversible energy loss (net or permanent pressure loss) by turbulent jet flow, the kinetic pressure difference represented by the instantaneous flow acceleration and deceleration, and pressure wave dispersion by eddy inertia of the jet flow. The study proposes instantaneous inertia and frequency-dependent models to describe the kinetic pressure difference. The traditional steady-state characteristics of an orifice are used to calculate the net pressure loss, and the wave dispersion by turbulent jet flow is considered by the wavespeed adjustment method.

Chapter 9 presents the effect of plastic pipe on transient pipe flows. A linear-elastic model is relatively accurate for describing hydraulic transients in metal or concrete pipes. However, recent tests in water distribution pipe networks show significant viscoelastic behaviour due to soil-pipe interaction, flexible pipe joints, or household water services. Polymer pipes, especially polyethylene pipe, have been increasingly used in water and gas industries due to their high resistant properties, low price, and cost-effective installation methods. A mechanical strain principle model (spring-dashpot element model) is used for

describing viscoelastic behaviour. Total strain can be decomposed into instantaneous and retarded wall strain. This research focuses on the analysis of hydraulic transients in pressurised pipeline system with local polyethylene pipe.

CHAPTER 2

REVIEW OF TRANSIENT ANALYSIS FOR PIPELINE CONDITION ASSESSMENT

Worldwide there is a great deal of construction activity to complete pipelines to meet future water and energy needs. Ageing pipeline systems are under repair and replacement continually. Pipeline construction world-wide totals around 1.6 million kilometres, of which 60% are over 20 years old [Al-Rafai & Barnes, 1999]. The American Water Works Association (AWWA) estimates that 19,000 kilometres of new water distribution pipelines are installed annually around the world [Smith et al., 2000]. Natural gas is currently one of the most widely used energy sources and the fastest growing fuel worldwide because of its clean combustion characteristics, low production costs, and thermal efficiency. Moreover, it is found all over the world and convenient to control with most natural gas being distributed through pipeline systems. During the last 30 years, large gas pipeline networks have been constructed in order to convey natural and industrial gases from the source of production to consumption sites across long distances. The international construction survey by *Pipeline & Gas Journal* indicates 96,434 kilometres (59,923 miles) of gas and oil pipelines are in various stages of construction or planned for construction [Tubb, 2001].

With the wide spread use of pipelines, a variety of pipeline failures, such as pipeline accidents and subsequent leaks are reported frequently. Leakage from pipelines may cause significant environmental damage as well as economic loss. Leaks are unintentional releases of quantities of product from pipelines into the environment. In some countries, the daily water loss by leaks from a pipe network is a major percentage of the total daily

water consumption in many towns. Water loss from unaccounted water may be from 10% - 30% even in well-maintained networks [Makar and Chagnon, 1999] and as high as 50% or higher in old or poorly maintained networks [Rao and Sridharan, 1996]. In addition to these direct losses, environmental pollution, land subsidence due to soil loss, and additional energy expenses due to pressure drop may be important. In particular, gas pipelines may be in danger of an explosion. If leaking gas comes in contact with a lit match or a spark from a vehicle, an explosion or fire could result. Taking into account that a considerable proportion of gas networks are installed in highly populated zones, the consequences of such an explosion could be severe [ORNL, 2002]. Leaks generally originate from one or several factors including outside damage of pipeline, corrosion of pipe wall, abnormal pressure surges, poor quality of fittings and workmanship, soil movement, traffic loading, ageing of pipelines, equipment failure, and errors in pipeline design and operation [Liou and Tian, 1995]. Blockages formed by chemical or physical deposition are another major problem in pipeline systems. Pipe flow can be severely curtailed by partial blockages, whose immediate impact is loss of deliverability and higher pumping or compression costs [Adewumi et al., 2001]. It also creates fluid quality problems because stagnant fluid is left for extended periods. These blockages can arise from condensation, solid deposition, partially or fully closed valves by operator error, discrete partial strictures, and extended pipe constrictions.

This chapter reviews current pipeline condition assessment methods, such as risk assessment and fault detection, and numerical models for transient pipe flow analysis. Reviews of the effects of unsteady friction (Chapter 5), leakages (Chapter 6), entrapped gas cavities (Chapter 7), orifices and blockages (Chapter 8), and viscoelastic pipes (Chapter 9) on transient pipe flows are introduced at the beginning of each of these chapters. The techniques for pipeline condition assessment are divided into two categories, hydraulic and non-hydraulic based methods. Non-hydraulic based methods commonly follow traditional procedures of online or offline observation and surveillance with simple techniques, sensing devices, and/or advanced technologies. Hydraulic based methods monitor internal pipeline parameters that are used for input data of computational pipeline monitoring methods based on flow or pressure change analysis and transient simulation models. Unfortunately none of the existing methodologies can offer good performance for all conditions. The literature review for transient analysis models mainly focuses on one-dimensional models that approximate the actual cross sectional velocity profile. This

review presents the basic equations for unsteady flow analysis, their numerical solutions, and underlying assumptions.

2.1 PIPE CONDITION ASSESSMENT AND FAULT DETECTION

If faults and abnormalities, such as pipe wall inside damage, corrosion, cracks, and blockages, are recognized in pipeline systems, a decision must be made to replace or repair them. These abnormalities have the potential of causing a burst, a leakage, or loss of deliverability. Leakage from pipelines may cause significant environmental damage as well as economic loss. As a result, the pipeline industry is always looking for methods to obtain more reliable and accurate information on fault locations and sizes including the probability of generation of inside damage, cracks, and blockages.

The best opportunity to reduce pipeline accidents and subsequent product loss comes from performing pipeline condition assessment by better pipeline monitoring and fault detection. However, in a real pipeline, the performance of fault detection and characterization is frequently difficult due to variability in product characteristics (density, viscosity), pipeline parameters (diameter, length, elevation profile), instrumentation and communication capabilities, and process instrumentation variables (flow, temperature, pressure) [ADEC, 2000]. That is the reason why each fault detection technique has strengths and weaknesses according to the objective of detection. None of the existing methodologies can offer good performance across all the attributes of pipeline systems. The characteristics of some techniques favor their use in certain pipeline systems and situations. Each condition assessment technology can be evaluated by the performance and suitability criteria provided in the Alaska Administrative Code [ADEC, 2000].

- ***Applicability*** of any technology selected for use on a fluid pipeline system is designed for the intended use.
- ***Availability*** refers to the commercial availability of a fault detection system and its components.
- ***Sensitivity*** is defined as the composite measure of the size of fault that a system is capable of detecting the fault.

- ***Accuracy*** is related to estimation parameters such as total product lost and fault location.
- ***Reliability*** is the ability of a system to render accurate decisions about the possible existence of a fault on a pipeline.
- ***Robustness*** is the ability of a system to continue to function and provide useful information, even under changing conditions of pipeline operation.
- ***Feasibility*** requires a close examination of expected pipeline operation conditions.
- ***Environmental Impacts*** may offset any anticipated benefits.
- ***Cost*** is related to the hardware and software cost, and the expense of implementation, installation, and maintenance of the instruments.

Current condition assessment and fault detection methods along a pipeline can be divided into two categories, hydraulic and non-hydraulic based methods. Non-hydraulic based methods detect the property of a pipe material, fluid, or noise emission using traditional procedures such as online or offline observation and surveillance as well as visual, acoustic, robotic pig, and sampling devices. Hydraulic based methods, also known as computational pipeline monitoring or computational based method, use instruments to monitor internal pipeline parameters, such as pressure, flow, and temperature. These parameters are input data for inferring faults of pipeline by use of processors. The use of computer systems in pipeline monitoring allows the greatest amount of data to be collected, analysed, and acted upon in the shortest amount of time. For these reasons, most pipeline systems employ some form of computer based monitoring. Computer-based systems are generally composed of a supervisory computer with associated software, instruments, and communication links.

2.1.1 Non-Hydraulic Based Techniques

1) Condition Assessment Based on Simple Techniques

Experienced personnel or trained dogs can look for unusual patterns near the pipeline, smell for substances which are released from the pipeline, and listen to noises generated by product escaping from pipeline damage. The application of a soap-water or other bubble forming solutions on exposed gas pipes may be used to determine the existence of leaks. This method may be used for testing exposed pipeline systems above the ground, joints, or

parts of repaired leaks. A listening stick, electronic listening stick, or ground microphone may be used to detect noise generated by leaks in buried pipes as shown in Fig. 2.1. The leak noise travels through the fluid and pipe wall. Direct listening at valves, hydrants, and other surfaces fitting by these devices can be used for detecting a leak. The electronic listening devices are simple and cost effective, and are able to detect leak noise outside the range of sounds detected by the human ear. Also, closed-circuit television (CCTV) is frequently used for pipeline interior inspection. An experienced technician reviews recoded images of pipeline inner surface. Although these manual assessment procedures largely depend on individual experience, and are labor intensive and time consuming, they are useful methods to confirm a fault if they are used in conjunction with other techniques [Zhang, 1996; Furness and van Reet, 1998].

NOTE: This figure is included on page 11 of the print copy of the thesis held in the University of Adelaide Library.

Figure 2.1 Electronic Listening Stick and Ground Microphone
(Source: www.primayer.co.uk)

2) Condition Assessment Based on Sensing Devices

Temperature Sensing Devices

Some leaks can be detected through the identification of temperature changes. The principle behind the use of temperature sensors for leak detection is that a leak from a ground or underground pipe changes the thermal characteristics of the adjacent soil or surroundings and makes it a more effective heat sink or source. Infrared thermography is usually used to detect the change of surrounding temperature after a leak [Eiswirth et al., 2001]. This method can be used from moving vehicles, helicopters, or portable systems and is able to cover several kilometres or hundreds of kilometres of pipeline per day. The recent development of advanced wide area temperature sensors makes the temperature

profile technique more practical. Also, multi-sensor electrical cables and fibre optic cables that are driven into the soil beneath or adjacent to the pipeline is used to detect the changes of temperature in the neighbourhood of a leak [MacLean et al., 2001].

Vapour and Gas Sensing Devices

Leak detection using vapour monitoring techniques is a fairly straightforward concept. When a leaking liquid seeps into the soil, vapours migrate into the surrounding soil pore spaces. The soil vapours are collected for laboratory or field analysis to differentiate possible pipe content vapours from naturally occurring background vapours. If the product inside a pipeline is highly volatile, a vapour monitoring system can be used to detect the level of hydrocarbon vapour in the pipeline surroundings. Hydrocarbon gas or vapour sensing systems are more frequently used in storage tanks. A multi-channel gas leakage monitoring system is designed by using complex programmable logic device (CPLD) chip for monitoring the leakage of natural gas from underground pipelines [Chung and Lee, 2001]. The CPLD chips can selectively detect methane or natural gas. The sampling can be done by carrying the device along a pipeline or using a sensor tube buried in parallel to the pipeline. The sensing tube for detecting a leak involves the installation of a secondary conduit along the pipeline. The conduit is a small diameter perforated tube attached to or encompassed with the pipeline. Gas samples are drawn into the tube and analysed by sensors to determine the presence of a leak. Sensing tubes are usually only employed on short pipelines because of the problems associated with any system installed along the entire length of a pipeline.

Liquid Sensing Devices

Liquid sensing cables are buried beneath or adjacent to a pipeline. A microprocessor continuously receives the energy pulse signals based on a map of the specific installation of the cable [ADEC, 2000]. When a leak occurs, the cable becomes saturated with fluid. The fluid alters the impedance of the sensing cable, which in turn alters the reflection pattern returning to the microprocessor. The change in signal pattern causes the microprocessor to register a leak alarm at the location of the altered impedance. Specific cable types are chosen for each application based on the specific fluid being monitored. The leak detection system based on liquid sensing is available to provide real-time

information of leaks. The advantage of this method is the relatively high accuracy in determining a leak location, but the installation costs are very high.

3) Condition Assessment Based on Nondestructive Methods

Acoustic Techniques

Leaking mass through an irregular opening in a pipeline wall generates acoustic waves (noise). The wave of the noise propagates in the pipeline wall and in the flowing fluid with a speed determined by the physical properties of the fluid and pipeline. The acoustic detectors affixed to the pipe outside or inside monitor noise levels, and the system processors can determine the existence and location of leaks from signal analysis because the received signal near the leak sites is stronger. Surface acoustic wave detection only allows for non-intrusive monitoring of the pipeline when detectors are in contact with the external pipeline surface. The power spectrum of each detector signal is compared in the computer controller with the corresponding average spectrum of the background signal stored in the computer memory. A leak is detected on the basis of a significant difference in the acoustic energy of the detected signal and the acoustic energy of the background signal. The indication of a leak is verified by additional signal sampling and processing to minimize false alarms (generation of a leak alarm when the pipeline is under normal condition) [Rajtar and Muthiah, 1997].

Another acoustic method has been introduced for detecting and locating a leak in a gas transport pipeline located between two pump stations. The pipeline is treated as an acoustic tube, similar to a wind instrument. The impulse response of the acoustic wave in a pipeline may be estimated from the acoustic signal detected at two terminal sites in the pipeline. When a leak occurs in the pipeline, the impulse response of the acoustic wave has a sharp pulse or a step at a certain time that can be directly related to the site of the leak [Watanabe and Himmelblau, 1986; Watanabe and Koyama, 1990]. Fig. 2.2 shows the acoustic method for detecting a leak. The acoustic leak detection method usually requires the installation of many sensors along the pipeline due to the limitation of the detection range, and these sensors have to discriminate leak sounds from other sounds generated by the surroundings.

NOTE: This figure is included on page 14 in the print copy of the thesis held in the University of Adelaide Library.

Figure 2.2 Acoustic Leak Detection Method (Source: Watanabe and Himmelblau, 1986)

Radioactive Techniques

Neutron and gamma ray backscatter probes can be used for detecting faults in a pipeline. Usually these probes have been used in geophysical boreholes for the detection of cracks as well as in ground water observation wells for the investigation of soil density, soil moisture content [Eiswirth et al., 2001]. A radioactive source emits gamma rays that produce various nuclear interactions with the surrounding matter. This method is based on the absorption and scattering of the gamma rays when they meet a fault in a pipeline. When the probe meets passing water or gas outflow at a leak, the rate of the backscattered gamma ray changes. The radioactive method is still in the development stage on the area of pipeline condition assessment. Fig. 2.3 shows the scattering of gamma rays.

NOTE: This figure is included on page 14 in the print copy of the thesis held in the University of Adelaide Library.

Figure 2.3 Scattering of Gamma Rays (Source: Eiswirth et al., 2001)

Magnetic Flux Techniques

The magnetic flux leak detection technique (MFL) is used for most of the natural gas industry. This method is based on the principle that when a magnetic field is applied inside the pipe, the flux lines pass through the pipe wall. When a change occurs in the pipe wall geometry as a result of wall thinning, cracks, or pitting, a sensor detects the fault of pipe by analysing the magnetic flux. For example, at areas of reduced wall thickness by corrosion, the amount of magnetic flux carried is less than that for the full wall thickness. The location and amount of magnetic flux indicate the site and size of the pipeline fault. Fig. 2.4 shows the schematic of a magnetic flux leak detection technique. The measured flux is dependent on the material characteristics of the pipe, wall thickness, stresses in pipelines and dimensions of the flaw. The MFL method is good for detecting corrosion, dents, or other anomalies. However, this method cannot detect axial stress corrosion cracks or seam weld cracks [Varma, 2001] and the range of detection is restricted and short. The MFL method is usually a useful technique to confirm a fault if it is used in conjunction with other techniques.

Figure 2.4 Schematic of Magnetic Flux Leak Detection (Source: Varma, 2001)

Electromagnetic Techniques

Electromagnetic techniques can measure the wall thickness of a pipeline by sensing the attenuation and phase delay of an electromagnetic signal passing through the pipe wall. The signal is induced into the pipe by an internally placed coil, which generates eddy currents and magnetic flux lines. A disadvantage of the technique is that the signal arriving at the detector is typically very small [Eiswirth et al., 2001].

Ground Penetrating Radar Techniques

Ground penetrating radar (GPR) can detect leaking substances at the source by the use of radar. This system uses a radar transmitter and receiver to find buried pipeline leaks without digging [Daniels, 1996]. GPR techniques may be used either from the ground surface or within the pipe. Data interpretation of GPR is dependent upon personal experience and training because the radar output is difficult to interpret. Also this method does not provide a complete picture of the condition of pipes due to reliance on a single mode of data collection. Therefore, GPR is generally integrated with electromagnetic techniques [Eiswirth et al., 2001].

Ultrasonic Techniques

The features of a pipeline will affect ultrasonic waves travelling through the walls of the pipe. Ultrasonic waves can be measured to interpret the condition of the pipe. The most common way of generating an ultrasonic wave is to use a piezoelectric device. Oak Ridge National Laboratory (ORNL)'s Nuclear Science and Technology Division (NSTD) developed new fault detection methods using electromagnetic acoustic transducer (EMAT) technology. The EMAT transmitter electromagnetically induces an ultrasonic horizontal shear wave and EMAT measures the amount of sound energy reflected from the pipe wall and the amount transmitted through the pipe wall. An algorithm developed for analysing the signal recognizes the differences in patterns of reflected and transmitted sound waves and correlates those differences with changes in the pipe material caused by corrosion, circumferential and axial flaw and pitting. General piezoelectric devices need contact with the material to provide a good coupling to induce an ultrasonic wave. Getting good contact is very difficult in an instrument that is moving along the pipe. Fig. 2.5 shows the electromagnetic acoustic transducer inside the pipeline.

NOTE: This figure is included on page 17 of the print copy of the thesis held in the University of Adelaide Library.

Figure 2.5 Electromagnetic Acoustic Transducer (Source: ORNL, 2002)

Micro-Cantilever Techniques

Oak Ridge National Laboratory (ORNL) developed a method to detect very small leaks of gas from pipelines. A micro-cantilever vibrates at the characteristic rate of material. If there is no leak in a pipeline, it will vibrate at the characteristic rate of material. If it is placed in the vicinity of a leak, the frequency of its vibration will change. The shift in frequency indicates the amount of leak through a pipe crack.

Internal Inline Inspection Tools Based on Robotic Pig

Internal inline inspection tools, known as robotic or smart pigs, are computerized and selfcontained devices that are inserted into the pipeline usually for pipe cleaning, and more recently pipeline monitoring [Furness and van Reet, 1998]. The studies for improving the ability of inline inspection tools have progressed over the past decade. Some tools are highly sophisticated and others achieve their purpose with less complexity. The inline pigs are slowly propelled through the fluid flow and record pipeline information as they go. Specialized robotic pigs rely on various technologies to detect the existence of fault and the characterization of features of the pipeline. Pipeline corrosion, crack, and geometry detection pigs commonly make use of magnetic field, ultrasound, or electromagnetic wave generating signals into the pipe wall to measure changes of pipe wall thickness, crack, internal diameter. The mechanism of detection is based on the analysis of reflected signals. Inline inspection tools can reliably detect pipeline features, such as blockages, dents, corrosion, cracks, material loss, and mechanical damage. However, current inline inspection tools have a difficulty to pass sharp curves, bends, and small diameter pipes in a system. Fig. 2.6 shows various pipeline monitoring pigs.

NOTE: This figure is included on page 18 of the print copy of the thesis held in the University of Adelaide Library.

Figure 2.6 Pipeline Monitoring Pigs (Source: www.new-technologies.org)

2.1.2 Hydraulic Based Techniques

1) Flow and Pressure Change Based Techniques

Although the flow and pressure in a pipeline fluctuate due to operational changes, statistically the total mass entering and leaving a pipeline system must be in balance. These techniques rely on the assumption that a high rate of change of flow or pressure at the inlet or outlet indicates the occurrence of a fault, especially a leakage. If the flow or pressure rate of change is higher than a predefined figure within a specific time period, a leak alarm is generated [Zhang, 1996].

Single Point Pressure Analysis

The single point pressure analysis technique for leak detection uses the pressure measurement data to detect the depressurisation that accompanies a leak. More recently, the single point pressure analysis has used statistical techniques as a leak detection technique to determine when a measured pressure is declining in a significant manner [Whaley et al., 1992]. The measured pressure data of two periods is used for determining the point of difference between two sets of data. The mean and variance of the two samples are computed by,

$$\bar{p}_{old} = \frac{1}{n_{old}} \sum_{i=1}^{n_{old}} p_i \tag{2.1a}$$

$$\bar{p}_{new} = \frac{1}{np - n_{old}} \sum_{i=n_{old}+1}^{np} \bar{p}_i \tag{2.1b}$$

$$\sigma^2{}_{old} = \frac{1}{n_{old} - 1} \sum_{i=1}^{n_{old}} (p_i - \bar{p}_{old})^2 \tag{2.1c}$$

$$\sigma^2{}_{new} = \frac{1}{np - n_{old} - 1} \sum_{i=n_{old}+1}^{np} (p_i - \bar{p}_{new})^2 \tag{2.1d}$$

where $\bar{p}$ is the average of the pressure data, p_i is the measured pressure at time i, σ^2 is the variance of the pressure data, np is the total number of data points, and n_{old} is the number of data points in the earlier part of the data. The subscripts new and old refer to the older and newer partitions of the data. A leak is suspected when the mean of the newer partition of the data is significantly lower than the mean of the older part of the data. Statistically, it is necessary to test the hypothesis of $\bar{p}_{\text{old}} = \bar{p}_{\text{new}}$ against the alternative $\bar{p}_{\text{old}} > \bar{p}_{\text{new}}$ [Whaley et al., 1992].

Although the simplicity of a single point pressure analysis method is the primary strength, the use of a pressure decline as a leak signature is the weakness because a pressure decline is not unique to a leak event only. This method can yield false alarms even when the leak signature is correctly identified. Also, the single point pressure analysis system does not provide the location of leaks and spill volume. This method seems to be effective when applied to small and simple pipelines transporting incompressible fluid that operate in a nearly steady state mode.

Real Time Statistical Detection Systems

Zhang [1993] introduced the statistical pipeline leak detection system incorporating advanced pattern recognition functions to overcome the difficulties and limitations of a dynamic model based leak detection system. This method does not use numerical solution procedures to calculate flow or pressure in a pipeline. Therefore, the method itself produces no numerical errors. Various flow, pressure or temperature measurement data of a pipeline generated by operational changes need to be have been previously registered.

The detection of faults is based on relative changes in the mean value and data pattern which accept errors as normal discrepancies [Al-Rafai and Barnes, 1999]. The pattern recognition function learns flow and pressure patterns about continual changes in the line and instruments through continuously monitoring a pipeline [Zhang, 2001].

The statistical fault detection system requires a long time period of operational data to achieve a reliable and sensitive fault detection system. Zhang and Mauro [1998] used normal operational data over one year period to detect leaks in a crude oil pipeline. The pipeline was 23 kilometres in length and an average internal diameter of 24 inches. The statistical parameters were tuned and learnt based on normal operational data to recognize the external events such as equipment failures, unusual load, supply changes, and leak. Fault determination was based on probability calculations at regular sample intervals. The deviation from the established balance was detected by an optimal statistical test method, the Sequential Probability Ratio Test (SPRT) [Zhang and Mauro, 1998; Zhang and Xu, 1999]. Various real time applications and field tests were executed for estimating the applicability and sensitivity of the statistical fault detection system [Hoeijmakers, 2002; Zhang and Twomey, 2000].

Mass or Volume Balance Methods

The volume and mass balance method, also known as line balance, is one of the earliest developed computer based methods to detect the presence of a leak in a pipeline. It is based on measuring the discrepancy between the incoming and outgoing product volumes or masses of a particular pipeline segment under the principle of conservation of mass. If the difference between an upstream and downstream flow data changes by more than an established tolerance considering uncertainties in line-packing and flow measurement, a leak alarm will be generated. The relationship [ADEC, 2000] is

$$Q_L = Q_{in} - Q_{out} > dQ_m + \frac{dL_s}{\Delta t} \tag{2.2}$$

where Q_L = flow rate of the leak, Q_{in} = measured inflow to the system, Q_{out} = measured outflow from the system, dQ_m = bound of uncertainty in flow measurement, and dL_s = bound of uncertainty in line-packing change over a time interval Δt. Volume balance

without any correction for changing line-packing is most often done on crude oil pipelines or other liquid pipelines that are not batched. However, it does not work very well for gas pipelines where the line-packing can change by very large amounts over a short amount of time. Including the change in line-packing in the volume balance equation greatly reduces the amount of error in the volume balance associated with the packing or drafting of the line. The line-packing due to pressure, temperature or product composition is considered by using various volume balance methods. A representative bulk modulus or dynamic bulk modulus is used for line-packing calculations. Mass balance method accounts directly for product density. The effectiveness of mass balance calculations for leak detection is shown in a comparison based on a major Canadian crude oil pipeline [Liou, 1996]. Scott and Yi [1999] used flow-testing methods to detect and characterize partial blockages in looped sub-sea flow lines. The presence and magnitude of a blockage can be determined by checking the reduced total volume of a pipe because blockage can reduce the volume of the pipe.

Although volume balance methods have the advantage of being able to identify small leaks, the response time of leak detection is generally slow compared to other leak detection methods. In order to keep the rate of false alarms at an acceptable level, time periods from one hour to one day are required. In many cases, the response times of one hour to one day are unacceptably long to detect leaks. Also, the methods cannot find the exact location of the leak in a pipeline. Algorithms based on pressure analysis are added to volume balance methods to find the location of a leak.

Pressure Analysis Method

The pressure analysis method, also known as rarefaction wave, negative pressure, or expansion wave monitoring, is based on the analysis of pipeline pressure variations. When the pipeline wall cracks by the pressure of product or an outside force, a sudden drop in pressure occurs at the location of the leak. The expansion wave of the resulting low-pressure propagates at the speed of sound both upstream and downstream from the leak site. For example, the rarefaction wave should reach the opposite ends of the line simultaneously, when the leak occurs in the middle of a line segment with uniform construction. Pressure transducers placed along the pipeline can be used to measure the pressure gradient with respect to time. The measurement data monitored at each end of

line or segment are used to calculate the location of the leak. Usually two sensors are used for each pipeline segment to help discriminate between noise and externally caused pressure drops. Most transient flow based and volume balance leak detection systems use pressure analysis to locate leaks. The pressure analysis leak detection method largely depends on the sensitivity and calibration of instruments.

2) Transient Model Based Techniques

A transient model based method involves computer simulation using hydraulic modelling. Unexpected flow and pressure deviations can be detected based on real time models [Theakston and Larnaes, 2002]. The advantages of using a transient model over a steady state model for detecting pipeline fault are a wider range of application and increased sensitivity. The American Petroleum Institute (API) discribed the advantage of the transient model based method over other methods in 1995. It has the ability to model all of the dynamic fluid characteristics (flow, pressure, temperature) and takes into account the extensive configuration of physical pipeline characteristics (length, diameter, thickness), as well as product characteristics (density, viscosity). This method can predict the size and location of faults by comparing the measured data for a segment of pipeline with the conditions predicted by the transient analysis model. However, it is a complex method that requires numerous instruments and extensive controller training and system maintenance. The sensitivity and calibration of instruments have a direct effect on the accuracy of the model.

Many fault detection methods based on transient flow analysis have been introduced previously. Liggett and Chen [1994] developed an innovative technique called the inverse transient method. Liou and Tian [1995] presented two leak detection algorithms that are leak discrepancy pattern methods using a Cauchy algorithm and a time-marching algorithm to avoid noise amplification. Brunone [1999] applied transient analysis for leak detection to outfall pipes. Leak detection systems for gas pipelines were developed by the online simulation method [Fukushima et al., 2000], by extended Kalman filtering [Benkherouf and Allidina, 1988] and by artificial neural networks for leak sizing and locating and processing the field data [Belsito et al., 1998]. The procedure of most transient model based leak detection method is similar to that shown in Fig. 2.7.

NOTE: This figure is included on page 23 of the print copy of the thesis held in the University of Adelaide Library.

Figure 2.7 Model Based Leak Detection Flow Diagram (Source: Zhang and Mauro, 1998)

Inverse Transient Method

Pudar and Liggett [1992] introduced the first application of inverse analysis for leak detection in water distribution systems based on a steady state model. As the improvement of the steady state inverse method by using a transient model, Liggett and Chen [1994] proposed the inverse transient method (ITM) for fault detection and system calibration. The technique is able to determine the locations and magnitudes of leaks and the friction factor for each pipe in a network. The leakage is described in terms of a lumped discharge coefficient, and leaks are assumed to occur only at nodal positions for computation in the modelled pipeline system [Vítkovský, 2001]. The challenge for the method is distinguishing the difference between transients affected by leaks and normally occurring transients in a pipeline. Minimization of the differences between measured values and expected values obtained by the transient model produces a solution for the objective function. A genetic algorithm has been used for the inverse transient method to improve the efficiency of the optimisation normally based on a gradient method [Vítkovský et al., 2000a; Kim, 2002; Nash and Karney, 1999]. The inverse transient method requires a highly accurate numerical model for simulating transients. However, the development of an appropriate and accurate numerical model is difficult because real pipeline systems contain numerous unknown parameters. These uncertainties decrease the accuracy of transient analysis models. In addition, unsteady friction and minor loss effects cause significant damping of pressure traces during transient events.

Transient Damping Method

The presence of a leak in a pipeline causes an increase in the damping rate of pressure trace measurement in a pipeline during a transient event. When the pressure waves are decomposed into Fourier components, the damping rate of each component is different according to leak characteristics in the pipeline. The frequency-domain analysis of these different damping rates provides a method for determining the location and size of the leak [Wang et al., 2002]. However, in a real pipeline system, there are a lot of system components, such as joints, connections, bends, complex internal boundaries that also cause pressure wave damping. The modelling of all of system components can be complicated and, in some cases, impossible.

Frequency Response Method

The frequency response method uses the analysis of transient response in the frequency domain by Fourier transformations that transform time-domain data into the frequency-domain data [Mpesha et al, 2001; Ferrante and Brunone, 2003a and 2003b]. Comparing the dominant frequencies with and without a leak can provide a method for leak detection because the effect of a leak is frequency-dependent. The reaction of the pressure and flow to a sinusoidal input at different input frequencies defines the system response of a pipeline system. The presence of a leak in a pipeline modifies this system response depending on the size and location of the leak. The input is often a valve movement and the output is the measured pressure. A mathematical operator relates the input to the output. Analysis of the ratio of any input and output rates can be used to detect and locate leaks in pipelines [Lee et al., 2002]. Also, the examination of the leak-induced influence on the resonant peaks in the transfer function leads to a leak detection method [Lee et al., 2003].

Wave Reflection Method

This technique is similar to the theory of waves in radar and sonar systems. A signal is sent out from a source with the aim of detecting objects. The signal propagates away from the source and when meeting a change in the media, part of the signal is reflected back in the direction of the source. The analysis of these reflected signals can detect the characteristics and location of an object. A pressure wave propagates from the generation point in both directions when a pressure disturbance is generated in a pipeline. When this

pressure wave meets a fault, part of the wave is transmitted and the other part is reflected. The timing and size of the reflected wave determines the location and size of the fault [Brunone and Ferrante, 2001; Jönsson, 2001]. Adewumi et al. [2001] verified the possibility of utilizing the interaction between a pressure pulse propagating in a pipe with the blockages, as a means of blockage detection and characterization.

2.1.3 Limitation of Techniques

Most of the non-hydraulic based techniques detect leaking product outside the pipeline and include traditional procedures such as inspection by patrols. These methods are frequently labor intensive, time consuming, expensive and only partially effective, and cannot monitor a pipeline continuously. Also the techniques based on sophisticated technology have many drawbacks. The disadvantages of pipeline condition assessment methods based on non-hydraulic techniques are

- Pipeline systems have many sharp curves, bends, junctions and small diameter pipeline parts that may be undetectable places with current inspection tools.
- Data interpretation of these techniques is dependent upon personal experience and training because the signal arriving at the detector is typically very small and the output is difficult to interpret. Also these methods do not provide a complete picture of the condition of pipes due to reliance on a single mode of data collection.
- Some devices need contact with the material to provide a good coupling to induce and receive signals. Getting good contact is very difficult in an instrument that is moving along the pipe.
- Most of sophisticated technology techniques are still in the development stage for the area of pipeline condition assessment.
- The biggest disadvantage is that these techniques cannot monitor a pipeline continuously.

The hydraulic based fault detection techniques can continuously monitor the flow conditions of pipeline. The most commonly used methods are line balance method and pressure analysis method. Although the simplicity of these methods is the primary strength, they have many drawbacks.

- The use of pressure variation as a leak signature is the weakness because pressure variation is not unique to a leak event only.
- Most of these methods do not provide the exact location of fault and spill volume.
- These methods often require a long time period of operational data to achieve reliable results.
- The response time of fault detection is generally slow compared to other methods.
- These methods largely depend on the sensitivity and calibration of instruments.

The performance of transient model based fault detection techniques is, so far, largely unsatisfactory because these methods required highly accurate transient models and largely depend on the sensitivity and calibration of instruments. However these techniques may represent the future direction of fault detection as well as real-time pipeline monitoring by improving pipeline modelling and system measurement.

A number of different pipeline condition assessment techniques have been presented in this chapter. Each method has its advantages and disadvantages. Unfortunately none of the existing methodologies can offer good performance for all the attributes. A common problem for most of these methods is high false alarm rate, generating an alarm when the pipeline is under normal operation. False alarms are undesirable because they generate extra work for operational personnel as well as a real leak may be overlooked. Each fault detection technique may be suitable for the specific operational condition of a pipeline while not applicable to others. The characteristics of some techniques favor their use in certain pipeline and surrounding situations. In a system with complex geometry, the best combination of various techniques must be used to produce optimum results.

2.2 TRANSIENT ANALYSIS

Pressurised pipe systems incur a wide range of operational and loading conditions that vary with time. The principal use of transient analysis is the prediction of maximum positive and minimum negative pressures in pipe systems to design a suitable pipe size and material and effective transient pressure control systems. However, transient effects in pipeline systems are particularly important when calculating the effects of short-term flow

disturbance (rapid flow change), such as resulting from the sudden adjustment of a valve, starting or stopping of a pump, turbine or compressor, and accidental events due to equipment failure. These disturbances may create travelling pressure waves of large magnitudes, excessive noise, fatigue, pitting due to cavitation, disruption of normal control of circuits, and the possibly destructive resonant vibrations. The areas of application of fluid transients as critical design factors range over a wide variety of subjects involving the problem of the transmission of energy or substance through fluid in nuclear and thermal power plant equipments, hydroelectric power generation, rocket and missile propellant pumping systems, fluidic system responses, fuel supply systems, compressor dynamics, hydraulic and pneumatic control systems, biological blood circulatory systems, acoustics, and especially oil, gas, sewer, slurry and water transport pipelines. Also, pipeline condition assessment and fault detection systems based on transient analysis models appears to be one of the most promising techniques because pressure transients propagate through the entire system interacting with the pipe or devices along the pipe and contain a large amount of information about physical characteristics of the systems. Therefore, the analysis of induced transient data provides the basis for characterising pipeline systems. The performance of a pipeline condition assessment and fault detection system based on a transient model highly depends on the accuracy of the model.

Mathematical models for transient flow are commonly described by partial differential equations. In general problems, the unknown quantities to be determined are the three velocity components, pressure, temperature, and density of the fluid that are functions of spatial and temporal coordinates. Therefore, six fundamental equations relating these unknowns are required to obtain their solutions. The equations below show the conservation form of the fundamental equations in the rectangular coordinate system [Anderson, 1995]. These equations are the continuity equation, the three motion equations, the energy equation and the equation of state of the fluid.

Continuity Equation

$$\frac{\partial \rho}{\partial t} + \nabla \cdot (\rho \mathbf{V}) = 0 \tag{2.3}$$

Momentum Equations (Navier-Stokes Equations)

$$\frac{\partial(\rho u)}{\partial t} + \frac{\partial\left(\rho u^2\right)}{\partial x} + \frac{\partial(\rho u v)}{\partial y} + \frac{\partial(\rho u w)}{\partial z} = -\frac{\partial p}{\partial x} + \frac{\partial}{\partial x}\left(\lambda \nabla \cdot \mathbf{V} + 2\mu \frac{\partial u}{\partial x}\right) + \frac{\partial}{\partial y}\left[\mu\left(\frac{\partial v}{\partial x} + \frac{\partial u}{\partial y}\right)\right] + \frac{\partial}{\partial z}\left[\mu\left(\frac{\partial u}{\partial z} + \frac{\partial w}{\partial x}\right)\right] + \rho B_x \tag{2.4a}$$

$$\frac{\partial(\rho v)}{\partial t} + \frac{\partial(\rho u v)}{\partial x} + \frac{\partial\left(\rho v^2\right)}{\partial y} + \frac{\partial(\rho v w)}{\partial z} = -\frac{\partial p}{\partial y} + \frac{\partial}{\partial x}\left[\mu\left(\frac{\partial v}{\partial x} + \frac{\partial u}{\partial y}\right)\right] + \frac{\partial}{\partial y}\left(\lambda \nabla \cdot \mathbf{V} + 2\mu \frac{\partial v}{\partial y}\right) + \frac{\partial}{\partial z}\left[\mu\left(\frac{\partial w}{\partial y} + \frac{\partial v}{\partial z}\right)\right] + \rho B_y \tag{2.4b}$$

$$\frac{\partial(\rho w)}{\partial t} + \frac{\partial(\rho u w)}{\partial x} + \frac{\partial(\rho v w)}{\partial y} + \frac{\partial\left(\rho w^2\right)}{\partial z} = -\frac{\partial p}{\partial z} + \frac{\partial}{\partial x}\left[\mu\left(\frac{\partial u}{\partial z} + \frac{\partial w}{\partial x}\right)\right] + \frac{\partial}{\partial y}\left[\mu\left(\frac{\partial w}{\partial y} + \frac{\partial v}{\partial z}\right)\right] + \frac{\partial}{\partial z}\left(\lambda \nabla \cdot \mathbf{V} + 2\mu \frac{\partial w}{\partial z}\right) + \rho B_z \tag{2.4c}$$

Energy Equation

$$\frac{\partial}{\partial t}\left[\rho\left(e_t + \frac{V^2}{2}\right)\right] + \nabla \cdot \left[\rho\left(e_t + \frac{V^2}{2}\right)\mathbf{V}\right] = \rho q + \frac{\partial}{\partial x}\left(k \frac{\partial T}{\partial x}\right) + \frac{\partial}{\partial y}\left(k \frac{\partial T}{\partial y}\right) + \frac{\partial}{\partial z}\left(k \frac{\partial T}{\partial z}\right) - \frac{\partial(up)}{\partial x} - \frac{\partial(vp)}{\partial y} - \frac{\partial(wp)}{\partial z} + \frac{\partial(u\tau_{xx})}{\partial x} + \frac{\partial\left(u\tau_{yx}\right)}{\partial y} + \frac{\partial(u\tau_{zx})}{\partial z} + \frac{\partial\left(v\tau_{xy}\right)}{\partial x} + \frac{\partial\left(v\tau_{yy}\right)}{\partial y} + \frac{\partial\left(v\tau_{zy}\right)}{\partial z} + \frac{\partial(w\tau_{zx})}{\partial x} + \frac{\partial\left(w\tau_{yz}\right)}{\partial y} + \frac{\partial\left(w\tau_{zz}\right)}{\partial z} + \rho \mathbf{B} \cdot \mathbf{V} \tag{2.5}$$

Equation of State

$$E_T = E_T(\forall,\ T)$$
$$S = S(\forall,\ T) \tag{2.6}$$

where x, y, and z are the distances in the Cartesian space, t is the time, u, v, and w are the x, y, and z components of velocity, ρ is the fluid density, V is the fluid velocity, **V** is the vector velocity in the Cartesian space, p is the fluid pressure, μ is the absolute viscosity coefficient, λ is the second viscosity coefficient, $B_{x,\,y,\,and\,z}$ is the body force, q is the rate of volumetric heat addition per unit mass (heat flux), e_t is the internal energy due to random molecular motion per unit mass, $V^2/2$ is the kinetic energy per unit mass, $e_t+V^2/2$ is the total energy per unit mass, k is the thermal conductivity, T is the absolute temperature, $\tau_{xx,\,yy,\,and\,zz}$ is the normal stresses in a fluid, $\tau_{xy,\,xz,\,yz,\,\ldots}$ is the shear stresses, **B** is the vector body force, $\forall$ is the volume, E_T is the total energy of the system, and S is the entropy.

These fundamental relations are too difficult to solve analytically and numerically because of their complexity and turbulence. Most engineering solutions involve approximations to simplify the general governing equations for a particular case. The assumptions for simplifying these equations have the effect of reducing complexities of these equations. They may be hyperbolic equations of the first or second order for transient pipe flows. Each of the transient models considered is derived from the fundamental equations of fluid dynamics and general considerations of the boundary and flow conditions according to the degree of simplification. The basic equations describing the phenomenon are based on a number of simplifying assumptions that must be satisfied if the mathematical model is to yield satisfactory results. The following choices in the Table 2.1 are made in developing the transient model in pipeline systems.

Table 2.1 Choices Used in the Derivation of the Models

1	Viscous or inviscid flow
2	Perfect gas or real gas law
3	Laminar or turbulent flow
4	Single or multiple phase flow
5	One or higher dimensional flow
6	Steady or unsteady flow friction
7	Axisymmetric or azimuthal flow
8	Body forces are negligible or not
9	Thermal effects are negligible or not
10	Compressible or incompressible flow
11	Homogeneous or non-homogeneous fluid
12	Expansion of pipe wall is negligible or not
13	Constant (average fluid properties) or variable coefficient
14	Non-linear convective acceleration terms are negligible or not
15	Isentropic or non-isentropic propagation of disturbances along the pipe

2.2.1 Waterhammer Analysis Models

1) Method of Characteristics (MOC)

Assuming one-dimensional flow averaged cross sectional velocity and pressure distribution in pressurised pipeline systems, the computational procedures for transient analysis are well-developed and proven and produce satisfactory results if properly utilized [Gibson, 1908; Rich, 1951; Parmakian, 1955; Fox, 1977 and 1989; Webb and Gould, 1978; Sharp, 1981; Chaudhry, 1987; Almeida and Koelle, 1992; Swaffield and Boldy, 1993; Wylie et al., 1993; Thorley, 2004]. The basic equations of continuity and motion governing one-dimensional transient flow in a pipeline are written below in a simplified form.

$$\frac{\partial H}{\partial t}+\frac{a^2}{gA}\frac{\partial Q}{\partial x}=0 \qquad (2.7a)$$

$$\frac{\partial Q}{\partial t}+gA\frac{\partial H}{\partial x}+\frac{f\,Q|Q|}{2DA}=0 \qquad (2.7b)$$

The dependent variables are the piezometric head H and discharge Q, x and t are the independent variables denoting distance along the pipeline and time, respectively, g is the gravitational acceleration, a is the wavespeed, A is the pipe cross-sectional area, and D is the pipe inside diameter. Frictional losses are assumed to be approximated by the steady state values at any instant and f denotes the Darcy-Weisbach friction factor. For most engineering applications, the convective terms, $V(\partial H/\partial x)$ and $V(\partial V/\partial x)$, are neglected because they are small compared to the other terms. The applicability of each model is governed by the fluid and pipe characteristics and by the time rate of change of a primary variable $\partial H/\partial t$ and $\partial V/\partial t$ at the boundary. The most commonly used technique for solving these hyperbolic partial differential equations is the method of characteristics (MOC) because of numerical simplicity of the explicit formulation and the fast computational time. The MOC can transform the partial differential equations into ordinary differential equations that apply along specific lines called characteristic lines in the space-time plane, and the simplified compatibility equations are solved along these characteristic lines.

The method of characteristics is computationally efficient when it can use a fixed-grid (fixed time and space interval) for computation. Therefore, it is considered to be an excellent means for the analysis of transient flow through pipeline systems with constant celerity of wave propagation. In this case, the pipeline can be divided into an integer number of equal reaches that satisfy the stability condition restricting the relationship between time and space-mesh parameters. In this case, the Courant number, the ratio of the physical celerity to the numerical celerity, is equal to unity. However, the method becomes problematic when it is applied to complex systems or systems with varying wavespeeds, material properties, multiple phase flows, or flow control devices for which the Courant number is not equal to unity. For these systems, MOC requires interpolation schemes or wavespeed/geometric adjustments, although they introduce very important attenuation and dispersion errors into the solutions.

2) Interpolation Schemes for a Fixed-Grid MOC

Interpolations may be accomplished in either space or time, or in some combination of the two. In a space-line interpolation scheme, the unknown variables, R and S are interpolated using the previously calculated known values, A, B, and C as shown in Fig. 2.8a [Fox, 1961]. Vardy [1976] proposed a reach-out space-line interpolation scheme that may be improved by reaching over to adjacent reaches in space as shown in Fig. 2.8b. Although this scheme can use large time steps, it causes major errors when the flow change is rapid and requires irregular treatment at the boundaries. In the time-line interpolation scheme, the characteristic lines are extended backward from the unknown time level (j+1) to intersect a known time level (j), the interpolation can be done along the line between j-1 and j as shown in Fig. 2.8c. This interpolation scheme was developed by Goldberg and Wylie [1983] and is called reach-back time-line interpolation. They found that this scheme is more accurate than space-line interpolation for the same discretisation. They considered another time-line interpolation problem within the current time step as shown in Fig. 2.8d. This provides a solution procedure that is implicit in the solution variable and is called an implicit time-line scheme. This scheme is not constrained by maximum time step limitations, and has advantages when using in other implicit numerical schemes. Ghidaoui and Karney [1994] suggested the wavespeed adjustment method that artificially changes the wavespeed, thus allowing the characteristic lines to directly reach from a known value

to an unknown value. This method can be applied to previous mentioned all space and time line interpolation schemes as demonstrated in Fig. 2.8e.

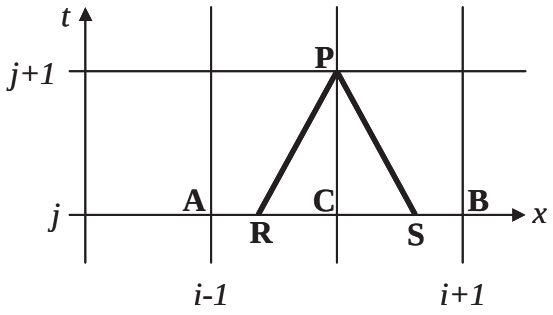

a) Space-Line Interpolation

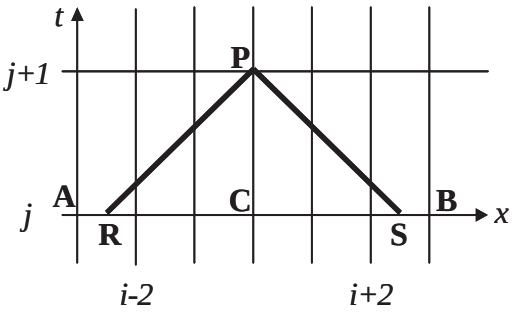

b) Reachout Space-Line Interpolation

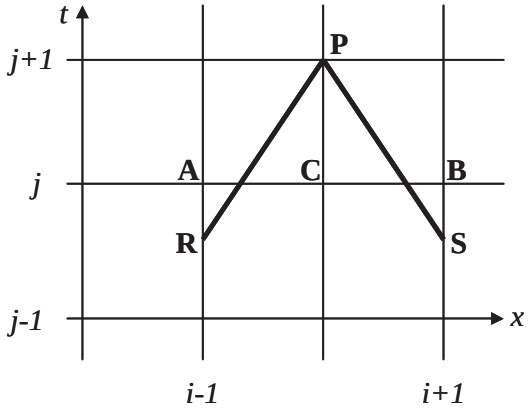

c) Reachback Time-Line Interpolation

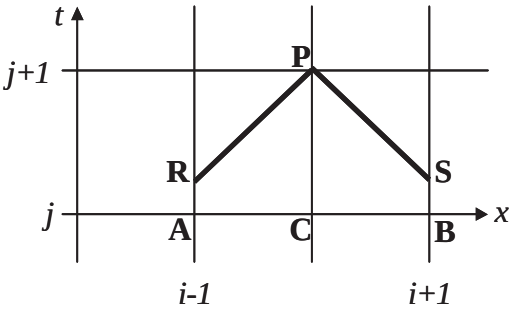

d) Implicit Time-Line Interpolation

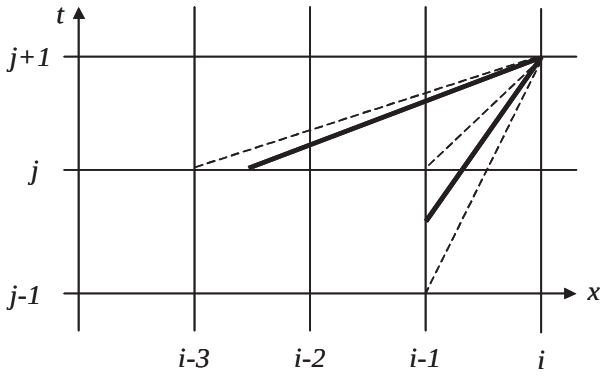

e) Wavespeed Adjustment Method

Figure 2.8 Interpolations for a Fixed-Grid MOC

Lai [1989] proposed a multimode interpolation scheme that combines various space and time line interpolations. Sibetheros et al. [1991] investigated the method of characteristics with cubic spline polynomials of interpolations for numerical waterhammer analysis in a

frictionless horizontal pipe. They compared the method with two-point fourth-order Hermite polynomial scheme developed by Holly and Preissmann [1977]. They noticed that the two schemes had similar accuracy and the overall accuracy with splines was improved compared to the MOC with linear interpolation. Yang and Hsu [1990] proposed a reach-back Holly-Preissmann scheme with reaching back in time more than one step for the advection-diffusion equation. Karney and Ghidaoui [1997] developed a hybrid scheme to combine and blend several interpolation schemes with wavespeed adjustment technique called a flexible discretisation algorithm. This method included interpolation along a secondary characteristic line, minimum-point interpolation and wave path adjustment. Minimum-point interpolation minimizes the distance from the interpolated point to the primary characteristic. Although the higher-order interpolations provide the expectation of improved accuracy in the solution compared with linear interpolations, they require more computation time and often introduce numerical diffusion [Chen, 1995].

3) Wave Plan/Characteristic Method

Wood et al. [1966] developed a wave plan method (later referred to as the wave characteristic method) that tracks the movement and transformation of pressure waves in transient pipe flows [Wood, 2005; Wood et al., 2005]. This method normally requires orders of magnitude fewer pressure and flow calculations, and has a simple physical model. However, the method requires flow disturbance functions that approximately calculate the behavior of flow disturbance systems, such as valve and joint. Even wall friction is modelled using the flow disturbance function. The effect of wall friction on a pressure wave is accounted for by modifying the pressure wave using a nonlinear characteristic relationship describing the corresponding pressure head change as a function of the line's flow rate. Therefore, this method cannot describe physical phenomena of unsteady wall shear stress.

4) Implicit Finite Difference Method (Implicit FDM)

It is possible to use finite difference methods (FDM) to solve partial differential equations in the conservative, non-conservative or simplified form for waterhammer. A number of finite difference schemes have been developed for other flow analysis fields. This section introduces the application of FDM into waterhammer analysis in closed-conduit. In the

implicit finite difference method, the unknown discharge and head at a section at the end of time step are expressed in terms of the unknown values of these variables at the neighboring sections. Therefore, the equations are solved simultaneously for the entire system at each time step [Chaudhry, 1987]. Bribiesca [1981] used an implicit FDM to evaluate waterhammer phenomena when column separation is expected. He developed a simple method for considering matrix properties to reduce computational time. Han [1983] modified the semi implicit method for pressure linked equation (called SIMPLE) by adding a density correction term to the pressure correction equation. This model permitted use for transient analysis of both high and low speed fluid flows. Various implicit schemes for FDM were tested for unsteady transport, flow equation, and friction-damping effects on pipe flow [Stephenson, 1986; Arfaie and Anderson, 1991; Szymkiewicz, 1995; Islam and Chaudhry, 1998; Anisimov et al., 1999; Samani and Khayatzadeh, 2003]. Arfaie and Anderson [1991] investigated the most suitable spatial weighting factor (0.515) of implicit FDM for rapid transient events. Verwey and Yu [1993] proposed a new implicit FDM called as space-compact high-order implicit scheme that had third-order accuracy in its truncation error. The scheme used only two adjacent grid points in space on a non-staggered grid and was defined on three levels in time. Therefore, the scheme gave the advantage of a simple solution algorithm and the preservation of the high-order characteristics. Salgado et al. [1994] and Schohl [2003] developed a hybrid method combining implicit FDM and MOC for unsteady flow in pipe networks. This method had proved to be efficient for modelling unsteady flows in complex pipe networks with greater flexibility than the MOC and FDM, particularly for large Courant numbers and avoids the interpolations required by MOC. The main advantage of implicit FDM is that the scheme is stable for large time steps. However, the time and space relationship should be specified by the Courant condition to achieve reasonable accuracy in most transient pipe problems. If the Courant number is not equal to unity, this method frequently generates high-frequency numerical oscillations behind steep wave fronts. Moreover, implicit FDM requires large computational times and storage because the entire system must be analysed for each iteration.

5) Explicit Finite Difference Method (Explicit FDM)

In the explicit finite difference method, the partial derivatives are replaced by finite difference approximations such that the unknown conditions at a point at the end of a time

step are expressed in terms of the known conditions at the beginning of the time step [Chaudhry, 1987]. Chaudhry and Hussaini [1985] introduced three second-order accurate explicit FDM including the MacCormack's method, the Lambda scheme, and the Gabutti Scheme to solve the quasilinear-hyperbolic partial differential equations describing the waterhammer phenomenon in closed conduits. They presented the details of these schemes and the treatment of boundary conditions for a simple frictionless pipe system where an analytical solution is available. They noticed that the second-order schemes required fewer computational nodes and less computational time when compared the first-order MOC when the Courant number is less than unity. However, there is little advantage in using the second-order methods over the first-order methods, if the Courant number is almost equal to unity. Chaudhry et al. [1990] used MacCormack's method and the Gabutti scheme to simulate transient conditions in a low Mach number flow and gas-liquid mixture flow with a very low void fraction. This research suggested that MacCormack's method is the most satisfactory for transient analysis in closed-conduit. Beauchemin and Marche [1992] investigated the application of MacCormack's method to the full waterhammer analysis model including non-linear convective acceleration terms and pipe slope terms. The first and second order explicit total variation diminishing (TVD) finite difference schemes have been adapted for the calculation of the unsteady flow in ducts of varying cross-sectional area to avoid numerical oscillations near shock waves and steep gradients [Corberan and Gascon, 1995].

6) Finite Element Method (FEM)

The finite element method (FEM) has been widely applied to fluid and solid mechanics problems, but its success in computing liquid pipeline transients has been limited. Usually, hybrid techniques involving finite elements in the spatial domain and finite difference in time domain are used for computing pipeline transients [Watt et al., 1980; Onorati et al., 1997]. The advantage of FEM is that easily treats the complex geomorphic systems and variable size system components. However, large computational times are the major disadvantage of the method. Davis and Cheng [1972] proposed a finite element method to simulate transient duct flow problems with constant axial conditions but arbitrarily prescribed initial conditions. Szymkiewicz and Mitosek [2005] proposed the modified FEM to solve the unsteady pipe flow equations. This approach produced a six-point implicit finite difference scheme for fixed mesh with two weighting parameters and

showed higher accuracy compared with standard versions of the finite element and difference method.

7) Finite Volume Method (FVM)

Although finite volume methods (FVM) have been successfully used to solve hyperbolic partial differential equation systems in gas dynamics and shallow water open channel flows, this approach has seldom been applied to water transient pipe flows because of the complicated boundary conditions for incompressible flows [Ghidaoui et al., 2005]. Hwang and Chung [2002] developed finite volume Godunov-type numerical method with second-order accuracy to simulate waterhammer problems in pipeline systems. In the Godunov approach, the implementation of boundary conditions and flow system components, such as valves and junctions, is similar to that of the method of characteristics. This model used a conservative form of the compressible flow equations including advective terms. Zhao and Ghidaoui [2004] proposed first and second-order explicit finite volume Godunow-type schemes. They found that the first-order Godunov scheme is identical to the MOC with linear space-line interpolation and the second-order scheme required much less memory storage and computational time than either the first-order scheme or the MOC.

8) Two-Dimensional Model for Waterhammer Analysis

A number of two-dimensional models using turbulence models have been proposed to describe waterhammer phenomena during transients by considering the actual velocity distribution across a section of pipe and unsteady wall resistance [Wood and Funk, 1970; Ohmi et al., 1985a; Bratland, 1986; Vardy and Hwang, 1991; Eichinger and Lein, 1992; Raabe and Olbrich, 1992; Brunone et al., 1995; Silva-Araya and Chaudhry, 1997 and 2001; Pezzinga, 1999 and 2000; Selcuk et al., 2002; Ghidaoui et al., 2002; Zhao and Ghidaoui, 2003]. Although these models can provide more detail of the physical phenomena than one-dimensional approaches and present information needed to assess the validity of one-dimensional models, until now the practical application of higher-dimensional models to extensive pipe network, real-time flow monitoring, pipeline fault detection and assessment using inverse analysis by evolution algorithm is unreasonable when considering the requirement of significant large computational time and memory space.

2.2.2 Transient Gas Flow Analysis Models

Assuming one-dimensional and single-phase flow, the basic equations and computational procedures for transient gas pipe flow analysis are similar to those for liquid flow. This section describes transient analysis models considering one-dimensional and single-phase flow in a natural gas pipeline. For transients in compressible flow, it is no longer the interaction between the slight compressibility of the liquid and the elasticity of the pipe wall, but rather the compressibility of the gas is the dominant physical process that needs to be modelled. The transient model for compressible flow can have a number of alternative assumptions according to the flow conditions, including isothermal, adiabatic, or generalized (non-isothermal and non-adiabatic) gas processes.

In previous research and practical applications, an isothermal or adiabatic gas process approach has been adopted due to the computational simplicity. Although the laws of thermodynamics must be satisfied for analysing real gas flows because the density of the fluid changes according to variation of both pressure and temperature, if the pipeline system being analysed maintains thermal equilibrium between the pipeline system and its surroundings, the fluid flow can be regarded as an isothermal process flow. Especially, for the case of slow transients caused by fluctuations in demand, it is assumed that the gas in the pipe has sufficient time to reach thermal equilibrium with its constant temperature surroundings. On the other hand, when transient events are fast, it is assumed that the pressure changes occur instantaneously, allowing no time for heat transfer to take place between the gas in the pipe and the surroundings. Therefore, the fluid flow is regarded as an adiabatic process flow [Osiadacz and Chaczykowski, 2001].

In isothermal or adiabatic gas process flows, the energy equation governing the heat transfer and the conversion of frictional work into thermal energy is not needed. A process exponent of a fixed value takes into account the heat exchange. Isothermal and adiabatic gas processes are idealized fluid flows. Real physical phenomena of compressible flows are heavily dependent on temperature variations of pipeline and its surroundings. Sometimes, it is impossible to accurately analyse compressible flow without considering the details of heat exchange. The generalized (non-isothermal and non-adiabatic) gas

process model includes the energy equation for simulating heat transfer between the pipeline and surroundings and the conversion of frictional work into thermal energy.

1) Method of Characteristics (MOC)

Some researchers have used the method of characteristics to provide a solution of the equations governing unsteady flow in natural gas pipelines under isothermal conditions [Stoner, 1969; Yow, 1972; Wylie et al., 1974]. Most of MOC formulations have neglected the inertia term in the momentum equation for computational simplicity. This assumption will definitely result in loss of accuracy of the simulation results for fast transients. Yow [1972] and Wylie et al. [1974] introduced the inertia multiplier to compensate for the absence of the inertia term in the momentum equation. However, the calculations based on the concept of inertia multiplier may yield very misleading results when the transient events are fast and abrupt, and when the time step for simulating transient flow is small [Rachford and Dupont, 1974]. Vardy and Pan [1997 and 2000] noticed that the method of characteristics is inherently less well suited to the solution of high speed gas flows (where flow velocities are important in comparison with wavespeeds) than in liquid flows in pipelines. With compressible flows, it is difficult to prevent distortion arising from errors in regions of steady and continuously varying flow, and these errors always exist in transient flows. Also, continuous changes of wavespeed due to the density variations can generate numerical errors from the fixed-grid of MOC. Issa and Spalding [1972] and Cronje et al. [1980] proposed transient analysis models based on the MOC to consider heat transfer in gas pipeline. Their procedure is based on the Hartree hybrid method that combines the use of a rectangular grid with the use of characteristics. The MOC generates additional characteristic lines for a temperature variable, which involves extra complications in computations. Although the MOC has been extended to deal with isothermal gas flows as well, the requirement of strict adherence to the time-space step relationship becomes a serious limitation in the case of non-isothermal gas flows, slow transients in gas pipelines and non-adiabatic gas flows that have variable wavespeeds [Greyvenstein, 2002].

2) Finite Difference and Element Method (FDM and FEM)

Various finite difference schemes have been applied to the simulation of transient gas pipe flows. Bender [1979] used a Lax-Wendroff scheme to simulate dynamic gas flows in networks including control loops. A major drawback of these explicit finite difference methods is that these methods are only conditionally stable. For most cases, the stability criterion is the same as that defined for the method of characteristics. Another disadvantage of explicit FDMs is their inability to solve for the boundary conditions naturally. In many cases, the boundary conditions are solved using the MOC, and then the calculations are complicated for networks with many branch pipelines [Thorley and Tiley, 1987].

Han [1983], van Deen and Reintsema [1983], Osiadacz [1983], Kiuchi [1994], and Greyvenstein [2002] proposed an implicit finite difference methods for transient analysis of compressible fluid flows based on the simultaneous pressure correction approach. The algorithm for solving partial differential equations of a pipe is based on an iterative convergence method with a sparse matrix technique. Usually, these methods include the calculation of the inertia terms. The disadvantage of the implicit FDM is the relatively large computational time for the simultaneous solution of a set of nonlinear equations at each time step. Although the stability analysis shows that these methods have theoretically unconditional stability, the accuracy and stability are dependent on a time-step weighting factor. The implicit FDM usually gives good solutions for both rapid and slow transient phenomena and in both isothermal and non-isothermal flows when compared with explicit methods. Perotti [1999] presented the discontinuous finite element method (DFEM) to solve one-dimensional Euler equations for unsteady gas dynamics in pipes. The DFEM shows some advantages with respect to FDM when dealing with non-uniform grids. However, this method is much more time consuming than an FDM having the same accuracy.

3) Hybrid Scheme

MacLaren et al. [1976] found a numerical scheme that combines the two-step leap-frog method in the pipes and the method of characteristics at the boundaries to improve computational efficiency of unsteady gas flow equations. Mulpuru [1983] introduced a

flux splitting method for the numerical simulation of one-dimensional compressible flow. He proposed two solution schemes based on the split conservation form of the basic equations. One is the first-order accurate upwind scheme and the other is a scheme similar to the second-order Lax-Wendroff scheme. This hybrid scheme that results from the weighting of the two schemes eliminates post-shock numerical oscillations of an ideal shock-tube problem, and this method can be extended to higher spatial dimensions through time splitting. Vandevoorde et al. [1998], Zhou and Adewumi [2000], Kessal [2000], and Dukhovnaya and Adewumi [2000] developed various hybrid schemes using the total variation diminishing (TVD) to achieve a higher-resolution capturing of transients propagation and to eliminate numerical oscillations and smearing usually characteristic of other methods. They used a Godunov scheme, a Roe scheme, a Lax-Wendroff scheme or a flux difference splitting technique with first or second order upwind fluxes for hybrid TVD schemes.

2.3 SUMMARY AND CONCLUSIONS

The performance of the pipeline condition assessment and fault detection system based on a transient model highly depends on the accuracy of a transient analysis numerical model. The most commonly used technique for solving the problems of pipeline hydraulic transients is the method of characteristics (MOC) because of numerical simplicity of the explicit formulation and the fast computational time. The MOC is considered to be an excellent means for the analysis of transient flow through pipeline systems with constant celerity of wave propagation (a system with a fixed-grid for computation). However, the method becomes problematic when it is applied to complex systems or systems with varying wavespeeds for which the Courant number is not equal to unity. In addition, the MOC generates an additional characteristics line for a temperature variable, which involves extra complications in computations. Although the MOC has been extended to deal with isothermal gas flows as well, the requirement of strict adherence to the time-space step relationship becomes a serious limitation in the case of non-isothermal and non-adiabatic gas flows that have variable wavespeeds due to density variations.

To improve the accuracy and applicability of transient analysis, a more robust scheme to analyse hydraulic transients in both liquid and gas pipelines based on a conservative finite difference solution scheme has been developed in this research. The conservation form of

the governing equations has been used to formulate the problem of unsteady flow in pipeline systems. The basic equations, derived from the conservation of mass, momentum, and energy, an equation of state for the fluid density, and an equation of state for the pipe area, include all terms. The conservative solution scheme directly calculates the fluid density and pipe wall distensibility at every computational time step. As a result, the wavespeeds at all computational nodes are updated at every time step. This procedure has big advantages for analysing systems with variable wavespeeds. The conservative solution scheme is discussed in Chapter 3.

Flow system components commonly encountered in pipelines create unique dynamic behaviours of pressure waves during transients, which cause a major obstacle in the development of a precise transient analysis model. The development of an advanced transient model for analysing these unsteady characteristics is essential prerequisite for pipeline condition assessment. To develop the advanced transient model, this research investigates the significant details of the effects of distributed energy loss component (unsteady pipe wall friction in Chapter 5) and local energy loss components (leakages in Chapter 6, entrapped air pockets in Chapter 7, orifices and blockages in Chapter 8, and viscoelasticity of localised polymer pipe sections in Chapter 9) that may affect the shape and phase of transient pressure waves. The dynamic characteristics of these system components are modelled based on the conservative solution scheme.

CHAPTER 3

TRANSIENT ANALYSIS FOR GASES AND LIQUIDS BASED ON A CONSERVATIVE SOLUTION SCHEME

This chapter presents the development of transient analysis models for both compressible (gases) and slightly compressible flow (liquids) in a pipeline. The accurate and appropriate simulation of pressure transients is an essential requirement for pipeline monitoring and fault detection systems. In this chapter, the governing equations in integral form derived from the Reynolds transport theorem are expressed in terms of partial differential equations suitable for a time-marching solution of one-dimensional flow. To improve the flexibility and sensitivity of transient analysis, this research uses a conservative solution scheme. The conservation form of the governing equations with all terms included has been used to formulate the problem of unsteady pipe flow. An implicit finite difference solution algorithm is used to solve the system of non-linear governing equations by a Newton-Raphson iterative procedure. The gas transient models developed in this research are able to analyse three different specified gas processes during unsteady pipe flows, namely, isothermal, polytropic, and generalized gas processes. These models can simulate one-dimensional gas transient problems including heat transfer and the conversion of frictional work into thermal energy. The conservative scheme solves four dependent variables (pressure, density, area, velocity) or five dependent variables with the addition of temperature. Numerical and laboratory experiments (presented in Chapter 5) of both gas

and water transients in pipeline systems have been carried out for the verification of the proposed conservative solution scheme.

3.1 GOVERNING EQUATIONS FOR TRANSIENTS

The behaviour of fluid in a flow system is described by a set of fundamental physical laws which are approximated by an appropriate set of equations, including the continuity, momentum, and energy equations. These equations specify the time rate of change of some system property, and are the mathematical statements of three fundamental physical principles. These include,

1. The law of conservation of mass (the mass of a system remains constant)
2. Newton's second law of motion, $F = ma$ (the time rate of change of momentum of a system is equal to the sum of all the forces acting on the system by its surroundings)
3. The laws of thermodynamics (the energy of a system is conserved)

There are two general approaches to observe fluid flow and to obtain the governing equations from basic laws [Anderson, 1995]. The first is the control volume approach which is referred to as the Eulerian flow description method. The flow is observed from a reference system fixed relative to the control volume (a geometric entity, in dependent of mass). From the control volume approach, information is obtained about the flow in terms of what happens at fixed points in space as the fluid flows past those points. The second approach, referred to as the Lagrangian flow description method, is the system approach that follows individual fluid particles as they move about and determines how the fluid properties associated with these particles change as a function of time (always the same atoms or fluid particles). We are usually interested in the flow through a region rather than the motion of a specified particle or a specified quantity of mass. Therefore, the control volume approach is usually applied to fluid mechanical problems to derive basic governing equations. The Reynolds transport theorem provides the key elements in the derivation of the control volume equations.

The Reynolds transport theorem is used for relating the fluid property (such as mass, energy, momentum), N, for a system (specified quantity of fluid mass) to the fluid property

for a particular control volume (specified region) [Munson et al., 2002]. Thus, it formulates the relation between equations applied to a system and those applied to a control volume. Eq. 3.1 is the general form of the Reynolds transport theorem for a fixed, non-deforming control volume. A detailed derivation of this equation can be found in Streeter and Wylie [1985], Liggett [1994], or Munson et al. [2002]. The time rate of change of N for the system is formulated in terms of the control volume.

$$\frac{DN_{SYS}}{Dt} = \frac{\partial}{\partial t}\int_{CV} \eta\rho \, d\forall + \int_{CS} \eta\rho \, \mathbf{v} \cdot d\mathbf{A} \tag{3.1}$$

where N is the total amount of some extensive property within the system at time t, the subscript SYS represents the system, η is the amount of this property per unit mass throughout the fluid (intensive property), $d\forall$ is the elemental volume inside the control volume, $d\mathbf{A}$ is the vector element representing an surface area of the inflow and outflow, ρ is the fluid density, $\mathbf{v}$ is the velocity vector, and the integrals are taken over the control volume (CV) and the control surface (CS). When the dot product of $\mathbf{v}$ and $d\mathbf{A}$ is equal to zero, there is no inflow or outflow through a control volume system boundary. D/Dt is the substantial or material derivative, which is physically the time rate of change of fluid property following a moving fluid element. This is different from $\partial/\partial t$, called a local partial derivative, which is the time rate of change at a fixed point.

Eq. 3.1 states that the time rate of increase of N (the term on the left) within a system is equal to the time rate of increase of the property N (the first term on the right) within the control volume (fixed relative to the Cartesian coordinate system, x-y-z axes) plus the net rate of efflux of N (the final term on the right) across the control volume boundary [Streeter and Wylie, 1985]. In the following section, continuity, momentum, and energy equations are derived by using the Reynolds transport theorem. Also, the governing equations of integral form derived from the Reynolds transport theorem are expressed in terms of partial differential equations suitable for a time-marching solution scheme appeal to one-dimensional flow.

3.1.1 Continuity Equation

The law of conservation of mass, *Dm/Dt = 0*, in Eq. 3.1 leads to the continuity equation. This principle states that the mass within a system remains constant with time. Let N_{SYS} be the total mass of the system (m) in Eq. 3.1. Then, η is the mass per unit mass (η=1). Thus,

$$0 = \frac{\partial}{\partial t}\int_{CV} \rho \, d\forall + \int_{CS} \rho \mathbf{v} \cdot d\mathbf{A} \tag{3.2}$$

The integral form of the continuity equation shows the time rate of change of mass inside the control volume is equal to the net rate of mass inflow/outflow to the control volume.

Flow through a closed conduit can be characterized as one-dimensional in terms of many practical problems. One-dimensional flow neglects variations in flow properties transverse to the main flow direction. The flow properties are assumed uniform across any given cross section. Therefore, conditions at a cross section are expressed by average values of fluid properties. To obtain a partial differential equation form of the continuity equation, Eq. 3.2 is applied to the shaded control volume shown in Fig. 3.1. This control volume is a slice of the pipe flow, where the infinitesimal thickness of the slice is *dx*.

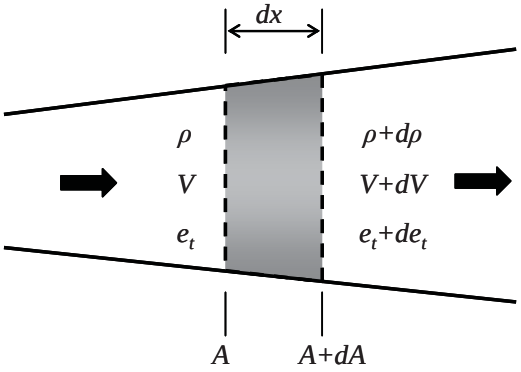

Figure 3.1 Control Volume for Deriving the Partial Differential Equations

The density, velocity, and internal energy, denoted by ρ, V, and e_t on the left side of the control volume, are uniform over the area A. Similarly, the density, velocity, and internal energy, denoted by $\rho+d\rho$, $V+dV$, and e_t+de_t on the right side of the control volume are uniform over the area $A+dA$. When we apply Eq. 3.2 to the control volume, the volume integral term in Eq. 3.2 becomes, in the limit as *dx* becomes very small,

$$\frac{\partial}{\partial t}\int_{CV}\rho\, dV = \frac{\partial}{\partial t}(\rho A dx) \tag{3.3}$$

where Adx is the volume of the control volume in the limit of dx becoming vanishingly small. The surface integral term representing the net rate of mass flow through the control surface in Eq. 3.2 becomes

$$\int_{CS}\rho\,\mathbf{v}\cdot d\mathbf{A} = -\rho AV + (\rho + d\rho)(A + dA)(V + dV) \tag{3.4}$$

The minus sign on the first term of the right hand side comes from the dot product of the vectors **v** and $d\mathbf{A}$ when we assume the inflow pointing toward the control surface of the control volume as negative. Expanding the triple product term on the right hand side of Eq. 3.4 gives

$$\begin{aligned}\int_{CS}\rho\,\mathbf{v}\cdot d\mathbf{A} = {} & -\rho AV + \rho AV + \rho V\, dA + \rho A dV + \rho\, dV\, dA \\ & + AV\, d\rho + V\, dA\, d\rho + A dV\, d\rho + d\rho\, dV\, dA\end{aligned} \tag{3.5}$$

The terms involving products of differentials can be dropped because they go to zero much faster than those terms involving only one differential. Thus,

$$\int_{CS}\rho\,\mathbf{v}\cdot d\mathbf{A} = \rho V\, dA + \rho A dV + AV\, d\rho = d(\rho AV) \tag{3.6}$$

Substituting Eq. 3.3 and Eq. 3.6 into Eq. 3.2,

$$\frac{\partial}{\partial t}(\rho A dx) + d(\rho AV) = 0 \tag{3.7}$$

Dividing Eq. 3.7 by dx and noting that $d(\rho AV)/dx$ is, in the limit as dx goes to zero, the definition of the partial derivative with respect to x [Anderson, 1995],

$$\frac{\partial}{\partial t}(\rho A) + \frac{\partial}{\partial x}(\rho AV) = 0 \tag{3.8}$$

Eq. 3.8 is the partial differential equation in conservation form of the continuity equation suitable for the time-marching solution of one-dimensional unsteady flow.

3.1.2 Momentum Equation

Newton's second law of motion, $\sum \mathbf{F} = D(m\mathbf{v})/Dt$, may be used to derive the momentum equation. This principle states that the time rate of change of momentum of a system is equal to the sum of all the forces ($\sum \mathbf{F}$) acting on the system by its surroundings. Let N_{SYS} be the momentum of the system ($m\mathbf{v}$) in Eq. 3.1, and let η be the momentum per unit mass ($\rho\mathbf{v}/\rho$). Thus for Eq. 3.1,

$$\Sigma \mathbf{F} = \frac{D(m\mathbf{v})}{Dt} = \frac{\partial}{\partial t}\int_{CV} \rho\, \mathbf{v}\, d\forall + \int_{CS} \rho\, \mathbf{v}\mathbf{v} \cdot d\mathbf{A} \tag{3.9}$$

The integral form of the momentum equation shows that the resultant force acting on a control volume is equal to the time rate of increase of momentum within the control volume plus the net efflux of momentum from the control volume across the control surfaces. There are two sources of the force for a moving fluid element. One comes from the body forces that act directly on the volumetric mass. Examples include gravitational, electric, and magnetic forces. The other sources are surface forces due to the pressure and viscous distributions acting on the surface.

To obtain a partial differential equation form of the x component of the momentum equation, the integrals in Eq. 3.9 are evaluated in the same manner as discussed above with regard to the continuity equation.

$$\frac{\partial}{\partial t}\int_{CV} \rho\, \mathbf{v}\, d\forall = \frac{\partial}{\partial t}(\rho V A dx) \tag{3.10}$$

$$\int_{CS} \rho\, \mathbf{v}\mathbf{v} \cdot d\mathbf{A} = -\rho A V^2 + (\rho + d\rho)(A + dA)(V + dV)^2 = d(\rho A V^2) \tag{3.11}$$

The evaluation of the resultant forces is carried out with the infinitesimal flow slice shown in Fig. 3.2 (pressure forces on the converging or diverging sides are neglected because those effects are negligible for general pipeline problems).

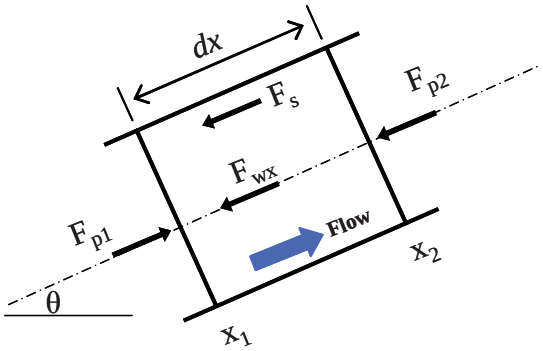

Figure 3.2 The Forces Acting on a Control Volume

Pressure forces at section 1 and 2,

$$F_p = -pA + (p + dp)(A + dA) = d(pA) \tag{3.12}$$

The gravitational force of the weight of the control volume along the pipe centerline is

$$F_{wx} = \rho g A dx \sin\theta \tag{3.13}$$

The shear force due to viscous distribution acting on the surface is

$$F_s = \tau \pi D dx \tag{3.14}$$

where p is the pressure, the subscripts refer to the corresponding sections, θ is the angle of the pipe from horizontal, τ is the shear stress between the fluid and pipe wall, and D is the internal diameter of the pipe. If we consider the downstream flow direction as positive,

$$\Sigma \mathbf{F} = -d(pA) - \rho g A dx \sin\theta - \tau \pi D dx \tag{3.15}$$

Substituting Eq. 3.10, Eq. 3.11, and Eq. 3.15 into Eq. 3.9 gives

$$\frac{\partial}{\partial t}(\rho A V dx) + d(\rho A V^2) + d(pA) + \rho g A dx \sin\theta + \tau \pi D dx = 0 \tag{3.16}$$

Dividing Eq. 3.16 by *dx*, taking the limit as *dx* goes to zero, and noting that $d/dx(\rho AV^2+pA)$ is the definition of the partial derivative with respect to *x* [Anderson, 1995],

$$\frac{\partial}{\partial t}(\rho AV)+\frac{\partial}{\partial x}(\rho AV^2+pA)+\rho gA\sin\theta+\tau\pi D=0 \tag{3.17}$$

Eq. 3.17 is the partial differential equation in conservation form for the momentum equation. If we assume that the energy losses by wall resistance during any flow condition are the same as in steady flow, the Darcy-Weisbach friction formula, $\tau=\rho fV|V|/8$, may be applied for the shear stress. Further details of energy dissipation by pipe wall resistance are discussed in Chapter 5 in relation to unsteady friction. Thus it follows

$$\frac{\partial}{\partial t}(\rho AV)+\frac{\partial}{\partial x}(\rho AV^2+pA)+\rho gA\sin\theta+\frac{\pi Df}{8}\rho V|V|=0 \tag{3.18}$$

where $V|V|$ automatically deals with reverse flows. f is the Darcy-Weisbach friction factor, and may be calculated using Hagen-Poiseuille equation for laminar flow and Colebrook equation for turbulent flow, which are the basis for Moody diagram [Streeter and Wylie, 1985]. Single explicit equations have been proposed with the same accuracy as the implicit Colebrook equation by Swamee and Jain [1976] and Chen [1979].

3.1.3 Energy Equation

For many dynamic fluid applications (especially gas), the assumption that a process has a constant temperature is often not valid. If the process is not an isothermal and heat transfer is considered, the conservation of energy must be included in the analysis. The energy principle states that the energy of a system remains constant with time. It is nothing more than the first law of thermodynamics. The laws of thermodynamics deal with interactions between a system and its surroundings as they respectively pass through equilibrium state. These interactions may be divided into two classes, work and heat interactions [Shapiro, 1953]. The first law states that the time rate of change of the total stored internal energy E_T of the system is the net time rate of energy addition by heat transfer Q_H in the system plus the net time rate of energy addition by work done W on the system due to body and surface forces depending only upon the initial and final states of the system. That is,

$$\frac{DE_T}{Dt} = \frac{\delta Q_H}{\delta t} + \frac{\delta W}{\delta t} \tag{3.19}$$

According to the laws of thermodynamics, for simple systems from the point of view of energy conservation, there are at most two (initial and final) independent state variables, on which the others depend algebraically [Wesseling, 2001]. The total energy in the left term of Eq. 3.19 is evaluated by two contributions, the internal energy (also called thermal energy) $\dot{e}$ due to random molecular motion and the kinetic energy due to translational motion of the fluid element. The kinetic energy per unit mass is simply $V^2/2$. It is important to realize the difference between heat and internal energy. Heat and work are forms of energy in transition depending on the process or path followed by the system in going from state 1 to state 2 (path function), which appear at the boundary of the system and are not contained within the matter. In contrast, the internal energy resides within the matter. It does not depend on the path (state function). Let N_{SYS} be the total energy of the system E_T in Eq. 3.1, and let η be the total energy per unit mass $e_t + V^2/2$. Thus,

$$\frac{\delta Q_H}{\delta t} + \frac{\delta W}{\delta t} = \frac{DE_T}{Dt} = \frac{\partial}{\partial t}\int_{CV}\left[\rho\left(e_t + \frac{V^2}{2}\right)d\forall\right] + \int_{CS}\left[\rho\left(e_t + \frac{V^2}{2}\right)\mathbf{v}\cdot d\mathbf{A}\right] \tag{3.20}$$

To obtain a partial differential equation form of the energy equation, Eq. 3.20 is applied to the shaded control volume shown in Fig. 3.1 and the infinitesimally small fluid element shown in Fig. 3.2 in the same manner as discussed above for both the continuity and momentum equations. That is,

$$\begin{aligned}&\frac{\partial}{\partial t}\left[\rho\left(e_t + \frac{V^2}{2}\right)A\,dx\right] + d\left[\rho\left(e_t + \frac{V^2}{2}\right)AV\right] \\ &\quad + d(pAV) + d(qA) + \rho g VA\,dx\sin\theta + \frac{\pi D f}{8}\rho V^3 dx = 0\end{aligned} \tag{3.21}$$

where q is the volumetric heat flux added externally per unit mass. Dividing Eq. 3.21 by dx and noting that d/dx is the definition of the partial derivative with respect to x [Anderson, 1995],

$$\frac{\partial}{\partial t}\left[\rho A\left(e_t+\frac{V^2}{2}\right)\right]+\frac{\partial}{\partial x}\left[\rho AV\left(e_t+\frac{V^2}{2}\right)\right] + \frac{\partial}{\partial x}(pAV)+\frac{\partial}{\partial x}(qA)+g\sin\theta\,\rho AV+\frac{\pi Df}{8}\rho V^3=0 \tag{3.22}$$

Eq. 3.22 is the partial differential equation in conservation form of the energy equation [Liggett, 1994]. This equation can consider heat transfer across the surface due to temperature gradients (thermal conduction) and the conversion of frictional work into thermal energy. Similar to the derivation for the momentum equation, the energy losses by wall friction may be calculated by the Darcy-Weisbach friction formula when the pipe wall shear stress during any flow condition is the same as in steady flow.

For the perfect gas law, the internal energy e_t depends temperature T only. Therefore, the specific heat at constant volume, C_v and the specific heat at constant pressure, C_p are constant by the relationship of the first law of thermodynamics. Eq. 3.22 can be rewritten by setting $e_t = C_vT = RT/(\gamma-1)$ that the details of derivation are given in Section 3.3. It may be more convenient to use temperature T instead of internal energy e_t.

$$\frac{\partial}{\partial t}\left[\rho A\left(\frac{R}{\gamma-1}T+\frac{V^2}{2}\right)\right]+\frac{\partial}{\partial x}\left[\rho AV\left(\frac{R}{\gamma-1}T+\frac{V^2}{2}\right)\right] + \frac{\partial}{\partial x}(pAV)+\frac{\partial}{\partial x}(qA)+g\sin\theta\,\rho AV+\frac{\pi Df}{8}\rho V^3=0 \tag{3.23}$$

where T is the absolute temperature, R is the gas constant, and γ is the ratio of the specific heat at constant pressure to the specific heat at constant volume.

3.2 FLUID COMPRESSIBILITY FOR LIQUIDS AND PIPE DEFORMABILITY

For most purposes, a liquid can be considered as a quasi-incompressible or slightly compressible fluid. However, the density of the fluid will change for fast and strong pressure disturbances in a confined flow inside a pipe. The changes of fluid density influence transients. The compressibility of a liquid is introduced with the definition of

bulk modulus of elasticity *K*. It is the ratio of the change in unit pressure to the corresponding density change per unit of volume, $K=dp/(d\rho/\rho)$. Thus, the equation of state for slightly compressible fluids may be expressed as

$$\frac{d\rho}{\rho} = \frac{dp}{K} \tag{3.24}$$

The deformation of pipe may be a function of the flow conditions as well as of the pipe wall characteristics. The pipe deformation can be neglected for moderate transient pressure variations in a gas distribution network. For pressurised liquid flow, however, pipe distensibility can be a vital part of the transient response of the pipe element. Pipe elastic characteristics depend on the wall material, cross section geometry, and structural constraints [Almeida and Koelle, 1992]. When the deformability of the wall is significant, an element spring-mass-dashpot model of the wall should suffice if secondary wall transmission is negligible. Most transient analysis models use the assumption of linear-elastic behaviour of pipe wall. Linear-elastic model is relatively accurate for describing hydraulic transients in metal or concrete pipes. However, rubber and plastic pipes in transients exhibit viscoelastic behaviour because these materials have a different rheological behaviour in comparison to metal and concrete pipes. Viscoelastic effect of pipes is discussed in Chapter 9. For a linear-elastic behaviour of pipe wall, the elasticity of the pipe wall and its rate of deformation are a function of pressure only [Wylie et al., 1993]. The equation of state for linear-elastic behaviour of pipe wall deformability is

$$\frac{dA}{A} = \frac{D}{eE}dp \tag{3.25}$$

where *e* is the pipe wall thickness and *E* is Young's modulus of elasticity for the pipe wall.

3.3 MATHEMATICAL MODELS FOR GAS TRANSIENTS

For transients in compressible fluid flows, it is no longer the interaction between the slight compressibility of a liquid and the elasticity of a pipe wall, but rather the compressibility of a gas that is the dominant physical process that needs to be modelled. The physical characteristics of a gas must obey the laws of thermodynamics. In addition, the heat generated by frictional processes should be considered.

The perfect gas is an idealized flow condition, and real gases will deviate from it to a greater or lesser degree. Deviations from the perfect gas theory are mainly due to two effects [Liepmann and Roshko, 1957]. At low temperatures and high pressures (nearly the critical pressure), the intermolecular forces become important. These are the so-called van der Waals forces, which account for the possibility of liquefying of a gas. At high temperatures (nearly the critical temperature) and low pressures, dissociation and ionization processes occur because these processes change the number of particles. Many equations of state have been proposed in the literature with either an empirical, semi-empirical or a theoretical basis for real gases and gases under the critical condition. Comprehensive reviews can be found in the works of Modisette [2000] and Wang [2003]. However it is reasonable to use the perfect gas law because temperature and pressure of most gas transmission and distribution pipelines do not reach the critical pressure and temperature. Transient models for compressible flow can have a number of alternative assumptions according to flow conditions including isothermal, adiabatic, isentropic, or specified heat transfer, to simplify analysis models based on the perfect gas law.

3.3.1 Perfect Gas Law

Thermodynamic relations and compressible fluid flow cases have been limited generally to perfect gases with constant specific heat because, at ordinary temperatures and pressures, most gases tend to obey the perfect gas law [Streeter and Wylie, 1985]. A perfect gas is defined as a substance that satisfies the perfect gas law. The equation of state for a perfect gas is a relation between the pressure, density and temperature of a gas.

$$p = \rho RT \tag{3.26}$$

For single component systems, the specific heats at constant volume and constant pressure respectively are defined as

$$C_v = \left(\frac{\partial e_t}{\partial T}\right)_v \qquad C_p = \left(\frac{\partial h}{\partial T}\right)_p \tag{3.27}$$

where h is the enthalpy per unit mass given by $h = e_t + p/\rho$.

The specific heat ratio γ of a gas is defined as

$$\gamma = C_p \Big/ C_v \tag{3.28}$$

The ratio of specific heats plays an important role in an isentropic process. Since the internal energy and enthalpy is a function only of temperature for a perfect gas, Eq. 3.27 becomes

$$e_t = C_v T \qquad h = C_p T \tag{3.29}$$

Substituting Eq. 3.29 into $h = e_t + p/\rho = e_t + RT$

$$C_p = C_v + R \tag{3.30}$$

Combining Eq. 3.29 with Eq. 3.28 and 3.30 gives

$$e_t = \frac{1}{\gamma - 1} RT \qquad h = \frac{\gamma}{\gamma - 1} RT \tag{3.31}$$

3.3.2 Specified Gas Transient Flows

If the pipeline system being analysed maintains thermal equilibrium between the pipeline system and its surroundings, the fluid flow can be regarded as isothermal flow. This flow relates to slow dynamic changes. For the case of slow transients in a pipeline caused by fluctuations in demand, heat generated by the flow (positive or negative) has sufficient time to reach thermal equilibrium with its constant temperature surroundings. Changes of temperature within the gas due to heat conduction are sufficiently slow to be neglected. This flow condition can be modelled in the form of Eq. 3.32 known as the universal gas law with the constant gas compressibility z which is a function of pressure and temperature.

$$p = z\rho RT \tag{3.32}$$

If the process takes place without the additional heat exchange from its surroundings, it is called adiabatic process. The process is called isentropic if it is frictionless and reversible adiabatic. When rapid transients are under consideration, the pressure changes are assumed instantaneous. It allows no time for heat transfer to take place between the fluid in the pipe and the surroundings. Adiabatic and isentropic flow usually relates to fast dynamic changes in the fluid. However, heat conduction effects by wall resistance or pressure variation cannot be neglected for any process [Osiadacz and Chaczykowski, 2001]. An isentropic process obeys the following relation. Heat conduction of the system is calculated by only an exponent of specific heat ratio.

$$p = \rho^{\gamma} RT \quad or \quad \frac{p_1}{\rho_1^{\gamma}} = \frac{p_2}{\rho_2^{\gamma}} \tag{3.33}$$

Finally, the relation between pressure and density in a polytropic process is given by

$$\frac{p}{\rho^n} = constant \tag{3.34}$$

where n is the polytropic process exponent. This process approximates actual processes to consider heat conduction by wall resistance or pressure variation and heat transfer between the fluid in the pipe and the surroundings when the process is reversible. In this situation, heat transfer occurs except when the process is the isentropic case ($n=\gamma$) [Streeter and Wylie, 1985]. In Eq. 3.34, the total heat exchange of the system is considered by only a polytropic process exponent.

3.4 VELOCITY OF WAVE PROPAGATION (WAVESPEED)

It is assumed that surface forces, body forces, inertia effects, column separation and reflected wave interferences are neglected. Then, the Allievi expression (generally attributed to Joukowsky) shows the calculation of the magnitude of transient caused by complete instantaneous valve closure at the end of a simple pipeline [Fox, 1977].

$$\Delta p = \pm \rho a \Delta V \tag{3.35}$$

Eq. 3.35 relates the change in velocity to the resulting change in pressure. The transient pressure rise is directly proportional to the wavespeed *a*. Therefore, it must be accurately evaluated for each system. The wavespeed in pressurised flows depends on the characteristics of the fluid, the characteristics of the pipe wall material, and the pipe geometry and restraints. Also, the dynamic behaviour of the pipe wall can influence the wavespeed and transient response.

For pipes with non-linear and non-elastic rheologic (viscoelastic) behaviour, for example, plastic and rubber pipes, the pipe deformability factor should be characterized for each particular influence of the pipe behaviour on the wavespeed because the wavespeed is a function of the unsteady pressure. Chapter 9 shows numerical and experimental results of the pipe distensibility of polyethylene pipe with mechanical viscoelastic models.

Eq. 3.36 is valid for linear-elastic pipes of slightly compressible flow.

$$a = \sqrt{\frac{K/\rho}{1+(K/E)(D/e)\psi}} \tag{3.36}$$

where ψ is the parameter for the pipe geometry and restraints that depends on Poisson's ratio μ. ψ is investigated for a thin-walled elastic pipe (D/e > 25) [Almeida and Koelle, 1992] and thick-walled elastic pipe (D/e < 25) [Wylie et al., 1993] with three different longitudinal support situations.

Table 3.1 ψ Values for Pipe Support Condition

Pipe Restraint Condition	ψ for Thin-wall	ψ for Thick-wall
Anchored at Upstream End Only	$1-\mu/2$	$\frac{2e}{D}(1+\mu)+\frac{D}{D+e}(1-\frac{\mu}{2})$
Anchored against Axial Movement	$1-\mu^2$	$\frac{2e}{D}(1+\mu)+\frac{D}{D+e}(1-\mu^2)$
Expansion Joints	1	$\frac{2e}{D}(1+\mu)+\frac{D}{D+e}$

Even a very small amount of entrained gas in the liquid pipeline may greatly alter the wavespeed. The effect of entrapped air pockets on transients in water pipelines is discussed in Chapter 7. Experimental results are also presented.

The wavespeed for a compressible fluid is given by

$$a^2 = \left(\frac{\partial p}{\partial \rho} \right)_s \tag{3.37}$$

where the subscript *s* presents the constant entropy. Since the disturbances of pressure and temperature produced by passage of a sound wave are extremely small, each fluid particle undergoes an almost reversible process. Also, fluid particles have no time to lose or gain heat because the process of passage of the wave is so fast with negligible temperature variations [Shapiro, 1953; Liepmann and Roshko, 1957]. Thus, the process is nearly adiabatic. Accordingly, the total process of the wavespeed for compressible flows can be considered a reversible adiabatic (isentropic) process in the perfect gas law.

$$a^2 = \gamma \frac{p}{\rho} = \gamma RT \tag{3.38}$$

The wavespeed of gas pipeline systems generally changes from section to section because friction effects and density variation change the temperature. In the case of isothermal flow, the wavespeed always remains constant. The wavespeed is a significant measure of the effects of compressibility when it is compared to the speed of the flow (Mach number).

3.5 HEAT TRANSFER THROUGH THE PIPE WALL

The fourth term of the left hand side in Eq. 3.22 represents heat transfer from the fluid to the pipe wall, through the pipe wall, and to the external environment. The term *q* is the rate of heat transfer per unit area of pipe wall. In pipeline systems, *q* may be calculated on a quasi-steady heat flow basis. This approach assumes that at any instant the steady flow of heat through the pipe wall is proportional to the temperature difference [Fox, 1989 and Lienhard IV and Lienhard V, 2004]. This ignores the heat required to raise (or lower) the temperature of the pipe wall material itself. More accurate methods of dealing with

unsteady heat flows are available using non-quasi-steady heat flow equations based on the heat diffusion equation and penetration depths. Fig. 3.3 shows the quasi-steady temperature distributions across the pipe wall.

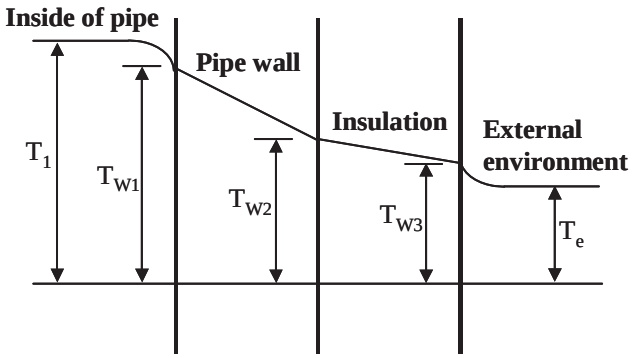

Figure 3.3 Temperature Distributions across the Pipe Wall

The heat transfer, through unit area per unit time, is represented by q, and is related to the temperature field by an expression analogous to the Newtonian friction law [Liepmann and Roshko, 1957],

$$q = k\Delta T \tag{3.39}$$

where k is the heat transfer coefficient (coefficient of thermal conductivity) and ΔT is the temperature difference. In steady state heat flow

$$q = k_c (T_1 - T_e) \tag{3.40}$$

where k_c is the compound coefficient of heat transfer. It is composed of the coefficient of heat transfer from the fluid to the wall, through the wall, through the insulation, from the insulation to the external environment. Therefore the heat transfer for pipe flow can be represented by the following equation [Wylie et al., 1993].

$$\frac{\partial}{\partial x}(qA) = k_c \pi D (T_1 - T_e) \tag{3.41}$$

3.6 SOLUTION BY THE METHOD OF CHARACTERISTICS

The most commonly used technique for solving hydraulic transient problems (especially, if the wavespeed of a system is constant) in closed conduits is the method of characteristics (MOC). It is numerically simple due to the explicit formulation and fast computational time. This method transforms the partial differential equations into ordinary differential equations that apply along specific lines called characteristic lines in the space-time plane. The simplified compatibility equations are then solved along these characteristic lines.

3.6.1 Simplified Governing Equations

For liquids, the pipe pressure transient analysis can be modelled by these simplified basic equations, also known as waterhammer equations with a number of assumptions [Chaudhry, 1987; Wylie et al., 1993; Thorley, 2004].

$$\frac{\partial H}{\partial t}+\frac{a^2}{gA}\frac{\partial Q}{\partial x}=0 \tag{3.42}$$

$$\frac{\partial Q}{\partial t}+gA\frac{\partial H}{\partial x}+\frac{f\,Q|Q|}{2DA^2}=0 \tag{3.43}$$

where H is the piezometric head and Q is the flow discharge. These equations neglect the variation of density ρ and flow area A due to variation of the pressure on the assumption that the fluid is slightly compressible, and the pipe wall has only slight linear-elastic deformation. However, the small variations of ρ and A are indirectly taken into account by the wavespeed in Eq. 3.36.

3.6.2 Characteristic Equations

Eq. 3.42 and 3.43 is a first order quasi-linear hyperbolic system of partial differential equations. The MOC transforms these equations into a pair of ordinary differential equations (Eq. 3.44 and 3.45) along characteristic lines C^+ and C^- on the *x*-*t* plane shown in Fig. 3.4 [Wylie et al., 1993; Chaudhry, 1987; Almeida and Koelle, 1992].

$$C^+ : \quad \frac{dQ}{dt} + \frac{gA}{a}\frac{dH}{dt} + \frac{f\,Q|Q|}{2DA} = 0 \qquad along \quad \frac{dx}{dt} = +a \tag{3.44}$$

$$C^- : \quad \frac{dQ}{dt} - \frac{gA}{a}\frac{dH}{dt} + \frac{f\,Q|Q|}{2DA} = 0 \qquad along \quad \frac{dx}{dt} = -a \tag{3.45}$$

These equations are referred to as compatibility equations. With a constant wavespeed and neglecting the convective terms from the basic equations, they are valid only along the straight lines shown in Fig. 3.4.

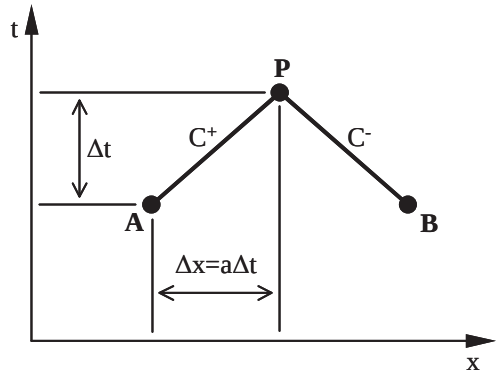

Figure 3.4 Characteristic Lines in x-t Plane

3.6.3 Stability and Accuracy

Both MOC and FDM are usually solved on a fixed grid in the time-space plane. The partial and ordinary derivatives are approximated by the characteristics of each approach on the fixed grid. The discretisation error is introduced through the approximation of partial and ordinary derivatives. The computational error is amplified or remains the same during a computation. The numerical scheme is said to be stable if the amplification of error remains bounded for all sections with time, and unstable if the error grows as time and solution progresses. Therefore, it is important to know the stability condition. If the scheme does not require any condition for stability, it is said to be unconditionally stable.

Although methods for determining the stability criteria for nonlinear equations are not available, the *Courant-Friedrichs-Lewy* (CFL) stability condition shows the stability condition of the finite difference scheme by neglecting the nonlinear terms of governing equations [Chaudhry, 1987].

$$\Delta x \geq a\Delta t \tag{3.46}$$

where Δt and Δx are the computational time and space step respectively. The Courant number C_N is defined as the ratio of the actual wavespeed a and the numerical wavespeed $\Delta x/\Delta t$. It is useful for the characteristic grid generation of MOC.

$$C_N = \frac{a}{\Delta x / \Delta t} = \frac{a\Delta t}{\Delta x} \tag{3.47}$$

3.6.4 Disadvantages of MOC

If the Courant number for stability criteria is equal to unity, the method of characteristics is quite straightforward, precise, and computationally efficient when analysing a single pipeline with constant celerity of wave propagation because of the possibility of dividing the pipeline into an integer number of equal reaches. However, MOC based techniques are frequently criticized for their shortcomings in practical implementation involving multiple and complex pipe systems or systems with variable wavespeeds.

In MOC, the time step for computational discretisation is limited by stability criteria based on the Courant number that restricts the relationship between time and space step for the whole computational domain. This limitation requires a specified time interval that is usually small for the accuracy of computation, and becomes problematic when it is applied to multiple pipe systems and single pipe systems with different wavespeeds, with varying pipe diameters and material properties, heat exchange flow, or multi-phase flows.

The MOC usually uses the initial wavespeed of a system for the whole computational domain, and it is an important factor for deciding the stability condition of solution. When the wavespeed is variable, the stability of solution using the initial wavespeed becomes unstable because the Courant number can change with location and time. If C_N is not equal to unity, MOC requires spatial and temporal interpolations, an adjusted wavespeed, or geometric adjustments that introduce important attenuation and dispersion errors into the solution.

The stability condition in Eq. 3.47 was derived by completely neglecting the non-linear friction term. If the friction effect is important due to a large friction factor, relatively long pipelines, large change in discharge, and/or small pipe diameters, then the solution of MOC may become unstable [Chaudhry, 1987]. The friction effect of fast transient events may be larger than that of steady state flows. There is additional energy dissipation by unsteady fluid behaviour during transients. Unsteady friction effects in pipeline systems will be discussed in Chapter 5 with numerical and experimental verification.

Another major difficulty of MOC based models is the extension to treat compressible transient flow. These models usually neglect the convective acceleration terms in the basic equations to achieve the required reduced form as two hyperbolic partial differential equations with constant coefficients. Although the numerical simplification can apply to system with low-Mach-numbers and slight compressibility, it may result in loss of accuracy of the simulation results when analysing compressible flow with high-Mach-numbers and high compressibility (high speed flows). The MOC of the complete set of governing equations may be used for modelling gas flows. However, the compatibility equations and grid generation are extremely complex.

3.7 DEVELOPMENT OF NEW TRANSIENT MODEL USING CONSERVATIVE SOLUTION SCHEME

To overcome the limitations of MOC based transient analysis models and to improve the sensitivity and applicability of transient analysis, a more robust high-resolution scheme to analyse hydraulic transients in both liquid and gas pipelines based on a conservative solution scheme (CSS) has been developed in this research. The conservation form of the governing equations has been used to formulate the problem of unsteady flow in pipeline systems. The basic equations, derived from the conservation of mass, momentum, and energy, an equation of state for the fluid density, and an equation of state for the pipe area, include all terms. With the above derivation of the governing equations in mind, the equations below are used for liquid and gas transient models.

Continuity Equation

$$\frac{\partial}{\partial t}(\rho A)+\frac{\partial}{\partial x}(\rho AV)=0 \qquad (3.8)\ \text{repeated}$$

Momentum Equation

$$\frac{\partial}{\partial t}(\rho AV)+\frac{\partial}{\partial x}(\rho AV^2+pA)+\rho gA\sin\theta+\frac{\pi Df}{8}\rho V|V|=0 \qquad (3.18)\ \text{repeated}$$

Energy Equation for a Generalized Gas Transient Model

$$\frac{\partial}{\partial t}\left[\rho A\left(\frac{R}{\gamma-1}T+\frac{V^2}{2}\right)\right]+\frac{\partial}{\partial x}\left[\rho AV\left(\frac{R}{\gamma-1}T+\frac{V^2}{2}\right)\right] + \frac{\partial}{\partial x}(pAV)+\frac{\partial}{\partial x}(qA)+g\sin\theta\,\rho AV+\frac{\pi Df}{8}\rho V^3=0 \qquad (3.23)\ \text{repeated}$$

where

$$\frac{\partial}{\partial x}(qA)=k_c\,\pi D(T_1-T_e) \qquad (3.41)\ \text{repeated}$$

The Equation of Area State for a Linear-Elastic Model

$$\frac{dA}{A}=\frac{D}{eE}dp \qquad (3.25)\ \text{repeated}$$

The Equation of State for a Liquid

$$\frac{d\rho}{\rho}=\frac{dp}{K} \qquad (3.24)\ \text{repeated}$$

The Equation of State for an Isothermal Gas Flow

$$p=z\rho RT \qquad (3.32)\ \text{repeated}$$

The Equation of State for a Polytropic gas flow

$$\frac{p}{\rho^n}=constant \qquad (3.34)\ \text{repeated}$$

The governing equations (continuity, momentum and energy equations) have the same generic form, given by

$$\frac{\partial \mathbf{u}}{\partial t} + \frac{\partial \mathbf{f}}{\partial x} + \mathbf{g} = 0 \tag{3.48}$$

Eq. 3.48 represents the entire system of governing equations in conservation form, when **u**, **f**, and **g** are interpreted as column vectors, given by

$$\mathbf{u} = \begin{Bmatrix} \rho A \\ \rho A V \\ \rho A\left(\frac{R}{\gamma - 1}T + \frac{V^2}{2}\right) \end{Bmatrix} \tag{3.49}$$

$$\mathbf{f} = \begin{Bmatrix} \rho A V \\ \rho A V^2 + pA \\ \rho A V\left(\frac{R}{\gamma - 1}T + \frac{V^2}{2}\right) + pAV + qA \end{Bmatrix} \tag{3.50}$$

$$\mathbf{g} = \begin{Bmatrix} 0 \\ \rho g A \sin\theta + \frac{\pi D f}{8}\rho V|V| \\ g\sin\theta\, \rho A V + \frac{\pi D f}{8}\rho V^3 \end{Bmatrix} \tag{3.51}$$

The column vectors **f** and **g** are called flux terms and source terms respectively. The **u** is called the solution vector because the dependent variables in *u* are usually obtained numerically in a time-marching solution. The system of equations is completed by adding the equations of state.

3.7.1 Developed Liquid and Gas Transient Models

The basic equations for liquid transients are composed of Eq. 3.8, 3.18, 3.25, and 3.24 when the effect of heat exchange is negligible. The dependent variables are pressure, fluid density, pipe cross sectional area, and flow velocity. The gas transient model developed in

this research can analyse three different specified gas processes during unsteady pipe flows, namely, isothermal, polytropic, and generalized gas process.

The isothermal process gas transient model does not consider the effect of heat exchange because the pipeline system is regarded to be in thermal equilibrium. The basic equations for analysing flows are made up of Eq. 3.8, 3.18, 3.25, and 3.32. However, a significant amount of heat exchange may take place due to heat transfer between the pipeline system and the external environment and frictional work during transient events. The polytropic process gas transient analysis model can consider the heat exchange by using a polytropic process exponent. This model does not use the energy equation. The effect of total and approximated heat exchange of a whole system is considered by only a polytropic process exponent in Eq. 3.34. The basic equations for this model are composed of Eq. 3.8, 3.18, 3.25, and 3.34.

The final model for gas transient analysis, named as generalized gas transient analysis model, can directly calculate temperature variation during a transient event at every computational node by using the energy equation. This model can simulate one-dimensional gas transient problems including heat transfer and the conversion of frictional work into thermal energy. The basic equations consist of Eq. 3.8, 3.18, 3.23, and 3.25 with the perfect gas law, Eq. 3.26. There are five unknown variables, pressure p, density ρ, area A, velocity V, and temperature T.

These systems of equations are solved by an implicit finite difference method (FDM) using the Preissmann scheme [Samuels and Skeels, 1990; Chaudhry, 1993]. The conservative solution scheme solves four (pressure, fluid density, pipe cross sectional area, and flow velocity) or five dependent variables including temperature rather than two in the standard MOC approach (pressure and velocity). The implicit solution algorithm based on a Newton-Raphson iterative procedure is used to solve the system of non-linear governing equations. The sparse matrix of the systems of equations is handled by the efficient banded diagonal matrix algorithms [Press et al., 1997]. All transient analysis models are coded by Fortran language in this research.

3.7.2 Characteristics of the Conservative Solution Scheme

For solutions based on the MOC, the wavespeed is an important factor for determining the criteria of accuracy and stability. The time step for computational discretisation is restricted by the specified relationship between time and space over the complete computational domain. In addition, the initial wavespeed of system determines the computational time of the whole domain. The requirement of this strict relationship becomes a serious limitation of MOC, when it is applied to the systems with variable wavespeeds, non-isothermal or non-adiabatic gas flow, slow transients, and complex network systems.

The conservative solution scheme proposed in this research is more flexible for the grid generation of computational discretisation by the implicit FDM. The scheme allows for the use of varying grid steps along a pipeline. In principle, the scheme is unconditionally stable and has no adjustment of the wavespeed. The conservative solution scheme directly calculates the fluid density and pipe wall distensibility at every computational time step. Thus, the wavespeed is updated at every step. This procedure has big advantages for analysing the systems with variable wavespeeds, such as systems with entrapped air pockets and viscoelastic behaviour of a pipe material. These systems are discussed in the Chapters 7 and 9 with laboratory test results.

The problematic convective acceleration terms in the momentum equation, which are often neglected in other methods, are retained when using a conservative solution scheme. These terms have a significant impact on the accuracy in the case of high speed flows. Another advantage of this scheme is the flexibility in dealing with a large variety of non-pipe elements and unsteady friction models because the governing equations in conservation form and subsidiary equations for specified condition can all be expressed by the same generic equations. Also, the scheme can simulate transient flows of various fluids, such as gas and oil, by slightly modifying the basic structure of solution.

The conservative solution scheme is slower than explicit MOC methods because the entire system must be solved for each iteration. However, the scheme has an advantage of its average speed over a range of problems including both fast and slow transients, and its stability and accuracy. The addition of area and temperature variables makes it possible to

analyse heat exchange flow and elastic or viscoelastic effect of pipe wall material. Numerical and laboratory experiments of both gas and water have been carried out for the verification of the proposed conservative solution scheme.

3.7.3 Numerical Scheme

The Preissmann (weighted four-point or box) implicit finite difference method (FDM) is used for solving the non-linear hyperbolic partial differential equations (PDE) described above without neglecting any term. In this scheme, time and space derivatives are approximated by weighted means in a computational grid of the time and space domains as follows [Abbott and Basco, 1989; Liggett and Cunge, 1975; Venutelli, 2002] and the computational grid is shown in Fig. 3.5.

$$\frac{\partial \mathbf{u}}{\partial t} \cong \beta \frac{(\mathbf{u}_{i+1}^{k+1} - \mathbf{u}_{i+1}^{k})}{\Delta t} + (1-\beta)\frac{(\mathbf{u}_{i}^{k+1} - \mathbf{u}_{i}^{k})}{\Delta t} \tag{3.52}$$

$$\frac{\partial \mathbf{f}}{\partial x} \cong \alpha \frac{(\mathbf{f}_{i+1}^{k+1} - \mathbf{f}_{i}^{k+1})}{\Delta x} + (1-\alpha)\frac{(\mathbf{f}_{i+1}^{k} - \mathbf{f}_{i}^{k})}{\Delta x} \tag{3.53}$$

$$\mathbf{g} \cong \alpha\left[\beta \mathbf{g}_{i+1}^{k+1} + (1-\beta)\mathbf{g}_{i}^{k+1}\right] + (1-\alpha)\left[\beta \mathbf{g}_{i+1}^{k} + (1-\beta)\mathbf{g}_{i}^{k}\right] \tag{3.54}$$

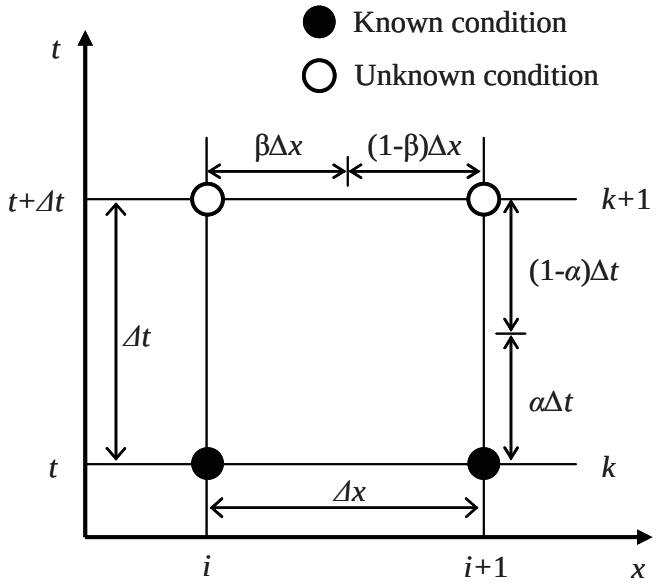

Figure 3.5 Computational Grid

where k and i refer to the time and space level respectively. α and β are the time and space step weighting coefficients respectively ranging 0 to 1 to balance accuracy and stability. The computation of the unknown quantities at all nodes on the end of time step (k+1 time level shown in Fig. 3.5) is done simultaneously subject to the relevant boundary conditions [IAHR report, 2000]. When $\alpha=\beta=1/2$, this scheme is a perfectly centred scheme (central difference approximation) and the truncation errors are second-order accuracy (Δt^2 and Δx^2). According to the linear stability analysis and truncation error analysis of the Preissmann algorithm [Abbott and Basco, 1989], all terms associated with numerical diffusion and truncation error terms disappear for the special case of $\alpha=\beta=1/2$ and Courant number=1. In this case, the numerical solution coincides with the analytical one (exact solution) and the weighted four-point scheme is stable and nondissipative. When putting more weight on the upper time level ($\beta=1/2$ and $\alpha>1/2$), the scheme introduces numerical dissipation (stable and dissipative). The truncation errors and numerical diffusion are presented.

The time derivatives are normally computed with $\beta=1/2$ as in Preissmann's original scheme [Chaudhry, 1993; IAHR report, 2000], although other weighting coefficients may be advantageous when unequal distance steps are used [Abbott and Basco, 1989]. Also, Evans [1977] emphasizes the importance of the time-weighting coefficient for stability and dissipation. Therefore, this research uses the fixed value of $\beta=1/2$ that gives an average time derivative at space address i+1/2 because equal space step is usually used for pipeline analysis. In this case, when $\alpha=0$, the scheme becomes fully explicit and gives the largest numerical damping, and when $\alpha=1$, the scheme becomes fully implicit and first-order accurate in time. If $\alpha=0.5$, the time integration is equivalent to that of the second-order Crank-Nicholson method. The method becomes unstable when $\alpha < 0.5$, and $0.5 < \alpha \leq 0.6$ offers a good result between accuracy and stability [Greyvenstein, 2002] and steep wave fronts are properly simulated for low values of α [Chaudhry, 1993]. Applying Eq. 3.52 to 3.54 to the basic equations, the finite difference forms of these equations are given below.

Finite Difference Approximation of Continuity Equation (Eq. 3.8)

$$\frac{1}{2\Delta t}\left[\left((\rho A)_{i+1}^{k+1}+(\rho A)_{i}^{k+1}\right)-\left((\rho A)_{i+1}^{k}+(\rho A)_{i}^{k}\right)\right]$$
$$+\frac{\alpha}{\Delta x}\left((\rho AV)_{i+1}^{k+1}-(\rho AV)_{i}^{k+1}\right)+\frac{(1-\alpha)}{\Delta x}\left((\rho AV)_{i+1}^{k}-(\rho AV)_{i}^{k}\right)=0 \qquad (3.55)$$

Finite Difference Approximation of Momentum Equation (Eq. 3.18)

$$\begin{aligned}
&\frac{1}{2\Delta t}\left[\left((\rho AV)_{i+1}^{k+1}+(\rho AV)_{i}^{k+1}\right)-\left((\rho AV)_{i+1}^{k}+(\rho AV)_{i}^{k}\right)\right]\\
&+\frac{\alpha}{\Delta x}\left((\rho AV^2)_{i+1}^{k+1}-(\rho AV^2)_{i}^{k+1}\right)+\frac{(1-\alpha)}{\Delta x}\left((\rho AV^2)_{i+1}^{k}-(\rho AV^2)_{i}^{k}\right)\\
&+\frac{\alpha}{\Delta x}\left((pA)_{i+1}^{k+1}-(pA)_{i}^{k+1}\right)+\frac{(1-\alpha)}{\Delta x}\left((pA)_{i+1}^{k}-(pA)_{i}^{k}\right)\\
&+g\sin\theta\left[\frac{\alpha}{2}\left((\rho A)_{i+1}^{k+1}+(\rho A)_{i}^{k+1}\right)+\frac{(1-\alpha)}{2}\left((\rho A)_{i+1}^{k}+(\rho A)_{i}^{k}\right)\right]\\
&+\frac{\pi Df}{8}\left[\frac{\alpha}{2}\left((\rho V|V|)_{i+1}^{k+1}+(\rho V|V|)_{i}^{k+1}\right)+\frac{(1-\alpha)}{2}\left((\rho V|V|)_{i+1}^{k}+(\rho V|V|)_{i}^{k}\right)\right]=0
\end{aligned}\tag{3.56}$$

Finite Difference Approximation of Energy Equation (Eq. 3.23)

$$\begin{aligned}
&\frac{1}{2\Delta t}\left[\begin{array}{l}\left(\left(\rho A\left(\frac{R}{\gamma-1}T+\frac{V^2}{2}\right)\right)_{i+1}^{k+1}+\left(\rho A\left(\frac{R}{\gamma-1}T+\frac{V^2}{2}\right)\right)_{i}^{k+1}\right)\\ -\left(\left(\rho A\left(\frac{R}{\gamma-1}T+\frac{V^2}{2}\right)\right)_{i+1}^{k}+\left(\rho A\left(\frac{R}{\gamma-1}T+\frac{V^2}{2}\right)\right)_{i}^{k}\right)\end{array}\right]\\
&+\frac{\alpha}{\Delta x}\left(\left(\rho AV\left(\frac{R}{\gamma-1}T+\frac{V^2}{2}\right)\right)_{i+1}^{k+1}-\left(\rho AV\left(\frac{R}{\gamma-1}T+\frac{V^2}{2}\right)\right)_{i}^{k+1}\right)\\
&+\frac{(1-\alpha)}{\Delta x}\left(\left(\rho AV\left(\frac{R}{\gamma-1}T+\frac{V^2}{2}\right)\right)_{i+1}^{k}-\left(\rho AV\left(\frac{R}{\gamma-1}T+\frac{V^2}{2}\right)\right)_{i}^{k}\right)\\
&+\frac{\alpha}{\Delta x}\left((pAV)_{i+1}^{k+1}-(pAV)_{i}^{k+1}\right)+\frac{(1-\alpha)}{\Delta x}\left((pAV)_{i+1}^{k}-(pAV)_{i}^{k}\right)\\
&+\frac{\alpha}{\Delta x}\left((qA)_{i+1}^{k+1}-(qA)_{i}^{k+1}\right)+\frac{(1-\alpha)}{\Delta x}\left((qA)_{i+1}^{k}-(qA)_{i}^{k}\right)\\
&+g\sin\theta\left[\frac{\alpha}{2}\left((\rho AV)_{i+1}^{k+1}+(\rho AV)_{i}^{k+1}\right)+\frac{(1-\alpha)}{2}\left((\rho AV)_{i+1}^{k}+(\rho AV)_{i}^{k}\right)\right]\\
&+\frac{\pi Df}{8}\left[\frac{\alpha}{2}\left((\rho V^3)_{i+1}^{k+1}+(\rho V^3)_{i}^{k+1}\right)+\frac{(1-\alpha)}{2}\left((\rho V^3)_{i+1}^{k}+(\rho V^3)_{i}^{k}\right)\right]=0
\end{aligned}\tag{3.57}$$

The equations of area and density state can be written in finite difference form by integrating over the time step. They are shown below in their homogeneous form.

The Equation of Area State for a Linear-Elastic Model (Eq. 3.25)

$$\ln A_i^{k+1} - \ln A_i^k - \frac{D}{eE}\left(p_i^{k+1} - p_i^k\right) = 0 \tag{3.58}$$

The Equation of State for a Liquid (Eq. 3.24)

$$\ln \rho_i^{k+1} - \ln \rho_i^k - \frac{1}{K}\left(p_i^{k+1} - p_i^k\right) = 0 \tag{3.59}$$

The Equation of State for a Polytropic gas flow (Eq. 3.34)

$$\frac{p_i^{k+1}}{\left(\rho_i^{k+1}\right)^n} - \frac{p_i^k}{\left(\rho_i^k\right)^n} = 0 \tag{3.60}$$

3.7.4 Method of Solution

Numerical experiments have been undertaken for the verification of the transient analysis models based on the conservative solution scheme (CSS) that have been developed in this research. The single pipeline system shown in Fig. 3.6 has been used.

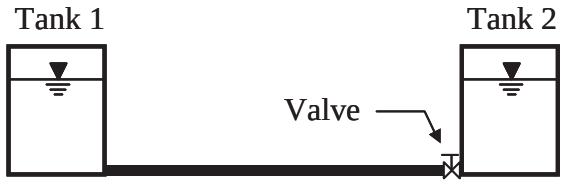

Figure 3.6 Single Pipeline System for Numerical Experiments

A computational grid is constructed by dividing the pipeline into n reaches of equal length Δx, resulting in a total of n+1 computational nodes. Because every node at the unknown time level contains four variables (pressure, density, area, and velocity; neglecting temperature variable), for n+1 nodes there are a total of 4(n+1) unknowns. Consequently 4(n+1) equations are required to solve the conditions at the unknown time level. Equations of continuity, momentum, and energy are applied over reaches, while equations of state are applied at individual nodes. Hence for n reaches there will be n equations of continuity, n equations of momentum, n+1 equations of area state, and n+1 equations of density state.

These account for $4n+2$ equations. Two remaining equations necessary to solve the system come from the known conditions at the two system boundaries. These boundary conditions may be a known pressure at a reservoir and a known velocity across a valve.

For a known reservoir pressure, the equation is written as

$$p_i^{k+1} - p_{reservoir}^0 = 0 \tag{3.61}$$

For a closed valve, the equation is written as

$$V_i^{k+1} = 0 \tag{3.62}$$

Unlike general explicit schemes, implicit schemes directly include the equations describing the boundary condition into the system of equations. Therefore, implicit schemes do not have to use the characteristic equations or the reflection procedures for boundary conditions. The numerical solutions to the equations of transient flows rely on knowing the system conditions at the previous time step. Thus, before the marching solution process can begin, it is necessary to define the starting conditions in the system at every computational node. These conditions may be determined directly from a steady state solution that solves the initial boundary conditions. Transient flow is imposed onto the system by suddenly altering its boundary conditions from those at steady state.

The set of $4(n+1)$ non-linear equations can be solved using the iterative Newton-Raphson method. This technique linearises each set of non-linear equations into a Jacobian matrix and a vector of residuals. In order to formulate the Jacobian matrix, it is necessary to define the partial derivative of each equation in its homogenous form (Eqs. 3.55 to 3.62) with respect to the unknown variables at the $k+1$ time level. Most of the entries in the Jacobian matrix will be equal to zero, except where the unknown variable appears within the equation. At each iteration, the resulting system of linearised equations is solved using standard linear matrix solving techniques to yield a correction vector which is added to the vector of unknowns [Vaculik et al., 2002]. Iteration is continued until the accuracy of the solution converges to a user-specified tolerance. This solution process is highly intensive on computational effort, especially when the pipeline is divided into a large number of reaches. Therefore, the sparse matrix of the systems of equations is handled by the efficient banded diagonal matrix algorithms [Press et al., 1997]. All transient analysis

models are coded by Fortran language in this research. Fig. 3.7 shows the flowchart of conservative solution scheme.

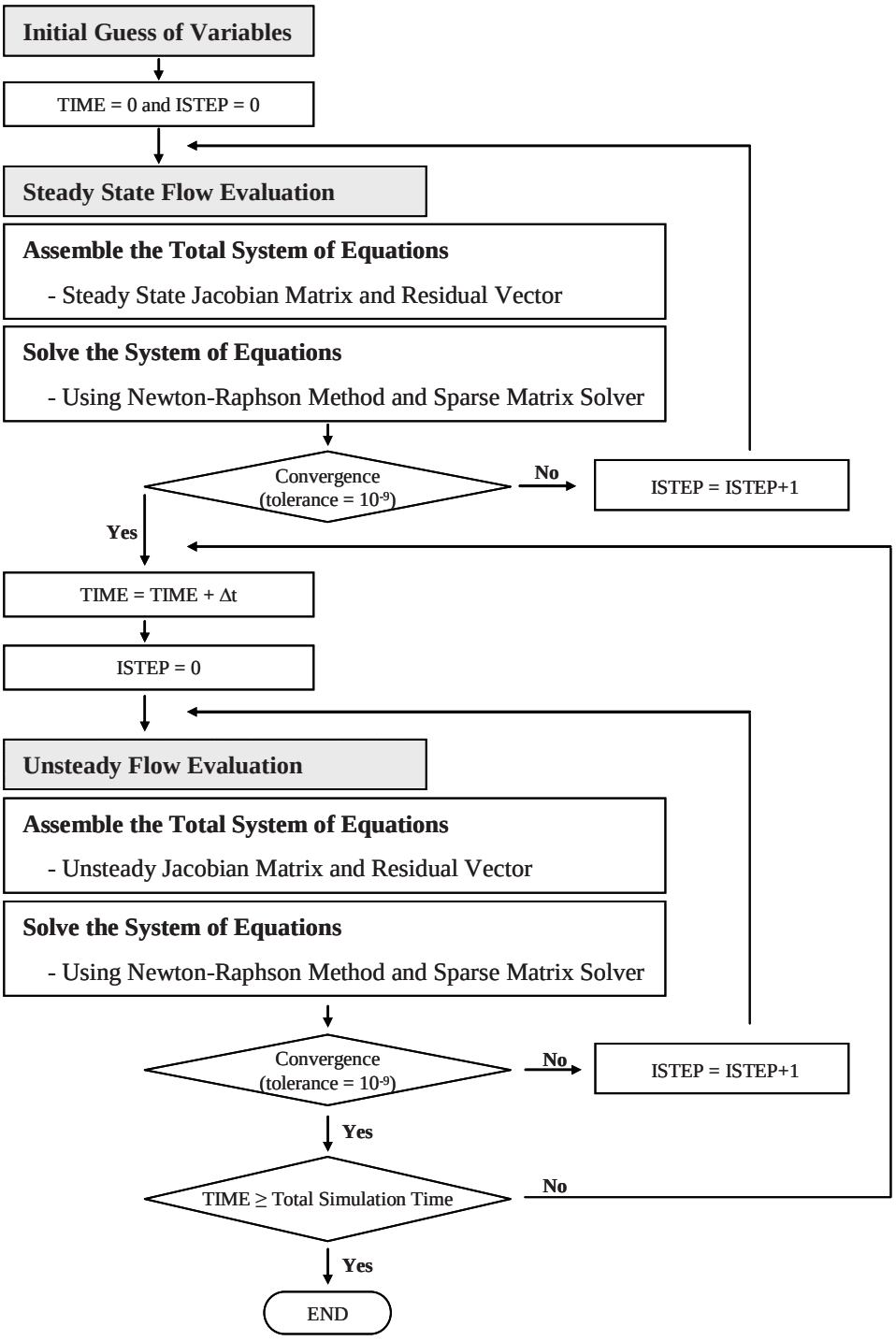

Figure 3.7 Flowchart of Conservative Solution Scheme

3.7.5 Numerical Experiments for Water Transients

Fig. 3.8 shows the simulation result of the proposed model based on CSS compared with the result of a MOC model for the water pipeline system in Fig. 3.6. The system is composed of a 37.53 m long pipe with an inside diameter of 22.1 mm and a wall thickness of 1.6 mm. The transient event is generated by instantaneous valve closure of an inline valve. The wavespeed is 1,320.3 m/s. The initial flow velocity is 0.298 m/s. The computational time and space step are $2.843*10^{-4}$ s and 0.3753 m (100 reaches) respectively. The Courant number for stability condition is nearly unity. A weighting coefficient of α=0.5 was used for implicit FDM solution. The pressure is observed at the valve and the middle point of the pipeline. The simulation results from the conservative solution scheme agree with the result of MOC model.

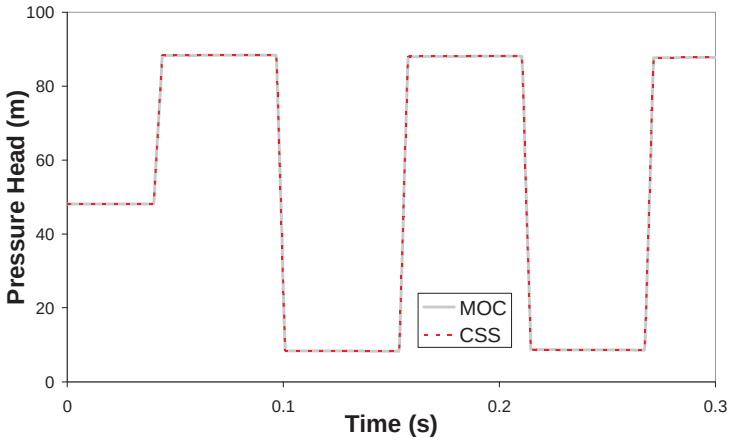

(a) Pressure Variation at the Valve

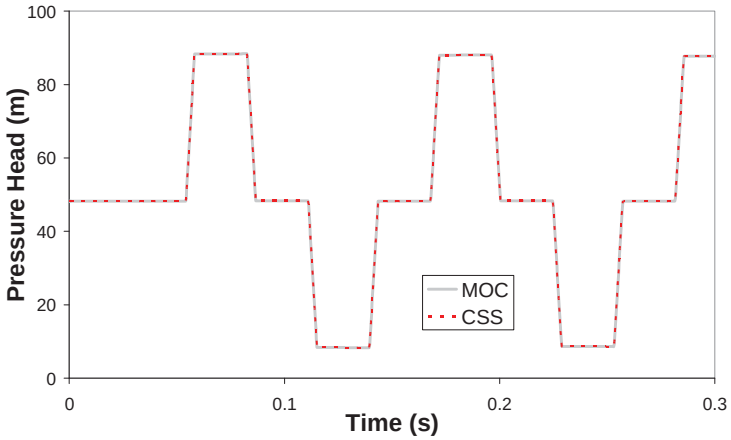

(b) Pressure Variation at the Middle

Figure 3.8 Numerical Experiment in Water Pipeline

3.7.6 Numerical Experiments for Gas Transients

For the same pipeline as described above (see Fig. 3.6), a numerical experiment for gas transients was carried out. Dry air of 20^{o}C is used for gas transient test. The wavespeed is 343.3 m/s. The flow velocity is 20.2 m/s. The computational time and space step are $2.733*10^{-3}$ s and 0.938 m (40 reaches) respectively. The weighting coefficient of α=0.525 was selected for implicit FDM solution. The pressure is observed at the valve and the middle. The polytropic process gas transient analysis model is used for this simulation. The polytropic exponent for heat exchange flow is n=1.20. Fig. 3.9 shows the pressure and density variation at the valve and the middle of pipeline during this air transient event. The compressibility of gas may be more dominant for transient damping effect. The line-packing is large compared with the result of water transients because of the effect of gas storage and compressibility.

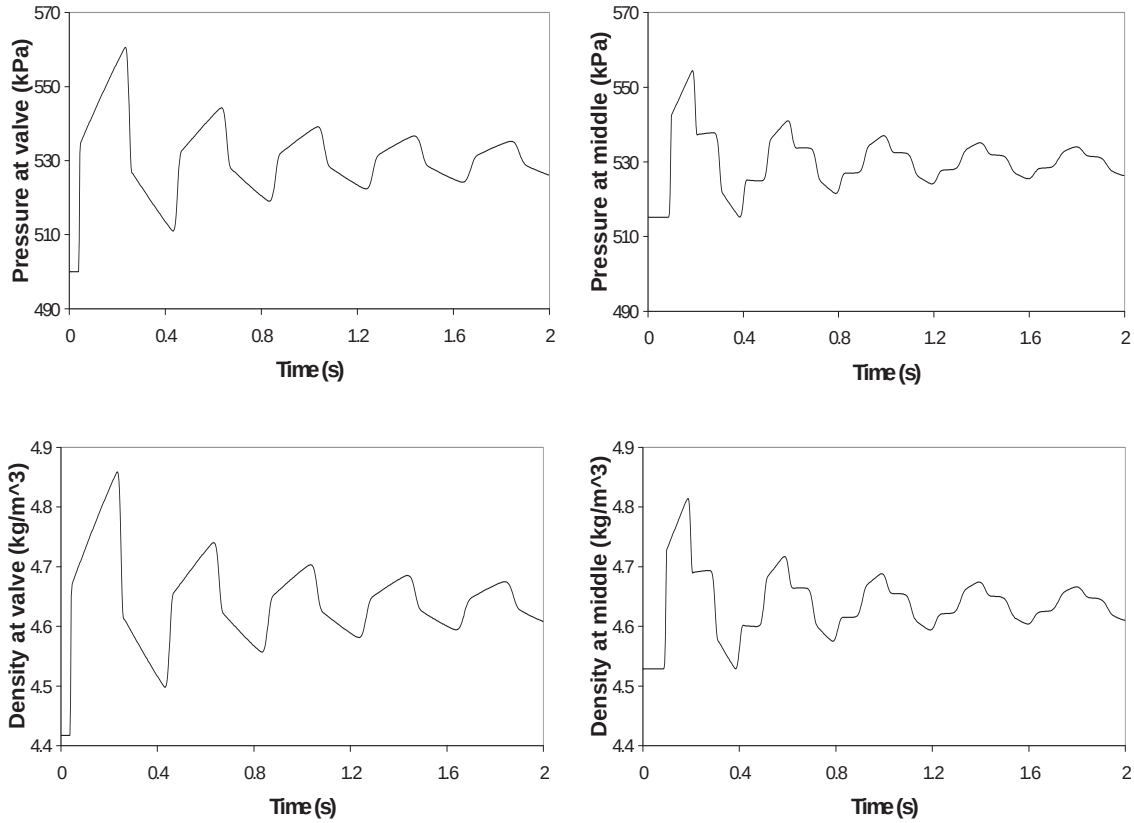

Figure 3.9 Numerical Experiment in Air Pipeline

3.7.7 Stability and Accuracy

The implicit FDM based on the Preissmann scheme is unconditionally stable. This means that the size of the time and space interval does not have to be restricted for the numerical scheme to be stable. However, the time interval cannot be arbitrarily increased to avoid violation of the validity of the replacement of the partial derivatives by finite difference approximations. Actually, the size of the time step is selected taking into consideration both the accuracy of the results and the stability of the scheme. If too large a value of time step is used, then the finite differences no longer approximate the partial derivatives of the governing equations. To ensure that the results computed by the implicit method are accurate, we have to use a computational time step that is nearly equal to that required for the stability of the method of characteristics, $C_N \approx 1$, despite the theoretically unconditional stability condition. Fig. 3.10 shows the convergence behaviour of the conservative scheme when a pipeline has various computational grid sizes. The same pipeline as described above (in Fig. 3.6 and Section 3.7.5) is used for numerical simulations. The pipeline is divided by various numbers of reach N (100, 40, 20, 10, and 5). However, the Courant numbers for all numerical simulations are unity. The pressure is observed at the valve.

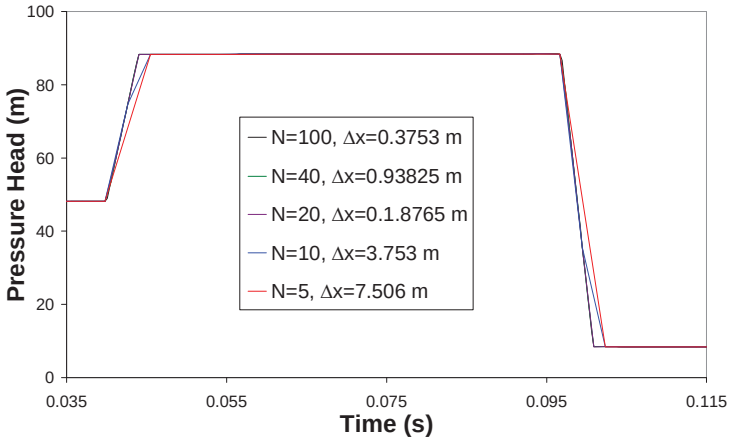

Figure 3.10 Convergence Behaviour according to Various Computational Grid Sizes

The simulation results of 20 and 40 reaches are almost similar to the result of 100 reaches. The results of 5 and 10 reaches show some discrepancies. These discrepancies come from the truncation error due to the use of large computational grid. However, the results show that the conservative solution scheme based on implicit FDM produces relatively good results under $C_N = 1$ condition. Fig. 3.11 shows the simulation results according to various

Courant numbers. The results have numerical oscillations when the Courant number is smaller than unity and these numerical oscillations increase as Courant number decreases.

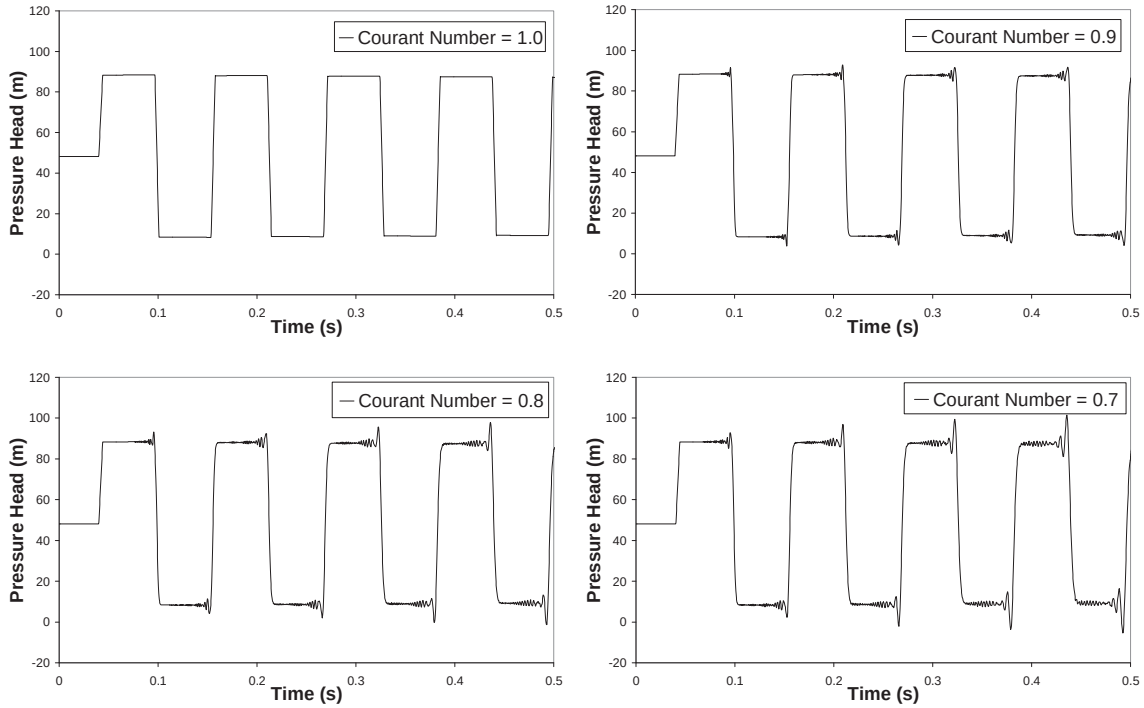

Figure 3.11 Simulation Results according to Various Courant Numbers

Figs. 3.12 and 3.13 show the effect of the numerical weighting coefficient α on the implicit FDM based on the Preissmann scheme. If the weighting coefficient is smaller than 0.5, the solution becomes unstable as shown in Fig. 3.12. There are high-frequency numerical oscillations behind the steep wavefront. If the weighting coefficient is bigger than 0.6, the solution undergoes increased numerical damping and the wavefront becomes progressively more smeared as shown in Fig. 3.13. The weighting coefficient of $0.5 < \alpha \leq 0.6$ offers a good result between accuracy and stability depending on the systems.

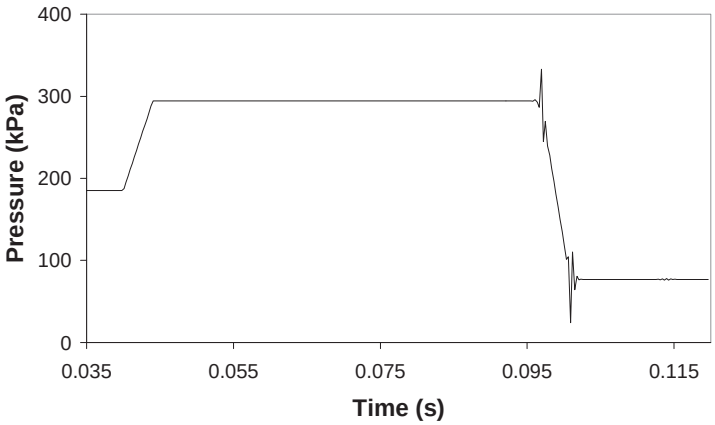

Figure 3.12 Numerical Oscillation (α < 0.5)

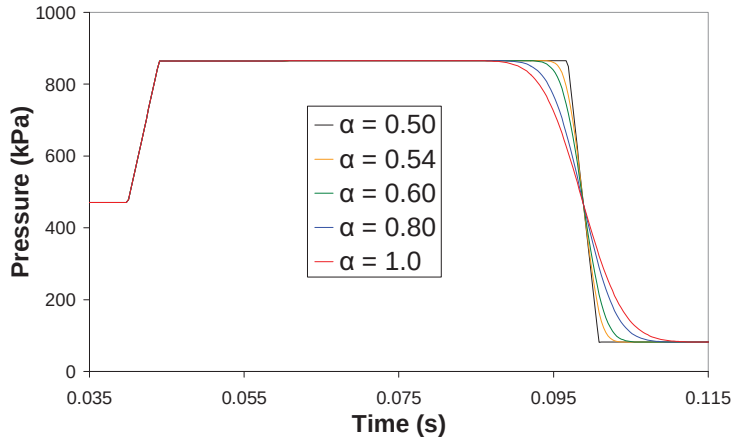

Figure 3.13 Numerical Damping

3.7.8 Numerical Experiments for Heat Exchange Flows

The generalized gas transient analysis model can analyse heat transfer and the conversion of frictional work into thermal energy due to the addition of energy equation and heat transfer equation in the formulation. Fig. 3.14 shows the fluid temperature variation by heat transfer from the external environment to the pipe wall according to different pipe materials. Dry air is used for gas transient flow with heat transfer for the system in Fig. 3.6. The wavespeed is 343.3 m/s. The flow velocity is 10.13 m/s. The pressure and temperature are observed at the middle of pipe, and transients are generated by the fast closure of a valve at the downstream tank. The temperature of all pipes is 293.15 Kelvin with the exception of the middle of the pipe, 303.15 Kelvin. The temperature of the surroundings is also 293.15 Kelvin, and it is constant during transient events. The simulations consider separately five pipe materials with different heat transfer coefficients,

chrome-nickel steel pipe (16.3 W/mK), carbon steel pipe (43.0 W/mK), iron pipe (73.0 W/mK), nickel pipe (93.0 W/mK), and an insulation pipe (no heat transfer). Fig. 3.15 shows the pressure variation of pipeline system with different heat transfer coefficients.

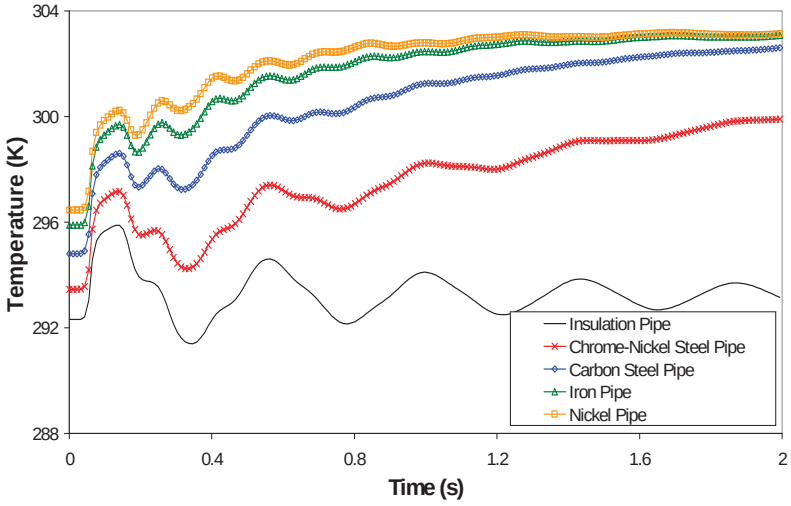

Figure 3.14 Temperature Variations due to Heat Transfer

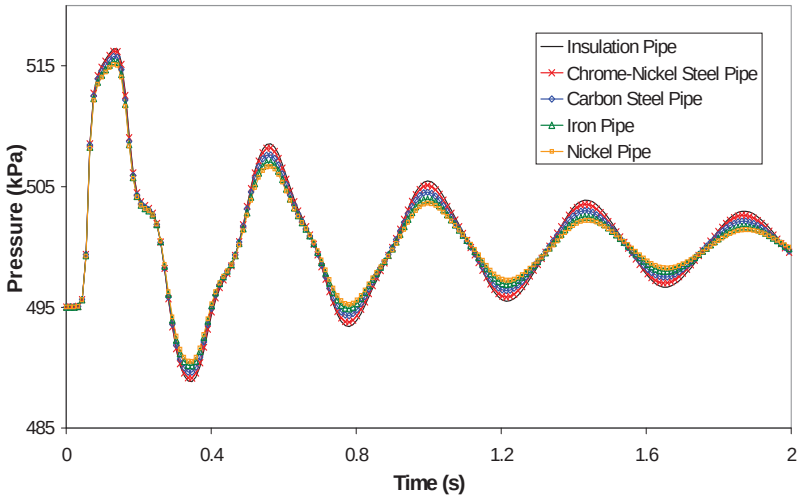

Figure 3.15 Pressure Variations due to Heat Transfer

3.8 SUMMARY AND CONCLUSIONS

To overcome the limitation of traditional transient analysis models and to improve the accuracy and applicability of transient analysis, this research has developed a conservative solution scheme to analyse hydraulic transients in both liquid and gas pipelines. The governing equations have been used in their conservative form and without neglecting any

terms within the basic equations. The conservative solution scheme proposed in this research is more flexible for the computational discretisation by the implicit finite difference method. The scheme is unconditionally stable and has no falsification of the wavespeed. The scheme directly calculates fluid density and pipe wall distensibility at every computational time step. Thus, the wavespeed is updated at every step. This procedure has big advantages for analysing systems with variable wavespeeds, such as systems with either entrapped air pockets or viscoelastic behaviour of the pipe material. Another advantage of this scheme is the flexibility in dealing with various non-pipe elements and unsteady friction models. The governing equations in conservation form and subsidiary equations for the specified conditions can all be expressed by the same generic equations. Also, the scheme can simulate transient flows of various fluids by only slightly modifying the basic structure of solution. The gas transient models developed in this research can analyse three different specified gas processes during unsteady pipe flows, namely, isothermal, polytropic and generalized gas process. These models can simulate one-dimensional gas transient problems including heat transfer and the conversion of frictional work into thermal energy. The scheme is slower than explicit methods when applied to fast transients in short pipelines because the entire system must be analysed for each iteration. However, it has an advantage of its average speed over a range of problems including both fast and slow transients in a relatively long pipeline system. Laboratory experiments and their simulation results of both gas and water transients in pipeline systems are presented in Chapter 5 for the verification of the proposed conservative solution scheme.

CHAPTER 4

PIPELINE APPARATUS FOR EXPERIMENTAL VERIFICATION

Laboratory experiments have been undertaken for the verification of the proposed liquid and gas transient analysis models based on the conservative solution scheme and for examining in significant detail the effect of unsteady pipe wall friction and pipeline system abnormalities (unsteady local loss elements) during transients. The experimental apparatus is a pipeline in the Robin Hydraulics Laboratory in the School of Civil and Environmental Engineering at the University of Adelaide [Bergant and Simpson, 1995]. The pipeline has been reconstructed for use in this research. The experimental apparatus is composed of a pipeline system, a pressure control system, and a data acquisition system. The pipeline is rigidly fixed to a foundation plate with special steel bracing to prevent structural vibration during transient events and connects two electronically controlled pressurised tanks by an air compressor. The pressure waves in the pipe are recorded by high-resolution pressure transducers and transferred via amplifiers and a 16-bit analogue/digital (A/D) converter card to a PC with data acquisition interface based on LabVIEW software. The characteristics of the experimental apparatus should be identified for accurate measurement of system data. The measurements of initial flow, pressure, and temperature are important factors for the transient analysis models. They have a direct effect on the simulation results of transient events. This chapter also presents the calibration of pressure transducers, generation of transients, wavespeeds, and measurement system data.

4.1 PIPELINE SYSTEM

The pipeline apparatus for liquid and gas transient experiments is located along the north wall of the Robin Hydraulics Laboratory. It was initially built by Bergant and Simpson [1995], and was reconstructed to minimize the variation of wavespeed by non-pipe elements with different wall thickness and to install adaptable sections (see Figs. 4.1 and 4.4) for investigating the effects of pipeline system abnormalities (unsteady minor loss elements) during transient events. These abnormalities include different pipe diameters, various pipe wall thicknesses and materials, entrapped air pockets, leakages, orifices, and blockages, and are studied in this research. The schematic and photographs of the pipeline are shown in Figs. 4.1 and 4.2 respectively.

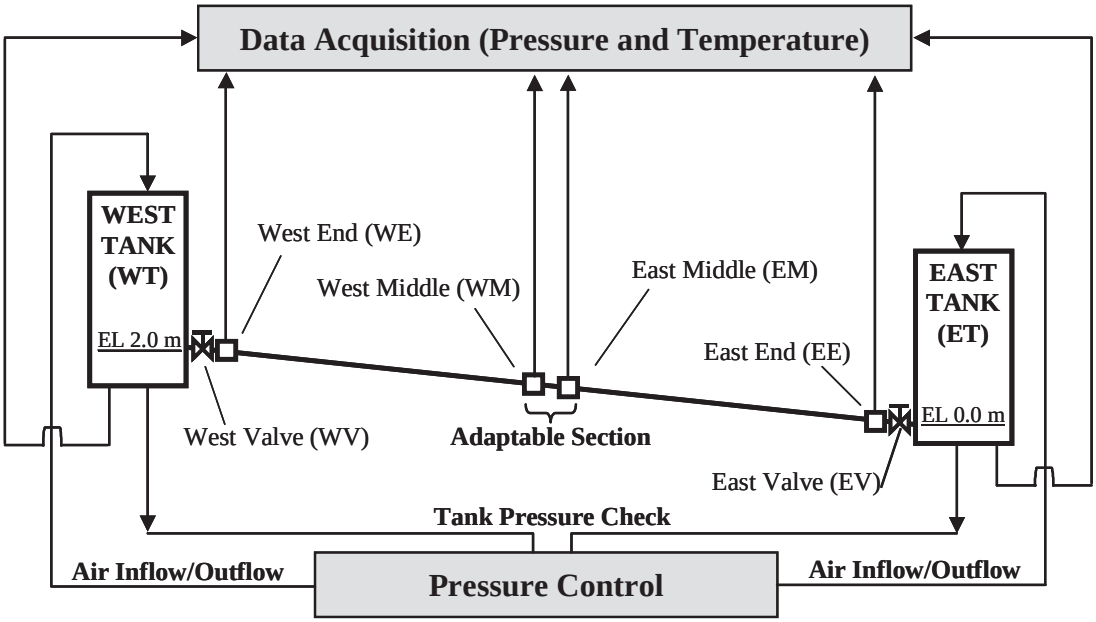

Figure 4.1 Pipeline Apparatus Schematic

(a) The Left End Section

(b) The Right End Section

(c) The Middle of Pipeline

(d) Foundation Plate and Wall Mounted Support Frames

Figure 4.2 Pipeline Apparatus Photographs

Pressure and temperature can be continuously monitored at four (WE, WM, EM, EE) brass blocks along the pipeline and at the bottom of both tanks (WT and ET). The pipeline is a straight 37.53 m long sloping copper pipe with an internal diameter of 22.1 mm and a wall thickness of 1.6 mm connecting two electronically controlled pressurised tanks. The roughness height of the interior surface of the pipe is estimated as 0.0015 mm by a manufacturer. The elevation difference between the two ends of the pipe is 2.03 m and the pipe slope is constant throughout with a vertical to horizontal ratio of 1:18.5. The pipeline is rigidly fixed to a foundation plate with special wall mounted steel construction frames (see Fig. 4.2d) at an interval of approximately 0.5 m in the axial direction to prevent fluid-structure interaction (FSI) during transient events. Demineralized water is used as the fluid to prevent corrosion of pipeline components for liquid transient tests. For gas transients, dry air is used as the fluid medium and supplied by an air compressor through air filters

after draining and drying pipeline and both tanks. Table 4.1 shows the specification of the copper pipe [KEMBLA, 2006].

Table 4.1 Specification of Copper Pipe

Specification	Value
Manufacturer	KEMBLA
Material	Phosphorus Deoxidised Copper
Internal Diameter (mm)	22.14 ± 0.28 (DN25)
Wall Thickness (mm)	1.63 ± 0.25 (Type A)
Standard Number	AS1432-2004 (Australia)
Thermal Conductivity (W/mk)	305-355
Modulus of Elasticity (MPa)	124.1
Poisson's Ratio	0.37
Safe Working Pressure (kPa)	4,750

The pipeline is composed of 9 or 11 pieces of copper pipe according to test conditions. Each pipe is coupled by high precision Swagelok 25.4 mm straight fittings (see Fig. 4.5a) [Swagelok, 2006]. The pipeline has one T-junction to extend the system for dead-end pipe and loop network system tests (see Fig. 4.5b), two 25.4 mm flow control valves (Whitey 65TF16, one-quarter-turn ball valve, inner diameter 22.2 mm, see Fig. 4.5c) located in the pipeline adjacent to both the pressurised boundary tanks, adaptable sections (see Figs. 4.4 and 4.5e) located in the middle of the pipeline for investigating the effects of pipeline system abnormalities during transient events, and four brass blocks (see Fig. 4.5d) for the connection of pressure transducers and temperature meters, leak units, and solenoid valves for transient generation. The layouts and photographs of pipeline system are shown in Figs. 4.3, 4.4, and 4.5.

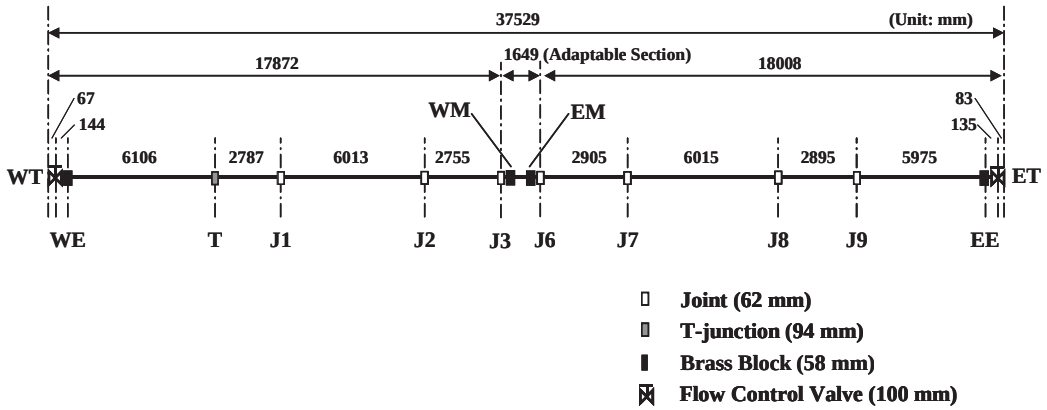

Figure 4.3 Pipeline System Layout

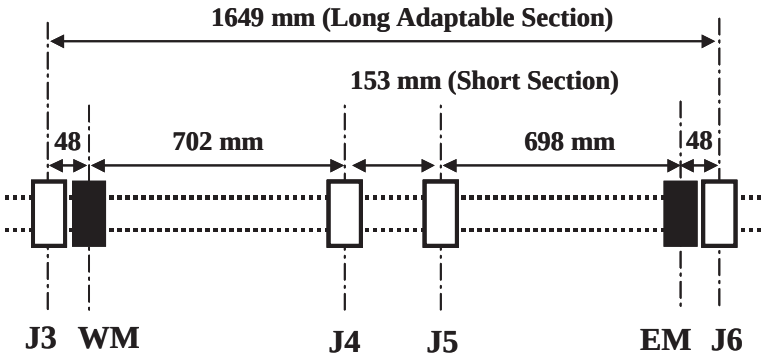

Figure 4.4 Adaptable Section Layout

(a) Joint

(b) T-junction

(c) Flow Control Valve

(d) Brass Block

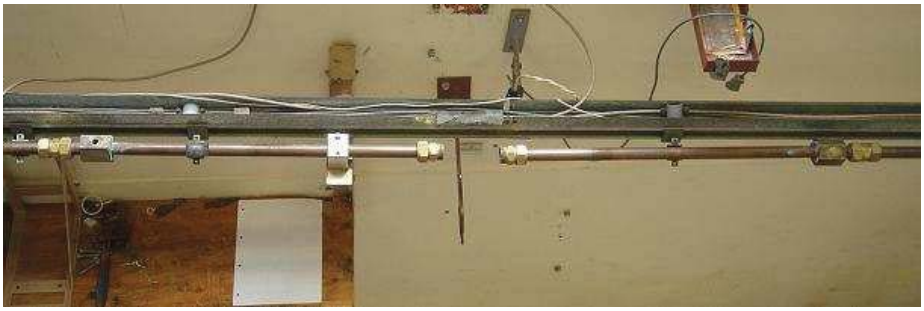

(e) Adaptable Section

Figure 4.5 Pipeline System Photographs

4.2 PRESSURE CONTROL SYSTEM

Two tanks at each end are pressurised through an air compressor that maintains the set pressures for initial pressure and flow in the pipeline during tests. An electronic pressure controller (called the blue box) regulates the specified pressure in each tank. The tanks are vertical standing cylindrically shaped on steel support stands. The specification of each tank is shown in Table 4.2 and Fig. 4.6.

Table 4.2 Specification of Tanks

Specification	West Tank (WT)	East Tank (ET)
Internal Diameter (mm)	485	566
Gross Height (m)	2.168	2.157
Volume of the Tank (m^3)	0.378	0.509
Maximum Allowable Pressure (kPa)	690	690

(a) West Boundary Tank **(b) East Boundary Tank**

Figure 4.6 Pressurised Boundary Tanks

Both tanks are equipped with a safety valve (consolidated type, 690 kPa, see Fig. 4.7a-1), two dial pressure gauges (at the top of a tank: AS 1349, 0 to 800 ± 10 kPa, see Fig. 4.7a-2; at the bottom of a tank: Dobbie, 0 to 700 ± 1 kPa, see Fig. 4.7b-1), an electronic pressure regulator (Fairchild T5700, maximum supply pressure 1,000 kPa, output pressure 20 to 820 kPa, see Fig. 4.7a-3) operated by a pressure controller, an electronic air exhaust valve (solenoid valve type, SMC VXD 21-40, see Fig. 4.7a-4) operated by manual switch at the pressure controller, and a sight glass protected by a polycarbonate tube (Lexan). The sight

glass is for visual inspection of water level in each tank. The dial pressure gauges are used for visual control of tank pressures. The precision regulator (SMC IR 202-02, maximum supply pressure 900 kPa, output pressure 5 to 700 kPa, see Fig. 4.7c-1) and air filter (see Fig. 4.7c-2) are installed in the air supply lines of each tank. The precision regulator attenuates pressure surges in air supply line. Fig. 4.7 shows the photographs of these devices.

(a) Top of a Tank

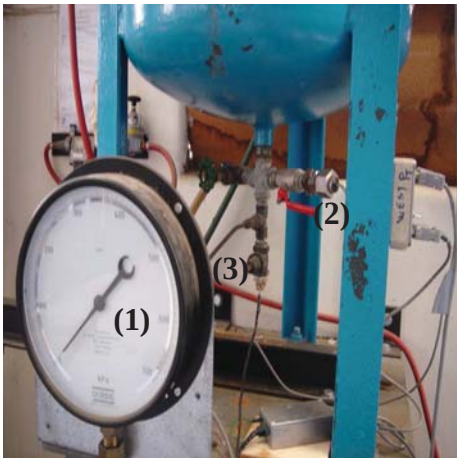

(b) Bottom of a Tank

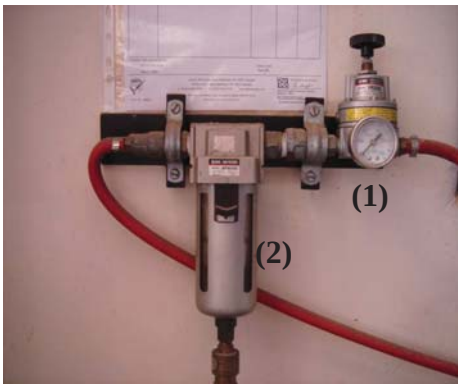

(c) Air Filter and Precision Regulator

(d) Electronic Pressure Controller

Figure 4.7 Pressure Control Devices

The electronic pressure controller operated by data acquisition software written in assembler language. The input data are the set pressure and the actual tank pressure measured by pressure transducers in each tank, and the output is the desired compressed air supply according to set tank pressure. The pressure controller compares the set and actual pressure in each tank. If the actual tank pressure is higher/lower than the set tank pressure, the pressure controller continuously adjusts the electronic pressure regulator to the required

pressure. This pressure control system can maintain the stable pressure condition of each tank during transient tests.

4.3 DATA ACQUISITION SYSTEM

4.3.1 Pressure Transducers

Pressure signals are measured at four positions along the pipeline (as indicated in Fig. 4.1) using Druck PDCR 810 high integrity silicon flush mounted diaphragm transducers with an absolute pressure range of 0 to 15 bars. The rise time is 5×10^{-6} s and the measurement uncertainty is rated at 0.1% of the full measurement span. This transducer also accurately responds to pressure below gauge (sub-atmospheric pressure) and the total error band is 0.5% for 0 to 50^{o}C. The excitation voltage is 0 to 10 volts and the output voltage range is 0 to 100 mV [Druck, 1997]. The flush diaphragm prevents high frequency interference between the fluid flow and the transducers. The transducers are mounted in brass blocks. The internal diameter of the brass block is designed to align smoothly with the inside of the pipe wall. The pressure in each tank is measured by Data Instruments AB/HP flush mounted diaphragm transducer (strain gauge type, gauge pressure range 0 to 689 kPa, uncertainty 0.25% of full span). An AB/HP transducer is installed at the bottom of each tank as shown in Fig. 4.7b-2. An amplifier is used for amplifying the small electrical output signal from the pressure transducers. Fig. 4.8 shows the photographs of transducers and brass block with a transducer.

(a) PDCR 810 Transducer **(b) AB/HP Transducer**

Figure 4.8 Transducer, Brass Block, and Amplifier

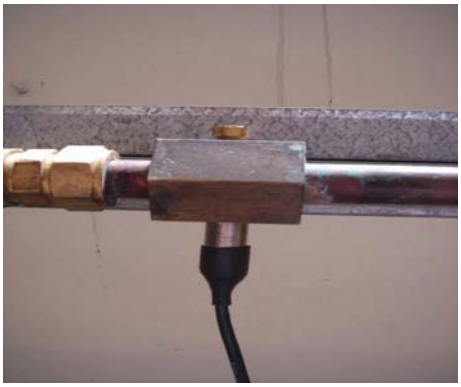

(c) Brass Block with a Transducer

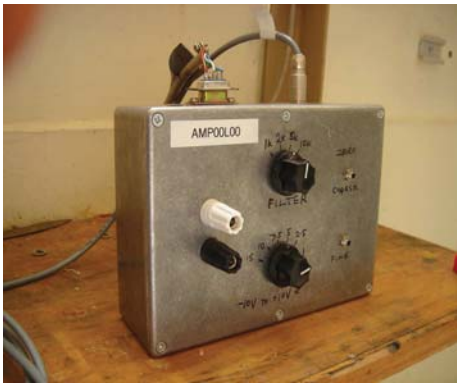

(d) Amplifier for transducer

Figure 4.8 Transducer, Brass Block, and Amplifier (continued)

4.3.2 Temperature Meters

Three temperature meters continuously measure the fluid temperature during experimental tests. They can be mounted at the bottom of each tank (see Fig. 4.7b-3) and at four positions of brass blocks along the pipeline. The nickel/chromium thermocouple temperature probe (RS Components, Type K) is inserted into the screw with inside hole and the probe is fixed by epoxy resin. The temperature range is -40 ^{o} to 1,200^{o}C with an uncertainty of 0.75% [RS Components, 2005]. The setting temperature range is 0 to 40^{o}C for the purpose of this research. The excitation voltage is $\pm$ 10 volts and the output voltage range is $\pm$ 100 mV. The temperature meters also have flush fitted face to be installed in the brass blocks. Fig. 4.9 shows a photograph of temperature meter and its amplifier.

Figure 4.9 Temperature Meter and Amplifier

4.3.3 Signal Module and Data Acquisition Interface

The data acquisition system measuring fluid pressure and temperature is performed on a personal computer using a universal serial bus (USB)-based analog and digital module (Measurement Computing, USB-1608FS, formerly known as PMD-1608FS) and a data acquisition interface based on LabVIEW software (National Instruments, version 7.1). The software provides an easy-to-use graphical user interface (GUI) of the data acquisition process. The data acquisition interface controls the number of input channels, sampling rates, processing of data, and storage of the data. The data acquisition module has 8 analog channels. The conversion of these analog signals to digital signals is performed with 16-bit resolution. The possible input ranges are ± 1, ± 2, ± 5, and ± 10 volts with external digital trigger input. The range of 0 to 10 volts is used in this research. The module provides on A/D converter per channel allowing simultaneous sampling over all 8 channels. It offers continuous single channel sample rates up to 50 kHz (kilosamples/sec) and multiple channel continuous sampling rates up to 100 kHz [Measurement Computing, 2006]. Fig. 4.10 shows data acquisition module and interface.

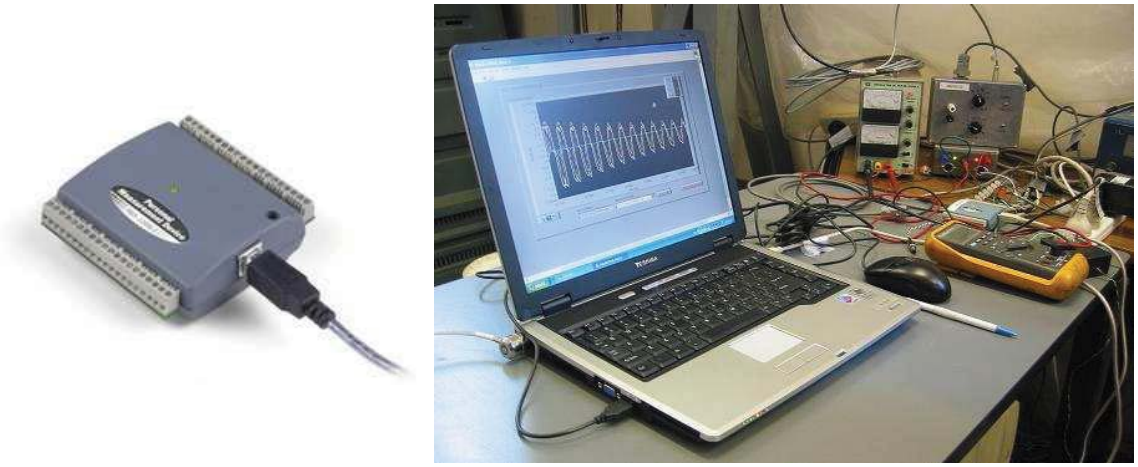

Figure 4.10 Data Acquisition Module and Interface

4.4 CALIBRATION OF PRESSURE TRANSDUCERS

The combination with pressure transducers and amplifiers is calibrated and adjusted using a portable pneumatic pressure tester (AMETEK, T662, pressure range 0 to 1,100 kPa) and a hydraulic dead-weight testing unit (Precision Eng., L-type) as shown in Fig. 4.11. The accuracy of the portable pressure tester is 0.5% of gauge span, and the operating fluid is air. The dead-weight tester is the basic primary standard for accurate measurement of pressure.

Pressure signals are artificially generated by specified weights. These signals are then used for calibration or adjustment of pressure transducers and amplifiers. The accuracy is better than 0.1% of reading.

(a) Portable Pressure Tester

(b) Dead-weight Pressure Tester

Figure 4.11 Pressure Testers

One of the important properties of pressure measurement is the observational error (measurement error). It is the difference between a measured value of quantity and its true value. The measurement error is composed of two additive parts. One is the systematic error that is associated with instruments. It always has the same value when the instrument is used in the same way. Another is the random error that may vary from observation to observation. It is due to factors that we cannot control.

In the experimental tests for this research, the noticeable systematic errors come from bit error (digital noise) and hydraulic noise. The bit error indicates the number of bits of a data stream over a communication channel that have been altered by noise. It is commonly referred to as bit error ratio (BER), the ratio of the number of failed bits to the total number of bits sent over the channel. This error is shown in Figs. 4.12 and 4.14 (for the same scale, 4 kHz sampling rate).

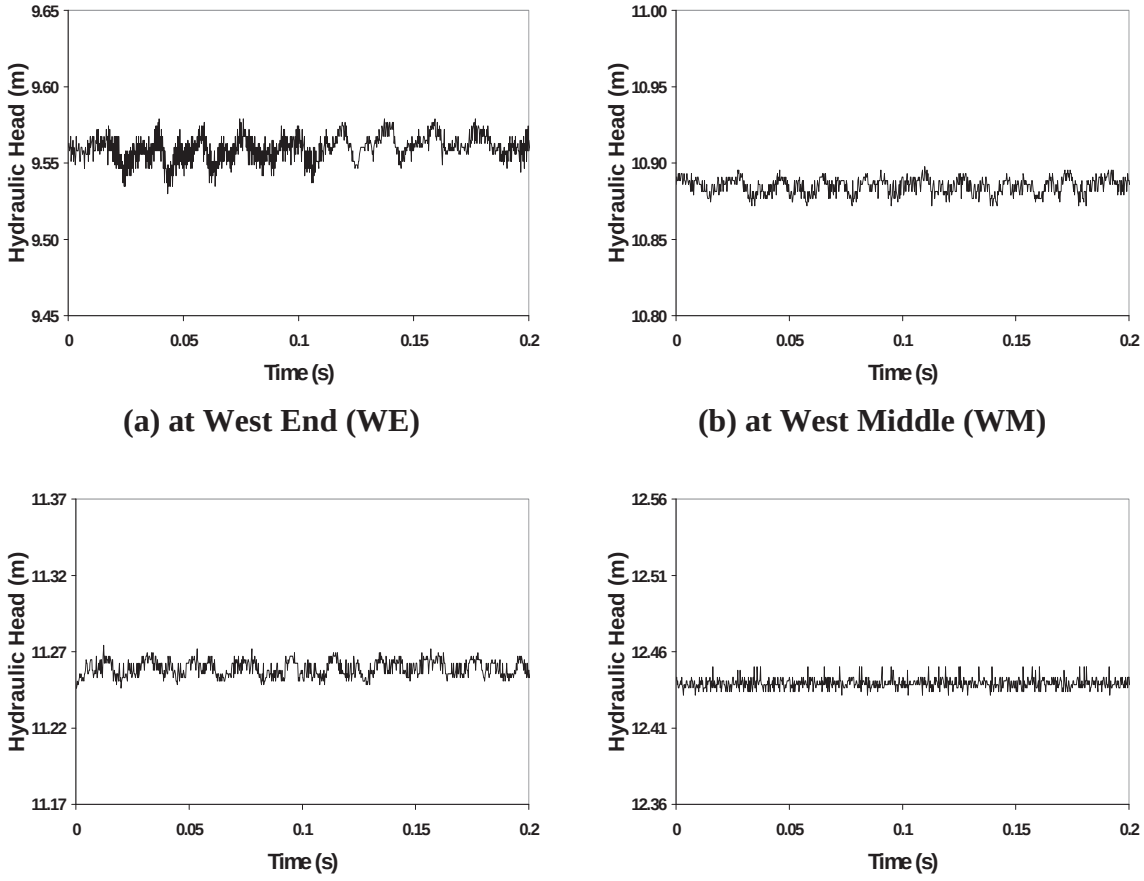

(a) at West End (WE) **(b) at West Middle (WM)**

(c) at East Middle (EM) **(d) at East End (EE)**

Figure 4.12 Pressure Measurement Noise (without Base Flow)

The random error is caused by electromagnetic interference (EMI) from environmental electromagnetic radiation of other random variations in currents. It causes unwanted signals (interference or noise) to be induced in the experimental devices and electric cables. The efficiency of the reduction of electromagnetic interference is dependent on ground connection and shielded electric cables. Although the experimental apparatus uses shielded cables and ground connections to minimize the random noise, Fig. 4.12 shows that there is an effect of electromagnetic interference. The random error by electromagnetic interference at the west end is larger than the error at the other positions because this position has many electric devices for controlling the system (see the right hand of Fig. 4.10). Fig. 4.13 shows the frequency spectrum of measured data at West End (as shown in Fig. 4.12a). The spike at the 50 Hz represents the random error by electromagnetic interference which is affected by normal electric devices with 0.02 second current cycle.

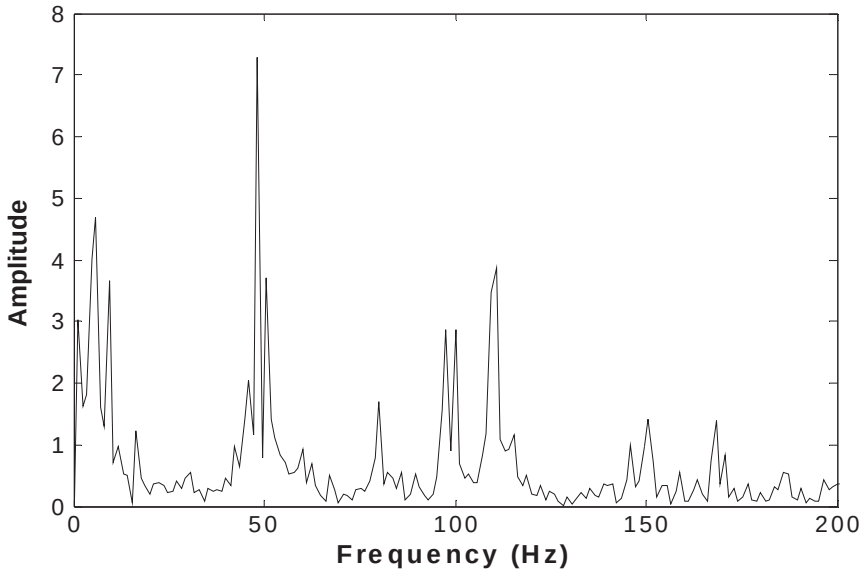

Figure 4.13 Frequency Spectrum of Measured Data with Random Noise

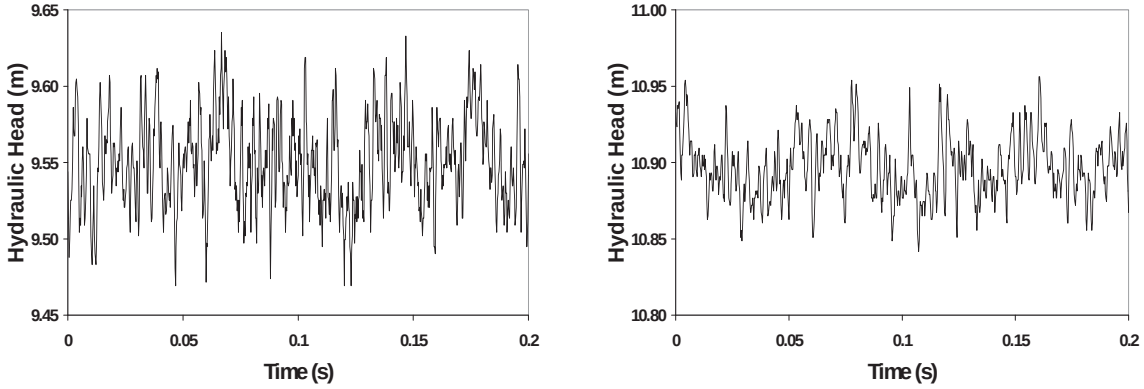

(a) at West End (WE)

(b) at West Middle (WM)

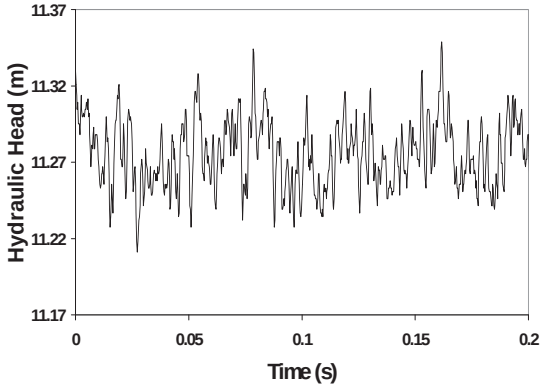

(c) at East Middle (EM)

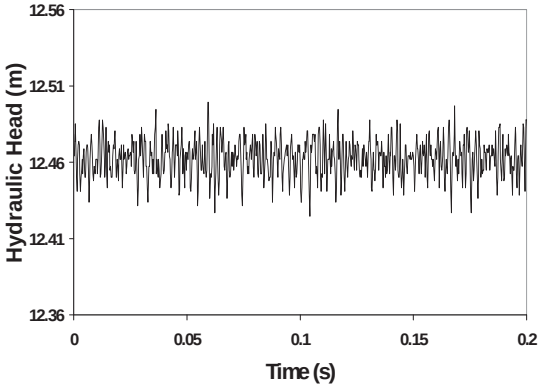

(d) at East End (EE)

Figure 4.14 Pressure Measurement Noise (with Base Flow)

In Fig. 4.14, the errors are measured when there is flow in the pipeline with discharge occurring from a fully open of side discharge valve at the near west end. The errors in the pressure signals are significantly amplified when the pipeline has flow. The reason for the larger error is caused by the hydraulic noise of the pipeline due to valve opening. The size of the error at each node is different and a function of the position of the side discharge valve. The random error is larger if the measured position approaches the valve opening as shown in Fig. 4.14.

The total range of the transducers is 153 m of hydraulic head, and the resolution of the data acquisition system is 16 bits (2^{16}). Thus, the possible resolution of measured pressure is 2.33 mm. Assuming that the error has a normal (Gaussian) distribution, the standard deviation of the total error for each node is shown in Table 4.3. Tests are conducted with six different flow conditions that are usually used for water transient tests in this research.

Table 4.3 Standard Deviation at Pressure Transducers

Flow Condition (Reynolds Number, Re)	Standard Deviation (mm)			
	WE	WM	EM	EE
No Flow	8.7	5.6	5.5	4.2
Condition 1 (1,483)	33.5	26.2	25.9	11.3
Condition 2 (2,039)	72.5	52.4	57.3	20.4
Condition 3 (2,552)	113.3	96.5	82.9	19.3
Condition 4 (2,991)	142.6	114.5	106.7	36.3
Condition 5 (3,385)	146.6	129.8	118.5	43.1
Condition 6 (3,699)	126.7	90.0	96.1	42.0

The standard deviations of the error at the transition flow zone (condition 4 and 5) are larger than other conditions. These may be caused by unstable flow of transition flow zone. The standard deviation of the condition 6 is more stable than these two values. The largest standard deviation of the error is 146.6 mm. This value of the error is quite reasonable for the transient test in this research without special data filtering. The estimated error can be used as a guide to quantify the magnitude of micro-reflection pressure waves by pipeline abnormalities.

4.5 TRANSIENT GENERATION

Transient events can be generated by flow control valves (in-line valves) or side-discharge solenoid valves in the experimental pipeline. The fast closure of an in-line valve is used as the traditional method. In-line valves are located near both tanks (west valve and east valve in Fig. 4.1). Side-discharge solenoid valves are another useful method for generating transients. They have fast operating time and can generate effective low amplitude transient signals. Also, the location of transient generation can be easily changed. A solenoid valve is an electromechanical valve controlled by starting or stopping an electrical current through a solenoid, thus changing the state of valve.

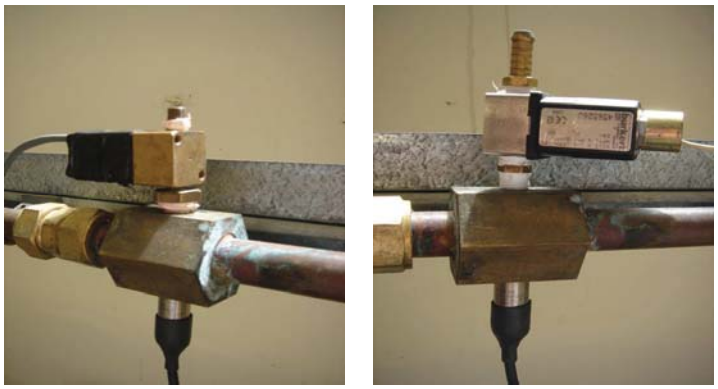

(a) For Water Transients **(b) For Gas Transients**

Figure 4.15 Solenoid Valve for Generating Transients

Solenoid valves for transient generation can be located in the four brass blocks (WE, WM, EM, EE in Fig. 4.1). Fig. 4.15 shows the solenoid valves installed in the brass blocks for liquid and gas transient events. A GEM-SOL solenoid valve (Fig. 4.15a) is used for water transient tests. The maximum operating pressure is 15 bars and the orifice diameter of the solenoid valve is 1.6 mm. For gas transient tests using dry air, a Burket (type 6013, Fig. 4.15b) solenoid valve is used. The maximum operating pressure and orifice diameter are 16 bars and 2.5 mm respectively. Both valves are two-way normally closed valves driven by 24 volts AC power and can move from fully opened to fully closed in 4 milliseconds (ms) theoretically. The effective valve closure times of both solenoid valves are measured by actual transient test data in water and air pipelines. The actual valve closure time can be represented by the time of pressure rising at the first wave cycle due to fast valve closure. An example for measuring effective valve closure time is shown in Fig. 4.16.

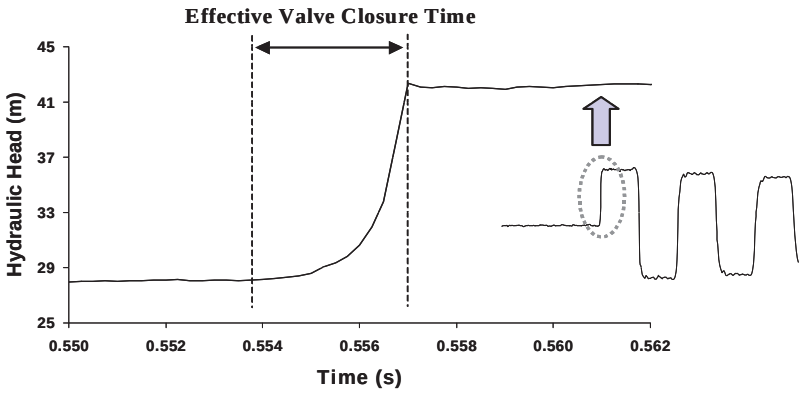

Figure 4.16 Estimation of Effective Valve Closure Time

The measured effective valve closure time ranges from 3.52 ms to 4.43 ms for water transient events (GEM-SOL solenoid valve) and from 4.14 ms to 6.69 ms for gas transient events (Burket solenoid valve). These values accord with theoretical values. They are considerably faster than the definition of a fast valve closure time in relation to the pipeline length (56 ms for water transients and 220 ms for gas transients) based on the *2L/a* period of the pipeline assuming a wavespeed of 1,340 m/s for water transients and a wavespeed of 340 m/s for gas transients.

4.6 CALIBRATION OF WAVESPEED

The wavespeed describes the speed of pressure waves travelling through a fluid medium. The wavespeed in a closed conduit is directly determined by the physical properties of conduit and fluid, thus it is a useful parameter for describing the pipeline system. The theoretical wavespeed is calculated using a relationship defined in Section 3.4. The theoretical value is verified by experimental methods for estimating the wavespeed.

4.6.1 Theoretical Wavespeeds

The theoretical wavespeed for water (20^{o}C) in the thick-walled copper pipeline is calculated by Equation 3.36.

$$a = \sqrt{\frac{\frac{K}{\rho}}{1+\frac{K}{E}\cdot\frac{D}{e}\cdot\psi}} = \sqrt{\frac{\frac{2.19\times10^{9}}{998.2}}{1+\frac{2.19\times10^{9}}{124.1\times10^{9}}\cdot\frac{22.14}{1.63}\cdot1.006}} = 1329 \text{ m/s} \qquad (4.1)$$

On the other hand, the theoretical wavespeed for air (15^{o}C) is calculated by reversible adiabatic (isentropic) process relationship in Equation 3.38.

$$a = \sqrt{\gamma RT} = \sqrt{1.401\times286.9\times(273.15+15)} = 340 \text{ m/s} \qquad (4.2)$$

4.6.2 Experimental Determination of Wavespeeds

The wavespeed can be determined by the time interval of the peaks of recorded pressure wave along the pipeline. The measured transient trace and the times of pressure peaks (31 points) are shown in Fig. 4.17. The wavespeeds calculated by the peak time intervals (30 intervals) is given in Fig. 4.18. The transients are generated 0.21 m away from the west tank by the closure of an initially open side-discharge solenoid valve (west end brass block, see Fig. 4.3). The test is conducted after closing the west flow control valve, thus the pipeline system is composed of reservoir (pressurised tank)-pipe-valve.

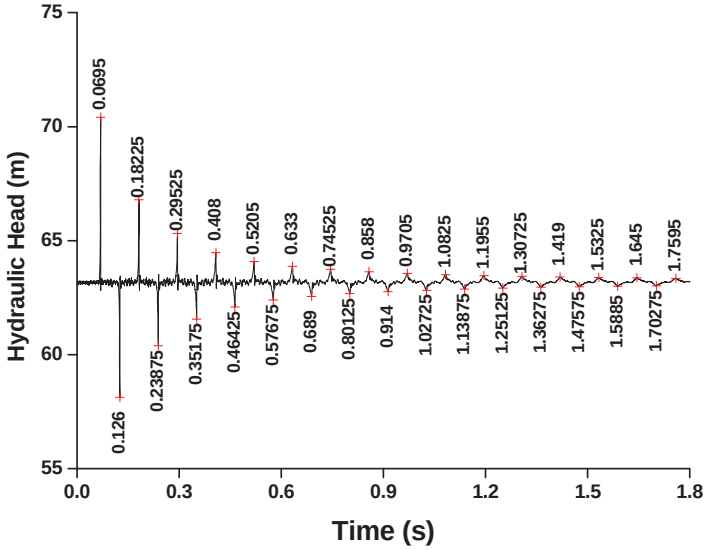

Figure 4.17 Peak Times of Measurement Data

The transients are measured 0.22 m away from the east tank (east end brass block, see Fig. 4.3). The sampling frequency for this test is 8 kHz. The measured transient data have the form of successive pressure spikes, because of the instant pressure reflection at the east tank. Fig. 4.17 shows the measured times of 31 pressure peaks during 1.8 s.

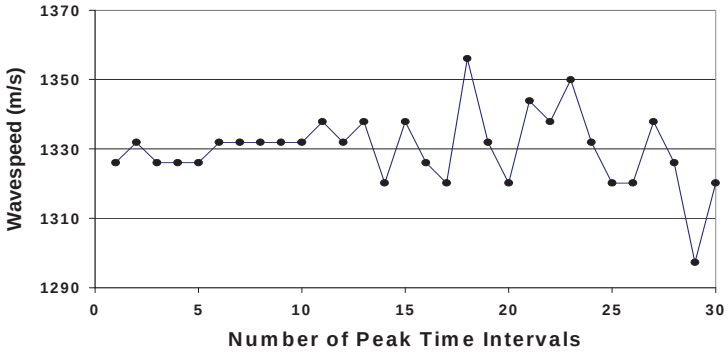

Figure 4.18 Wavespeeds by Peak Time Intervals

The average time it takes for the pressure wave to travel from peak to peak is 0.05633 s, which gives a wavespeed of 1,330 m/s. However, Fig. 4.18 shows the variability of measured wavespeeds with time. This may be due to the uncertainties in the water and pipe properties or deterioration of the speed of pressure wave in process of time. Therefore, the initial stage of peak time intervals is chosen for calculating wavespeed. The wavespeed is 1,328 m/s.

Another method for estimating the wavespeed is to find the best fit between the measured pressure data and calculated pressure data by transient analysis model. The wavespeed is calculated based on an inverse fitting. It is determined by trial and error to give the best match of the frequency of the measured transients. Fig. 4.19 shows the result of the best fit. The test condition is same as the above test to find peak time of pressure waves and the measurement position of transients is the west end brass block (see Fig. 4.3). The wavespeed is determined as 1,340.5 m/s during the long period of pressure wave (10 seconds). This value is slightly higher than the wavespeed of previous methods.

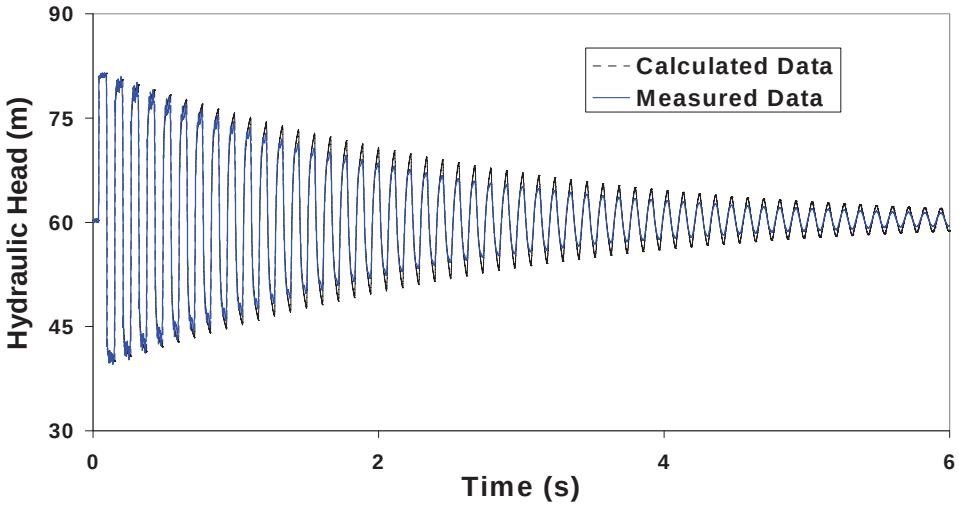

Figure 4.19 Wavespeed by Best Fit

The wavespeed for air is estimated by the same above methods. The wavespeed in the pipeline with air transients is determined to be 342 m/s, which is used in the further analysis of the experimental tests.

4.7 MEASUREMENT OF FLOW DATA

The initial steady state velocity of the flow in the pipeline can be measured by volumetric methods, the Joukowsky pressure rise formula (see Equation 3.35), and the relationship of the variation of pressure and mass in the tank with constant volume (called the variable pressure tank boundary model in this thesis) depending on the system boundary conditions and the flow medium.

4.7.1 Volumetric Methods

When the pipeline system for tests is composed of tank-pipe-tank, the flow velocity is determined by observing the changes in water levels of the supply and delivery tanks (east tank and west tank). The transients are generated by the flow control valve near the tanks. The change in water level over a period of time in both tanks is proportional to the flow velocity in the pipe. The two tanks are fully calibrated [Bergant and Simpson, 1995]. The steady state velocity V_0 is estimated by the following simplified equation.

$$V_0 = \frac{\Delta z}{t_{\Delta z} \cdot c_v} \tag{4.3}$$

where Δz is the change of water level, $t_{\Delta z}$ is the time for water level change, and c_v is the calibrated volumetric constant for a tank. The volumetric constants are 2.104×10^{-3} for the west tank and 1.540×10^{-3} for east tank.

When the pipeline system for tests is composed of tank-pipe-valve, the transients are generated 0.21 m away from the west tank through the closure of an initially open side-discharge solenoid valve (see Fig. 4.3). The test is conducted after closing the inline west flow control valve. Therefore, the pipeline system can be regarded as simple tank-pipe-valve system. The flow velocity is calculated by directly measuring the flow rate through solenoid valve with a 6 litre volumetric cylinder. In this case, this solenoid valve generates transient events. This boundary condition of the test system (tank-pipe-valve, transients by side-discharge valve) is usually used for tests conducted in this research. Table 4.4 shows the specified 6 different flow conditions for transient tests. The initial velocities are adjusted by the pressure conditions of the boundary tank pressurised by air compressor.

Table 4.4 Specified Six Different Flow Conditions

Flow Conditions	Tank Pressure (kPa)	V_0 (m/s) by the Volumetric Method	V_0 (m/s) by the Joukowsky Equation
Condition 1	117.6	0.0599	0.0597
Condition 2	200.0	0.0824	0.0824
Condition 3	297.2	0.1031	0.1033
Condition 4	397.4	0.1208	0.1209
Condition 5	502.2	0.1368	0.1366
Condition 6	612.1	0.1495	0.1497

4.7.2 Use of Joukowsky Formula

The Joukowsky pressure rise formula (Equation 3.35) can be used to calculate the initial velocity resulting from fast closure of a valve. The following equation is the rearranged Joukowsky formula and Table 4.4 shows the comparison of the initial velocity values by the volumetric method and the Joukowsky equation according to the specified six different flow conditions. There is good agreement between the two results.

$$V_0 = \frac{\Delta p}{\rho \cdot a} \tag{4.4}$$

4.7.3 Variable Pressure Tank Boundary Model for Gas

It is difficult to directly measure the mass flow rate or flow velocity in gas flows. This research uses the relationship of the variation of the pressure and mass in the constant tank volume to calculate the mass flow rate of air. This relationship can be represented by the equation of state.

$$\Delta p_t \cdot \forall_t = \Delta m_{out} \cdot R \cdot T \tag{4.5}$$

where Δp_t is the variation of tank pressure, $\forall_t$ is the volume of the tank, and Δm_{out} is the decreased mass from the tank during a test. If we neglect the temperature variation in the tank during tests, the variation of mass flow rate is a function of pressure only. The tank pressure can be easily measured by a pressure transducer. This relationship is incorporated into boundary condition to calculate the mass flow rate and the flow velocity of a gas pipeline at every time step.

A laboratory experiment was undertaken for the verification of the proposed variable pressure tank boundary model. Fig. 4.20 shows the layout of the pipeline system for the test. The west and east tanks were pressurised by air compressor after closing the east inline valve and the air was used as the fluid medium for tests. Fig. 4.21 shows the comparison between measured pressures at both tanks and their computed pressures by using variable pressure tank boundary model after the fast opening of the east inline valve.

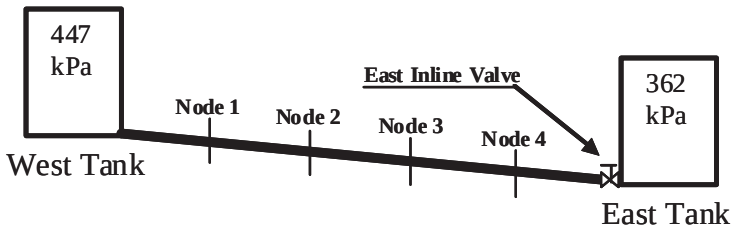

Figure 4.20 Layout of Experimental Pipeline Apparatus

The pressure of the west tank rapidly decreases and the pressure of east tank rapidly increases before the pressures of both tanks equilibrate at approximately 4.5 seconds. The model accurately simulates the phase of the experimental data. Fig. 4.22 shows the computed velocities at each node by using the variable pressure tank boundary model during this test. The velocities of all nodes abruptly decrease until the velocities are zero and the graph shows mild fluctuation of velocity profiles after 4.5 seconds.

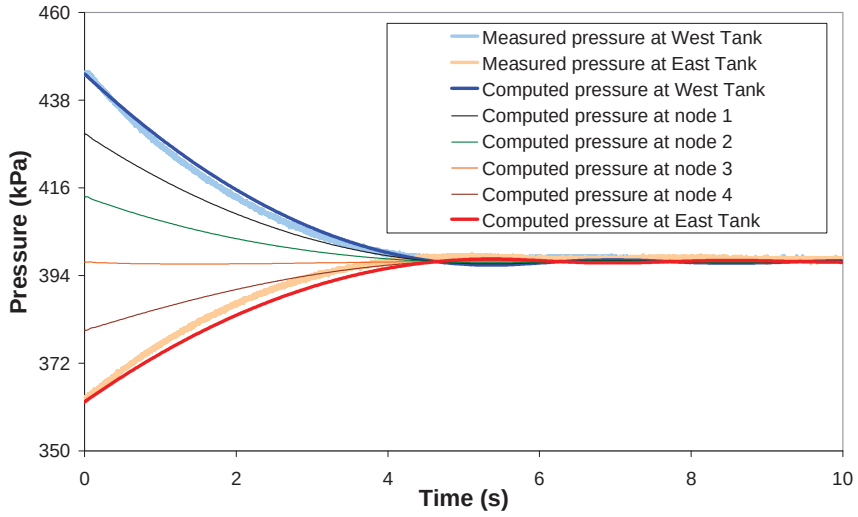

Figure 4.21 Measured and Computed Variable Pressure Tank Boundary

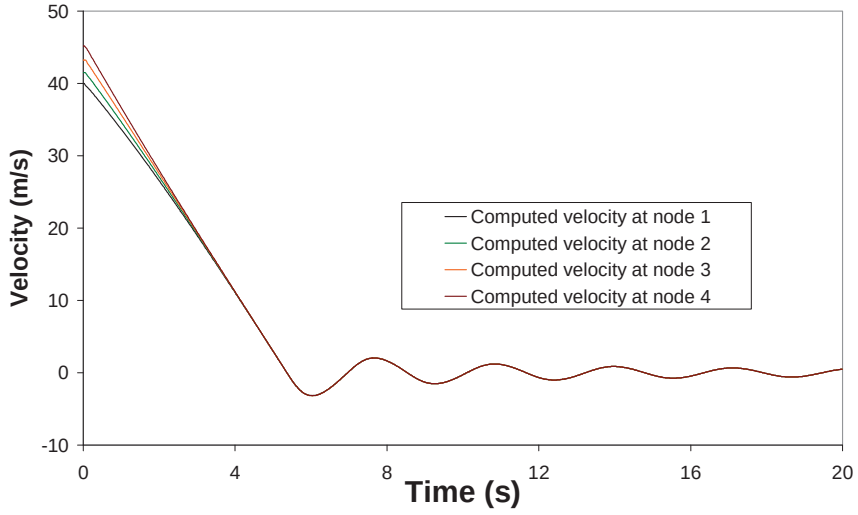

Figure 4.22 Computed Velocities by using Variable Pressure Tank Boundary Model

4.8 CONCLUSIONS

This chapter presents information of the pipeline apparatus that is needed for verification of the liquid and gas transient analysis models based on the conservative solution scheme. Also, the pipeline apparatus is used for examining in significant detail the effect of a distributed energy loss component (unsteady pipe wall friction) and local loss components (pipeline system abnormalities or flow control components) during a transient event. Experimental validation plays an important role in the overall contribution of this research. Comprehensive experimental tests have been carried out including the effects of unsteady pipe wall friction (Chapter 5), pipe leakage (Chapter 6), entrapped air pockets (Chapter 7), orifices and blockages (Chapter 8), and the non-linear elastic deformability (viscoelastic) of polyethylene pipe (Chapter 9) on transients in water and gas pipelines. Also, these tests are repeatable.

CHAPTER 5

UNSTEADY FRICTION IN THE CONSERVATIVE SOLUTION SCHEME

Understanding the unsteady hydraulic resistance behaviour caused by pipe wall shear stress is of great importance for the dynamic calculation in system design and calibration. This is especially true for long simulation times (beyond the first wave cycle of transient pressure) and practical applications (pipeline fault detection or assessment using transient flow data). The friction models based on the assumption of steady friction loss cannot accurately describe the real physical phenomena of fast transient events. Previously, various unsteady friction models have been used to evaluate energy dissipation by wall friction in waterhammer models based on the method of characteristics (MOC).

This chapter reviews a number of unsteady friction models for transient pipe flow and shows the application of unsteady friction models within a conservative formulation using the finite difference method (FDM). Various unsteady friction models based on convolution weighting functions are incorporated and modified in the conservative solution scheme for both transient laminar and turbulent flows. These models are compared with the measurement data of laboratory experiments for water and gas transient flows. The unsteady friction models based on the convolution weighting functions, originally developed for water (slightly compressible) transient flow, are applied to gas transient flows to verify their effectiveness for compressible flows.

5.1 REVIEW OF FRICTION MODELS FOR TRANSIENT FLOW

Pipe friction in transient flow is a high-dimensional physical complex phenomenon. A number of two-dimensional axisymmetric models have been proposed to describe unsteady friction during transients by including the actual velocity distribution across a section of pipe [Wood and Funk, 1970; Ohmi et al., 1985a; Bratland, 1986; Vardy and Hwang, 1991; Eichinger and Lein, 1992; Silva-Araya and Chaudhry, 1997 and 2001; Pezzinga, 1999; Ghidaoui et al., 2002; Zhao and Ghidaoui, 2003]. While these models provide more detail of the physical phenomena than one-dimensional approaches, the practical application (extensive pipe network, real-time flow monitoring, pipeline fault detection and assessment using inverse analysis by evolution algorithm) of these models has been difficult when considering the requirement of significant large computational time and memory space for such a rapidly varying flow. Current one-dimensional methods to represent physical phenomena of wall shear stress during flow disturbances may be classified into two categories based on correction coefficients for instantaneous accelerating/decelerating flow and based on convolution weighting functions for past velocities/accelerations. The unsteady friction models based on correction coefficients are the most commonly used and practical method due to relatively easy applicability. The extra energy loss during transients is proportional to a correction coefficient that is determined empirically or theoretically. The unsteady friction models based on convolution weighting functions consider the physical phenomena of flow turbulence viscosity and the relationship for the decay of the wall shear stress following a sudden velocity change. These approaches do not require a correction coefficient that must be calibrated for analysing certain flow conditions and take into account the two-dimensional behaviour of velocity profile.

5.1.1 Quasi-Steady Friction Models

The pipe friction that results from the pipe wall shear stress during transient events has been traditionally approximated by a steady-state friction relationship, which is usually described based on the Darcy-Weisbach friction formula.

$$h_f(t) \cong h_{sf}(t) = \frac{f(t) \cdot V(t) \cdot |V(t)|}{2gD} \tag{5.1}$$

where h_f is the total head loss due to pipe wall friction, h_{sf} is the quasi-steady head loss as a function of time (t), and f is the Darcy-Weisbach friction factor. In laminar flow, the friction factor f can be determined by the Hagen-Poiseuille law, $f = 64/N_R$, which indicates a direct relationship between the friction factor f and the Reynolds number N_R. The pipe flow is hydraulically smooth (see Eq. 5.2a). When the Reynolds number approaches a higher value (N_R *>2,000*), the flow becomes turbulent. At high Reynolds number, the value of f becomes independent of the Reynolds number and depends only on the relative roughness (pipe material roughness height/pipe diameter) ε/D. In this case, the pipe behaves as a hydraulically rough pipe (see Eq. 5.2b). In between these two extreme cases for transition turbulent flow, the pipe behaves neither smoothly nor completely roughly. Eq. 5.2c represents this intermediate range. The equations below show the relationship between friction factor and pipe wall condition from hydraulic smooth to rough pipe flow based on laboratory experimental data [Hwang and Houghtalen, 1996].

Completely hydraulic smooth pipe flow

$$\frac{1}{\sqrt{f}} = 2\log\left(\frac{N_R\sqrt{f}}{2.51}\right) \tag{5.2a}$$

Completely hydraulic rough pipe flow

$$\frac{1}{\sqrt{f}} = 2\log\left(3.7\frac{D}{\varepsilon}\right) \tag{5.2b}$$

For transition turbulent flow

$$\frac{1}{\sqrt{f}} = -2\log\left(\frac{\frac{\varepsilon}{D}}{3.7} + \frac{2.51}{N_R\sqrt{f}}\right) \tag{5.2c}$$

Many experimental studies have tested the validity of the assumption of steady friction models for transient analysis. This assumption is satisfactory for very slow transients, where the cross-sectional velocity profile is maintained in the steady-state flow, and for the first pressure wave cycle (initial pressure rise) after generating a transient event. However, the initial pressure rise is nearly independent of friction, and thus it can be easily calculated with the Allievi expression (generally attributed to Joukowsky, Eq. 3.35) where surface forces, body forces, inertial effects, friction, and reflected wave interferences are ignored.

Experimental validation of steady-state friction models for fast transients has showed significant discrepancies in pressure wave attenuation (damping) and dispersion (wave phase shift) when the simulation time exceeds the first pressure wave cycle. These inaccuracies lead to erroneous prediction of real-time flow monitoring and pipeline fault detection. To consider extra energy losses during transients, the total energy loss by pipe wall friction can be expressed as a sum of the quasi-steady energy loss component h_{sf} and unsteady energy loss component h_{uf}.

$$h_f(t) = h_{sf}(t) + h_{uf}(t) \tag{5.3}$$

The unsteady friction component represents the transient-induced changes in the velocity profile, which often involves flow reversal and large energy gradients (no-slip condition) near the pipe wall [Ghidaoui et al., 2005]. The following two sections review a number of unsteady friction models used for transient pipe flow.

5.1.2 Unsteady Friction Models Based on Correction Coefficients

In this approach, the additional energy dissipation due to wall shear stress during transients is related to a correction coefficient C for acceleration terms of momentum equation. Correction coefficients considered the additional transient effects on boundary resistance and momentum flux of local velocity.

$$h_f = h_{sf} + \frac{C}{g}\frac{\partial V}{\partial t} \tag{5.4}$$

where $\partial V/\partial t$ = temporal acceleration. While this approach is easy to implement in a numerical scheme, the need to determine the correction coefficients is a significant disadvantage. Numerous studies have attempted to deduce the correction coefficients based on experiments and higher dimensional models.

Early studies show that flow acceleration and deceleration play an important role for boundary resistance in unsteady flow motion. They found that pipe wall shear stress at any instant during accelerated or decelerated flow was slightly different from the equivalent

steady-state case through a uniform conduit. Daily et al. [1956] and Shuy [1996] obtained two distinct correction coefficient values for accelerating flows and decelerating flows through experimental data. The coefficient of Carstens and Roller [1959] is a function of *n* in the universal power law for the velocity distribution, which is dependent on the Reynolds number.

A modification of these early studies was introduced by the research group in Italy [Greco, 1990; Brunone et al. 1991a and 1991b]. They proposed that the correction coefficient has an effect on both temporal acceleration and spatial acceleration.

$$h_f = h_{sf} + \frac{k_3}{g}\left(\frac{\partial V}{\partial t} - a\frac{\partial V}{\partial x}\right) \tag{5.5a}$$

where a = wavespeed, $\partial V/\partial x$ = convective acceleration, and k_3 = correction coefficient for unsteady friction, which is determined empirically by trial and error for certain flow conditions. Vardy and Brown [1995] analytically deduced shear decay coefficients to predict the correction coefficient k_3 and Pezzinga [2000] used a more physically detailed model to obtain the coefficient by two-dimensional approach. Brunone et al. [2003] and Bouazza and Brunelle [2004] showed that the correction coefficient varied with time and space. Recent history of pressure head maximums was used as feedback to update correction coefficient during transients.

Bergant et al. [1999], Vítkovský et al. [2000b], and Pezzinga [2000] modified the Brunone et al. [1991a and 1991b] model because the equation fails to predict the correct sign of the convective term under particular flow and pressure wave directions in acceleration and deceleration phases. Eq. (5.5b) gives the correct sign of convective term for all possible flows and wave directions.

$$h_f = h_{sf} + \frac{k_3}{g}\left(\frac{\partial V}{\partial t} + a \cdot sign(V)\left|\frac{\partial V}{\partial x}\right|\right) \tag{5.5b}$$

Recently, Vítkovský et al. [2006] showed that even the modified Brunone et al. model failed to correctly simulate some types of transient events, such as valve opening events. They pointed out that this general deficiency of the model is a significant disadvantage for

simulating more complex pipelines or pipe networks, where various types of transient flow conditions occur simultaneously.

5.1.3 Unsteady Friction Models Based on Convolution Weighting Functions

Many researchers have dealt with frequency response characteristics of fluid lines to find analytical expressions for transient response in laminar flow in the frequency domain. Their methods are based on the classical linear theory of transfer operators for pressure and flow at two cross sections of pipelines. The wall shear stress becomes a function of frequency as well as mean velocity (frequency-dependent). The higher frequency components of the Fourier or Laplace spectrum of the wave are subjected to greater attenuation owing to increased wall shear. Brown [1962] developed analytical solution of frequency-dependent viscous effects in the propagation of pressure waves for both liquids and gases. He derived the characteristic impedance function and propagation operator, which could determine transient response and related the flow to the pressure. D'Souza and Oldenburger [1964] derived transfer matrix relating dynamic pressure and velocity variables for small diameter hydraulic lines. These functions included the effects of fluid viscosity and compressibility during transients. Holmboe and Rouleau [1967] performed two experiments with high-viscosity and low-viscosity liquids to verify the frequency-dependent friction models. They could accurately predict the distortion and decay of transients in constant diameter lines.

Zielke [1968] showed the successful implementation of the analytical solutions (as shown in Appendix A) of frequency-dependent wall shear stress for the method of characteristics (MOC) in the time domain. In his model, wall shear stress for transient laminar pipe flow is related to the instantaneous mean velocity and to the weighted past velocity changes in the pipe cross-section under the assumptions of fully developed flow and axisymmetric velocity profile during transients.

$$h_f = h_{sf} + \frac{16\nu}{gD^2}\int_0^t \frac{\partial V}{\partial t}(u)W(t-u)du \qquad (5.6)$$

where v = kinematic viscosity based on the initial flow conditions, W = weighting function, and u = time used in the convolution integral. The weighting functions are defined in terms of the dimensionless time $\tau=4vt/D^2$. This formulation takes into account two-dimensional behaviour of the velocity profile that results in frequency-dependent attenuation and slight frequency-dependent dispersion of transient pressure waves.

The weighting function for laminar flow was analytically derived by assuming a constant kinematic viscosity across the pipe that preserved and was an unchangeable condition for the duration of transients. The residue theorem and series expansion was applied. The resulting weighting function was split into two parts because of slow convergence of the exponential series for $\tau \leq 0.02$.

$$W(\tau)=\begin{cases}\sum_{j=1}^{6} m_j \tau^{\frac{1}{2}j-1} & for\ \ \tau \leq 0.02 \\ \sum_{j=1}^{5} e^{-n_j \tau} & for\ \ \tau > 0.02\end{cases} \tag{5.7}$$

where m_j = {0.282095, -1.25, 1.057855, 0.9375, 0.396696, -0.351563} and n_j = {26.3744, 70.8493, 135.0198, 218.9216, 322.5544}.

This convolution integral must be evaluated using all the previous time steps. This increases the computation time and requires a large amount of memory to store all previously calculated velocities. Efficient algorithms that provide an approximation to the convolution integral exist for the solution. Trikha [1975] and Suzuki et al. [1991] improved the computation speed by approximating Zielke's weighting function using a sum of exponential terms. Kagawa et al. [1983] provided a more accurate solution by fitting a higher number of exponential terms. In these approaches the flow history is lumped into the quantities at the previous time step, therefore the calculated quantities for the previous time step only need to be stored in the computer memory and there is no need to calculate the convolution integral from the beginning of simulation.

Other researchers have extended Zielke's approach to find weighting functions for transient turbulent flows. The derivation of a weighting function for turbulent flows is difficult because of the presence of eddy viscosity that varies with time. Vardy et al.

[1993] suggested a weighting function for low Reynolds number turbulent flows in smooth pipes by using two different viscosity distribution layers. The turbulent flow is assumed to have laminar viscosity in a layer close to the pipe wall and uniform infinite viscosity in the core region. Vardy and Brown [1995 and 1996] improved their weighting function for transient turbulent flows in smooth pipes by using linearly varied viscosity in the shear layer (see the Appendix B), but still uniform viscosity in the core. This model provided accurate results for various Reynolds number flows ranging from laminar to highly turbulent regime. The below equation is Vardy and Brown's weighting function.

$$W(\tau) = \frac{A^* e^{-B^* \tau}}{\sqrt{\tau}} \tag{5.8}$$

where A^* and B^* are coefficients for weighting function. Vardy and Brown [2003 and 2004b] further developed their coefficients for smooth and fully rough pipe turbulent flows by using linearly varied viscosity in the shear layer and uniform finite viscosity in the core region. The coefficients for smooth and fully rough pipe turbulent flows are calculated by the equations below.

For smooth pipe turbulent flows ($2{,}000 < N_R < 10^8$)

$$A^* = \frac{1}{2}\sqrt{\frac{\nu_w}{\pi \nu_{lam}}}, \quad B^* = \frac{N_R{}^{k_t}}{12.86} \quad with \quad k_t = \log_{10}(15.29 N_R{}^{-0.0567}) \tag{5.9}$$

For fully rough pipe turbulent flows ($10^{-6} < \varepsilon/D < 10^{-2}$)

$$A^* = 0.0103\sqrt{N_R}\left(\frac{\varepsilon}{D}\right)^{0.39} \quad and \quad B^* = 0.352 N_R \left(\frac{\varepsilon}{D}\right)^{0.41} \tag{5.10}$$

where ν_{lam} = laminar kinematic viscosity, ν_w = kinematic viscosity at the wall, and ε/D = relative roughness.

Similar to Zielke's model, the implementation of Vardy and Brown's models results in many convolutions that require significant computation time and memory storage of flow information for all past times. Efficient and accurate approximations of convolution integral type unsteady friction models for transient turbulent pipe flows are developed. Ghidaoui and Mansour [2002] examined the evolution of convolution integrals by seeking

a recursive approximation to Eq. 5.6. This approach is critically dependent on the choice of a simple numerical parameter that relates convolution integrals and their approximation. Vítkovský et al. [2004] and Vardy and Brown [2004a] developed improved implementations of the method by using the approximation of weighting function with a series of exponential terms. Vítkovský's method has the potential to simplify the treatment of turbulent flow weighting functions.

These unsteady friction models based on convolution weighting functions for laminar and turbulent flows were compared with measured data and numerical data by two-dimensional turbulent models [Vardy and Hwang, 1991 and Ghidaoui and Mansour, 2002]. The results were in good agreement with both laboratory and numerical experiments over a wide range of Reynolds numbers and wave frequencies.

5.2 IMPLEMENTATION OF UNSTEADY FRICTION MODELS

The governing equations for compressible and slightly compressible unsteady pipe flow were introduced by using the conservative solution scheme (CSS) in Chapter 3. This section shows the implementation of unsteady friction models based on convolution weighting functions for laminar and turbulent flows into the conservative scheme. Three different types of unsteady friction models are integrated in the conservative scheme. The first type is the original full convolution weighting function models for laminar and turbulent flows developed by Zielke [1968] and Vardy and Brown [2003 and 2004b] respectively. The second type is the approximated weighting function models by using a series of exponential terms. The original convolution weighting function models are approximated by Kagawa et al. [1983] and Vítkovský et al. [2004] approaches respectively. The final type is the modified models of previous two different models to improve computation time in the conservative scheme.

5.2.1 Original Convolution Weighting Function Models

Using the implementation of the implicit finite difference method for the conservative scheme, as shown in Fig. 5.1, the integral convolution in Eq. 5.6 for unsteady energy loss at point $P_{i,k}$ can be calculated from its first-order approximation as a full convolution in the scheme. The integral is approximated using the trapezoidal rule.

$$h_{i,k}(t) = 4\pi\nu\rho\sum_{j=1}^{k-1}(V_i^{k-j+1} - V_i^{k-j})W(j\Delta t) \tag{5.11}$$

where the weighting functions can be calculated from Eq. 5.7 for transient laminar flows and Eq. 5.8 for transient turbulent flows as functions of the dimensionless time τ.

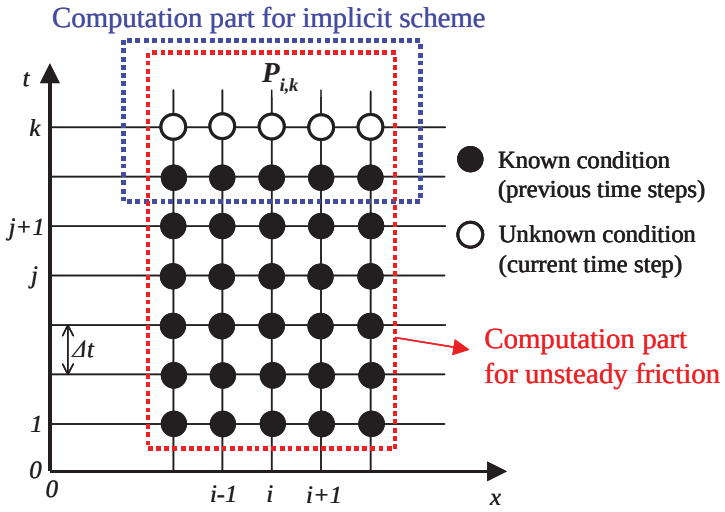

Figure 5.1 Computation Grid for Original Weighting Function Model

The unknown condition at a section is expressed in terms of the unknown values of these variables at the neighboring sections in the implicit finite difference method for the conservative scheme. Therefore, equations for the entire system have to be solved simultaneously as shown in Fig. 5.1. The four-point-centered implicit scheme in Eq. 3.54 discretises the Eq. 5.11 as

$$\begin{aligned} h_{i,k}(t) = {} & 2\pi\nu\alpha\left[\begin{array}{l}\rho_i^k\sum_{j=1}^{k-1}(V_i^{k-j+1} - V_i^{k-j})W(j\Delta t) \\ +\rho_{i-1}^k\sum_{j=1}^{k-1}(V_{i-1}^{k-j+1} - V_{i-1}^{k-j})W(j\Delta t)\end{array}\right] \\ & +2\pi\nu(1-\alpha)\left[\begin{array}{l}\rho_i^{k-1}\sum_{j=1}^{k-2}(V_i^{k-j} - V_i^{k-j-1})W(j\Delta t) \\ +\rho_{i-1}^{k-1}\sum_{j=1}^{k-2}(V_{i-1}^{k-j} - V_{i-1}^{k-j-1})W(j\Delta t)\end{array}\right] \end{aligned} \tag{5.12}$$

5.2.2 Approximated Weighting Function Models

The computation of original weighting function models requires full convolution at every space step by using all previous velocity history, therefore the computation time dramatically increases as the simulation time grows. Kagawa et al. [1983] provided an efficient solution to improve computational speed by approximating Zielke's weighting function with a sum of exponential terms.

$$W(\tau) \cong W_{app}(\tau) = \sum_{s=1}^{N} m_s e^{-n_s \tau} \tag{5.13}$$

where n_s and m_s are the fitted exponential sum coefficients for approximating the original weighting function (shown in Table 5.1), and the unsteady energy loss is expressed by a sum of N components $y_s(t)$ at time t.

$$\begin{aligned} h_{i,k}(t) &= 4\pi\nu\rho \int_0^t \frac{\partial V}{\partial t}(u) W(t-u)\, du \\ &\cong 4\pi\nu\rho \sum_{s=1}^{N} y_s(t) = 4\pi\nu\rho \int_0^t \frac{\partial V}{\partial t}(u) m_s e^{-n_s R_t (t-u)}\, du \end{aligned} \tag{5.14}$$

where $R_t = 4\nu/D^2$, which converts the time t into the dimensionless time τ. The component $y_s(t+\Delta t)$ at time $t+\Delta t$ splits the integral into the range 0 to t and t to $t+\Delta t$.

$$y_s(t+\Delta t) = \int_0^t \frac{\partial V}{\partial t}(u) m_s e^{-n_s R_t (t+\Delta t-u)}\, du + \int_0^{t+\Delta t} \frac{\partial V}{\partial t}(u) m_s e^{-n_s R_t (t+\Delta t-u)}\, du \tag{5.15}$$

The constant exponential part of the first term in Eq. 5.15 can be taken out of the integral and the final term is simplified by first-order approximation.

$$y_s(t+\Delta t) \cong e^{-n_s R_t \Delta t} \left\{ \int_0^t \frac{\partial V}{\partial t}(u) m_s e^{-n_s R_t (t-u)}\, du \right\} + m_s e^{-n_s 0.5 R_t \Delta t} \{V(t+\Delta t) - V(t)\} \tag{5.16}$$

The term in the first bracket is $y_s(t)$ that is calculated at a previous time step. Therefore, the final form for the component y_s is

$$y_s(t+\Delta t) \cong e^{-n_s R_t \Delta t} y_s(t) + m_s e^{-n_s 0.5 R_t \Delta t} \{V(t+\Delta t) - V(t)\} \tag{5.17}$$

All flow history is lumped into the quantities at the previous time step in this approach, therefore only the calculated quantities for the previous time step are stored in the computer memory and there is no need to calculate the convolution function from the beginning of simulation. The computation for unsteady friction in the conservative scheme is executed with three time step information (current and previous two time steps) after applying four-point-centered implicit discretisation as shown in Fig 5.2. Eq. 5.18 is the unsteady energy loss component of the approximated weighting function for the conservative scheme.

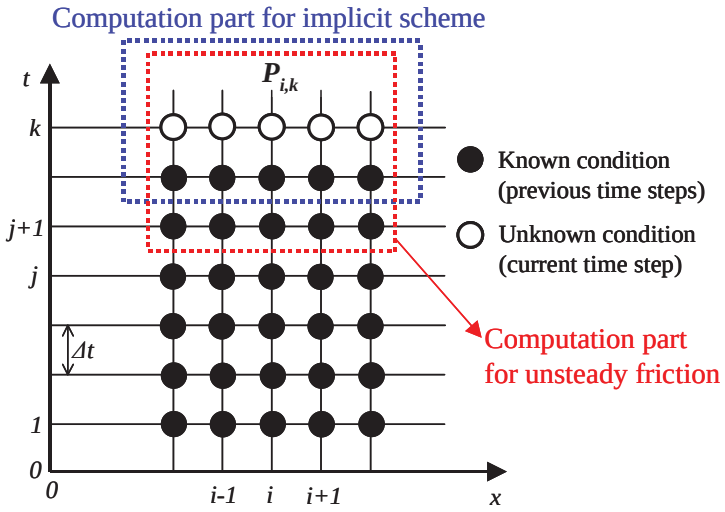

Figure 5.2 Computation Grid for Approximated Weighting Function Model

$$h_{i,k}(t) = 2\pi v\alpha \left[\begin{array}{l} \rho_i^k \sum_{s=1}^{N} \{e^{-n_s R_t \Delta t} \cdot y_s(t)_i^{k-1} + m_s \cdot e^{-n_s 0.5 R_t \Delta t} \cdot (V_i^k - V_i^{k-1})\} \\ + \rho_{i-1}^k \sum_{s=1}^{N} \{e^{-n_s R_t \Delta t} \cdot y_s(t)_{i-1}^{k-1} + m_s \cdot e^{-n_s 0.5 R_t \Delta t} \cdot (V_{i-1}^k - V_{i-1}^{k-1})\} \end{array} \right]$$

$$+ 2\pi v(1-\alpha) \left[\begin{array}{l} \rho_i^{k-1} \sum_{s=1}^{N} \{e^{-n_s R_t \Delta t} \cdot y_s(t)_i^{k-2} + m_s \cdot e^{-n_s 0.5 R_t \Delta t} \cdot (V_i^{k-1} - V_i^{k-2})\} \\ + \rho_{i-1}^{k-1} \sum_{s=1}^{N} \{e^{-n_s R_t \Delta t} \cdot y_s(t)_{i-1}^{k-2} + m_s \cdot e^{-n_s 0.5 R_t \Delta t} \cdot (V_{i-1}^{k-1} - V_{i-1}^{k-2})\} \end{array} \right] \tag{5.18}$$

Similar to Kagawa's approximation of the weighting function for transient laminar pipe flow, Vítkovský et al. [2004] proposed the efficient implementation of Vardy and Brown [2003 and 2004b] weighting functions for transient turbulent pipe flows by sum of exponential terms.

$$W(\tau) = \frac{A^* e^{-B^*\tau}}{\sqrt{\tau}} \cong \sum_{s=1}^{N} m_s e^{-n_s \tau} \tag{5.19}$$

where A^* and B^* are coefficients for the weighting functions that are dependent on Reynolds number of the flow and relative roughness of the pipe (Eq. 5.9 and 5.10). Therefore, the exponential coefficients n_s and m_s have to be refitted every time for the changes of pipe roughness and flow condition. Vítkovský et al. [2004] suggested the scaling procedure using A^* and B^* to avoid this problem. Rearrangement of Eq. 5.19 by the scaled exponential coefficients $m_s^* = m_s/A^*$ and $n_s^* = n_s - B^*$ produces

$$W^*_{app}(\tau) = \sum_{s=1}^{N} m_s^* e^{-n_s^* \tau} \tag{5.20}$$

where W^*_{app} is the approximate scaled weighting function. One set of fitted exponential coefficients m_s^* and n_s^* can be scaled to any weighting function given A^* and B^* (shown in Table 5.1). The same method as in the Kagawa's approximation is used for calculating the unsteady energy loss with Eqs. 5.14 to 5.18.

Table 5.1 Best Fit Exponential Sum Coefficients

		Kagawa et al. [1983] model			**Vítkovský et al. [2004] model**	
s		**m_s**	**n_s**		**m_s^***	**n_s^***
1		1.0	26.3744		5.03362	4.78793
2		1.16725	72.8033		6.48760	51.0897
3		2.20064	187.424		10.7735	210.868
4		3.92861	536.626		19.9040	765.030
5		6.78788	1570.60		37.4754	2731.01
6		11.6761	4618.13		70.7117	9731.44
7		20.0612	13601.1		133.460	34668.5
8		34.4541	40082.5		251.933	123511
9		59.1642	118153.0		476.597	440374
10		101.590	348316.0		932.860	1590300

5.2.3 Modified Weighting Function Models for Conservative Scheme

This section introduces a more efficient computation approach for the original and approximated weighting function models to improve computational time in the conservative solution scheme. The unsteady energy loss models are discretised by four-point-centered implicit finite difference approximation using the current and previous time step information in conservative scheme. The current unknown variables at a section are solved simultaneously with the current unknown variables at the neighboring sections and previous known variables. This procedure causes an increase in the computational time when incorporating unsteady friction models into the conservative scheme. Eq. 5.12 is based on original full convolution weighting functions and Eq. 5.18 is based on approximated weighting functions that can be simplified by dropping the current time step of computational part for unsteady energy loss (see Fig. 5.3).

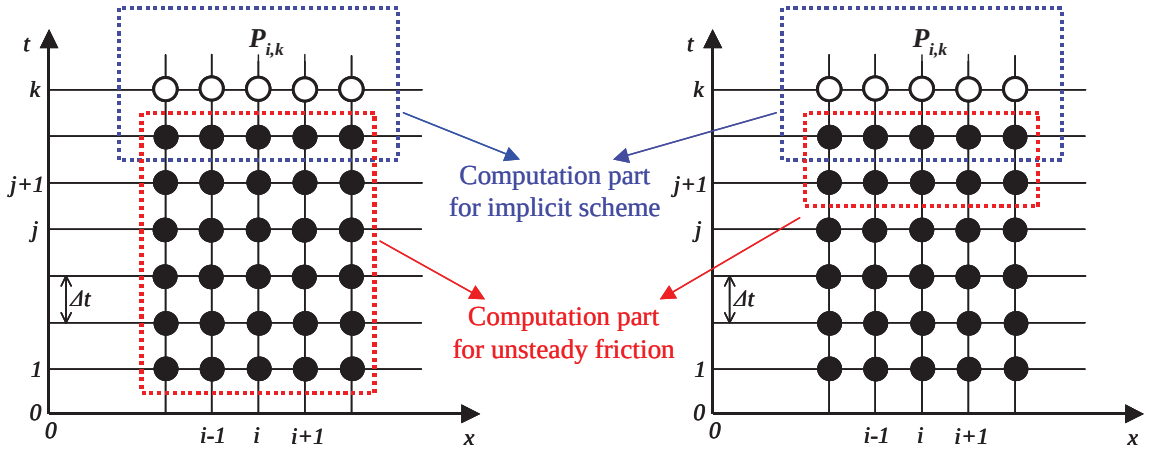

a) For Original Weighing Functions **b) For Approximated Weighting Functions**

Figure 5.3 Computation Grid for Modified Weighting Function Model

In this simplification, the computation part for implicit scheme does not directly calculate unsteady friction quantities at the current time step. The unsteady friction values at the previous time step are substituted for the unsteady friction of computation part for the implicit scheme. Therefore, the unknown current velocity variables V_i^k are dropped from Eq. 5.12 and 5.18. The equations below show the modification of the original and approximated weighting function models for the conservative scheme. The computational parts almost become half when compared to the Eq. 5.12 and 5.18.

Modified model for original convolution weighting function model

$$h_{i,k}(t) = 2\pi v * \left\{\alpha\rho_i^k + (1-\alpha)\rho_i^{k-1}\right\} * \left[\sum_{j=1}^{k-2}(V_i^{k-j} - V_i^{k-j-1})W(j\Delta t)\right] + 2\pi v * \left\{\alpha\rho_{i-1}^k + (1-\alpha)\rho_{i-1}^{k-1}\right\} * \left[\sum_{j=1}^{k-2}(V_{i-1}^{k-j} - V_{i-1}^{k-j-1})W(j\Delta t)\right] \tag{5.21}$$

Modified model for approximated weighting function model

$$h_{i,k}(t) = 2\pi v * \left\{\alpha\rho_i^k + (1-\alpha)\rho_i^{k-1}\right\} * \sum_{s=1}^{N}\{e^{-n_s R_t \Delta t} * y_s(t)_i^{k-2} + m_s * e^{-n_s 0.5 R_t \Delta t} * (V_i^{k-1} - V_i^{k-2})\} + 2\pi v * \left\{\alpha\rho_{i-1}^k + (1-\alpha)\rho_{i-1}^{k-1}\right\} * \sum_{s=1}^{N}\{e^{-n_s R_t \Delta t} * y_s(t)_{i-1}^{k-2} + m_s * e^{-n_s 0.5 R_t \Delta t} * (V_{i-1}^{k-1} - V_{i-1}^{k-2})\} \tag{5.22}$$

5.3 APPLICATION OF UNSTEADY FRICTION MODELS FOR GAS TRANSIENTS

This section considers the possibility of the application of unsteady friction models based on weighting functions to transient gas flows. The assumptions involved in developing weighting function type unsteady friction models are (i) the convective terms are negligible, (ii) the incompressible continuity equation is used, therefore the influence of mass storage on velocity profile is negligible, and (iii) the temperature variations are small enough so that the fluid viscosity across the pipe is considered to be constant or linearly varied frozen viscosity for the duration of the transients.

Unsteady friction models based on weighting functions were developed by neglecting the nonlinear convective acceleration terms $V\partial p/\partial x$ and $V\partial V/\partial x$ to simplify computational solution. These terms are usually very small when compared to the other terms in slightly compressible flows. However, in the systems with high-Mach-number (compressible flow with relatively high speed flow and low wavespeed), the neglecting of convective terms

may result in loss of accuracy of the simulation results. The convective acceleration terms are fully retained in the governing equations for the conservative scheme. These basic equations consider the inertial effect of compressible flow. Also, the velocity is very low near the pipe wall when considering the no-slip condition. The flow can be regarded as low-Mach number flow near the pipe wall. Therefore, the inertial effect due to wall shear stress is small and the convective terms can be neglected for developing unsteady friction models. In the same manner, the compressibility near the pipe wall is also relatively small. The unsteady friction can be developed using the incompressible continuity equation, although the compressibility of a gas is the dominant physical process for transient gas flow analysis. The equation of state in the conservative scheme considers gas compressibility during the simulation process.

Flow situations may be divided into two categories for analysis purposes, slow and fast transients. Slow transient are caused by changes in demand, for example, on a daily cycle and fast transients are caused by rapid shut-down or start-up of a system and short-term emergency, such as equipment failure and line-breakage. For the case of slow transients, the gas in the pipe has sufficient time to reach thermal equilibrium with the constant surrounding temperature. The flow completely exchanges heat with the outside, which is regarded as being a heat storage unit of infinite capacity with constant temperature (isothermal flow). Similarly, for the case of fast transients, pressure changes occur instantaneously. Therefore, there is no time for heat transfer to take place between the gas in the pipe and the surroundings. The flow has no heat exchange with the outside (adiabatic and, more especially, isentropic flow) [Osiadacz and Chaczykowski, 2001]. So, the temperature variations are small enough so that the fluid viscosity across the pipe is considered to be constant or linearly varied frozen viscosity for the duration of the transients, although the flow viscosity depends on local temperature. However, for many dynamic gas applications, the temperature profile of gas is a function of pipeline distance with local heat source or sink (non-isothermal and non-adiabatic flow). This heat transfer is calculated by the energy equation in the conservative scheme. The energy equation can consider heat transfer across the surface due to temperature gradients (thermal conduction) and the conversion of frictional work into thermal energy.

5.4 NUMERICAL INVESTIGATION FOR UNSTEADY FRICTION

Numerical experiments are presented to show the effect of the proposed unsteady friction models based on weighting functions for water and gas transient flows in a reservoir-pipeline-valve system (shown in Fig. 5.4). The transient analysis models incorporating unsteady friction term based on the conservative solution scheme simulate the system with compressible and incompressible fluids. The pipeline system is composed of a straight 40 m long copper pipeline (for numerical simulations of transient gas flows, 37.53 m pipeline with various pipeline materials is used) with 22.1 mm internal diameter and 1.6 mm wall thickness connecting two tanks. The test apparatus is almost equivalent to the laboratory apparatus in Chapter 4.

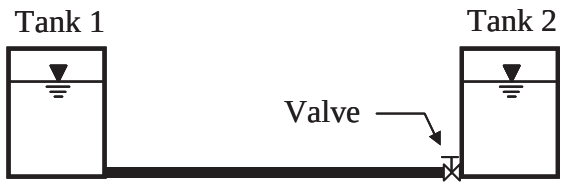

Figure 5.4 Pipeline System for Numerical Experiments

5.4.1 Numerical Experiments for Transient Flows in Water

Numerical experiments are executed for three different flow conditions, transient laminar flow and transient turbulent flows in smooth and rough pipe. Each flow condition is simulated with five different friction estimation models, including the steady friction model and unsteady friction models based on original, approximated, and modified weighting functions in the conservative scheme. A total of 12 different unsteady friction models are used for numerical experiments. Table 5.2 shows the used unsteady friction models and their shortened names. The transient event is generated by the rapid closure of a downstream end valve at a tank. Water and surrounding temperatures are assumed to be 20^{o}C and it is assumed that there is no temperature variation during a test. The wavespeed is 1,335 m/s in the copper pipe. The flow information is observed at the middle of pipe and the downstream valve.

Table 5.2 Unsteady Friction Models for Water Transients

Flow Condition	Unsteady Friction based on Weighting Function Model (WFM)	Shortened Name
Laminar Flow	**Original WFM** (Eqs. 5.12 and 5.7)	Original
	Modified original WFM (Eqs. 5.21 and 5.7)	Mod-original
	Approximated WFM (Eqs. 5.18 with coefficients in Table 5.1)	Approx
	Modified approximated WFM (Eqs. 5.22 with coefficients in Table 5.1)	Mod-approx
Turbulent Flow in Smooth Pipe	**Original WFM** (Eqs. 5.12, 5.8, and 5.9)	Original
	Modified original WFM (Eqs. 5.21, 5.8, and 5.9)	Mod-original
	Approximated WFM (Eqs. 5.18, 5.9, and 5.20 with coefficients in Table 5.1)	Approx
	Modified approximated WFM (Eqs. 5.22, 5.9, and 5.20 with coefficients in Table 5.1)	Mod-approx
Turbulent Flow in Rough Pipe	**Original WFM** (Eqs. 5.12, 5.8, and 5.10)	Original
	Modified original WFM (Eqs. 5.21, 5.8, and 5.10)	Mod-original
	Approximated WFM (Eqs. 5.18, 5.10, and 5.20 with coefficients in Table 5.1)	Approx
	Modified approximated WFM (Eqs. 5.22, 5.10, and 5.20 with coefficients in Table 5.1)	Mod-approx

Fig. 5.5 shows the simulation results for transient laminar flow at the end of pipe and at the middle of pipe. The initial flow velocity and Reynolds number are 0.075 m/s and 1,640 respectively. The thick gray line is the simulation result using steady-state friction approximation during transients. The steady-state friction model shows significant discrepancies in the magnitude of pressure wave compared with the results of unsteady friction models when the simulation time exceeds the first pressure wave cycle. The situation is similar for transient turbulent flows in smooth and rough pipe (shown in Figs. 5.6 and 5.7). The results using four different unsteady frictions based on original weighting function model (original) and its modified model (mod-original), and approximated weighting function model (approx) and its modified model (mod-approx) are presented and are shown to plot on the same line. This means that the modified models for the conservative scheme have excellent agreement with the original and approximated weighting function models. The results of unsteady friction models show serious pressure attenuation due to the additional unsteady energy loss and slight dispersion of transient pressure waves.

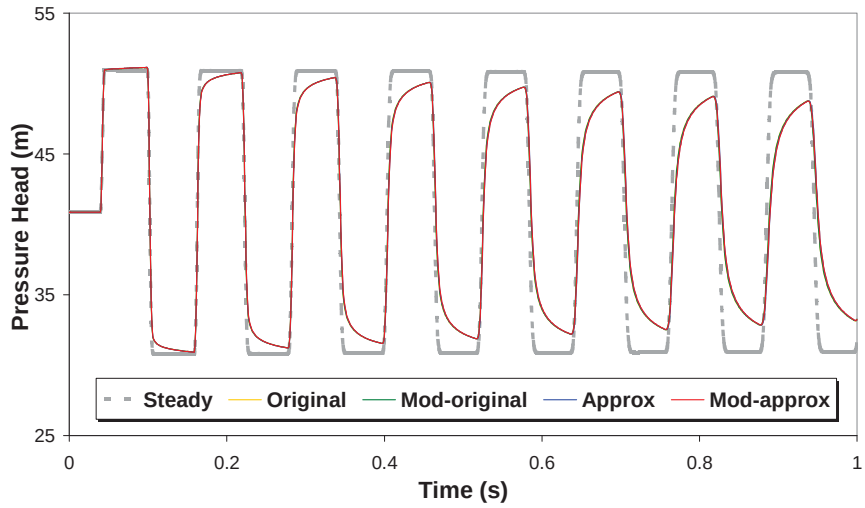

(a) Pressure Data at the Downstream Valve

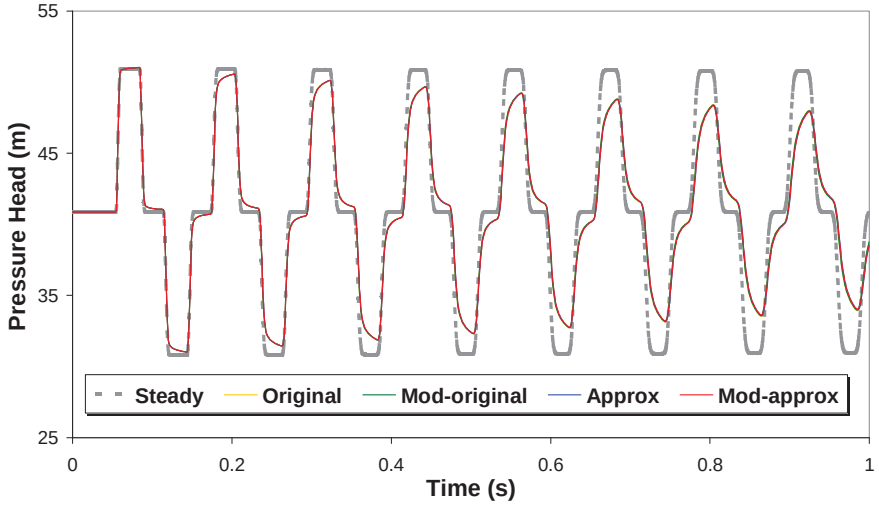

(b) Pressure Data at the Middle of Pipe

Figure 5.5 Results for Transient Laminar Flow

Fig. 5.6 shows the simulation results for transient turbulent flow in smooth pipe flow. The initial flow velocity and Reynolds number are 0.744 m/s and 16,393 respectively. The results of steady and unsteady friction models are similar to the results for transient laminar flow. The steady friction model underestimates the damping of pressure wave and does not predict the evolution of the shape of the pressure oscillations, demonstrating its inability to model strong frequency-dependent attenuation. The modified models have the same results as the original and approximated weighting function models.

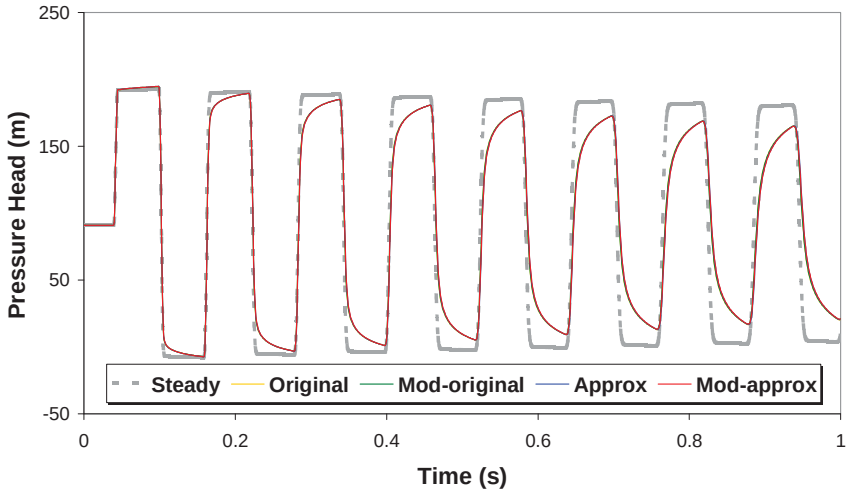

(a) Pressure Data at the Downstream Valve

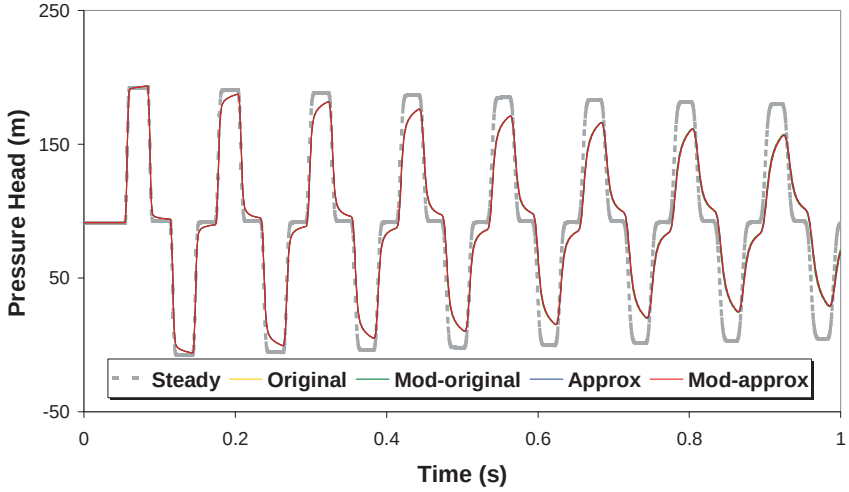

(b) Pressure Data at the Middle of Pipe

Figure 5.6 Results for Transient Turbulent Flow in a Smooth Pipe

Fig. 5.7 shows the simulation results for transient turbulent flow in rough pipe flow. The initial flow velocity and Reynolds number are 0.744 m/s and 16,393 respectively. The relative roughness is 0.009. The results are similar to the above two flow conditions.

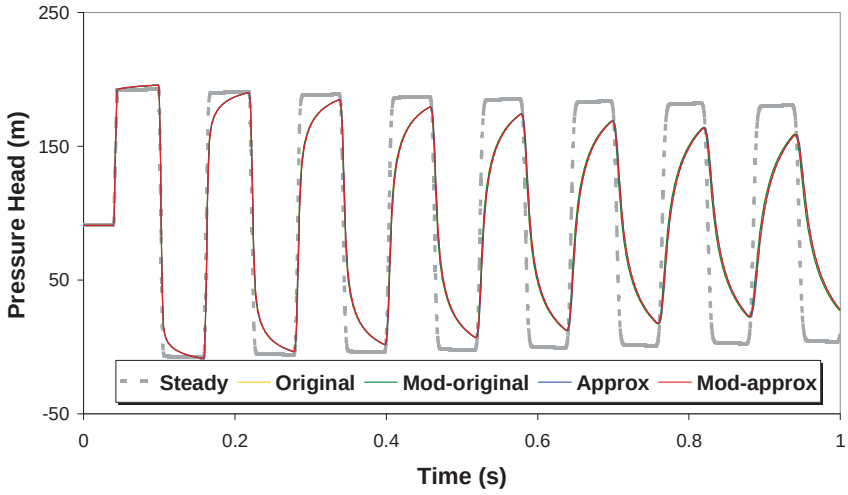

(a) Pressure Data at the Downstream Valve

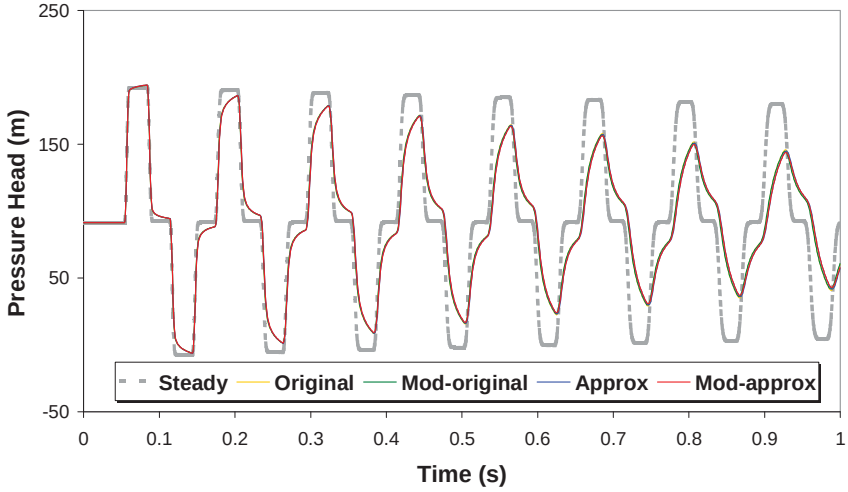

(b) Pressure Data at the Middle of Pipe

Figure 5.7 Results for Transient Turbulent Flow in a Rough Pipe

Table 5.3 shows the central processing unit (CPU) time ratios for the above simulations. The simulation time of steady friction model is taken as the standard for each flow condition to compare the simulation times for unsteady friction models. The simulation times for original weighting function models are significantly larger because of their full convolution at every space step by using all previous velocity history. They require serious computation intensity. The approximated weighting function models dramatically reduce the computational time. The modified original models dramatically decrease the simulation times of the original and approximated models. The simulation times of modified approximated models almost reach the simulation times for steady friction models.

Table 5.3 Computational Time Ratios for Friction Models

Flow Condition	Shortened Name for Friction Model	CPU Time Ratio
Laminar Flow	Steady	1.00
	Original	10.62
	Mod-original	7.68
	Approx	1.28
	Mod-approx	**1.13**
Turbulent Flow in Smooth Pipe	Steady	1.00
	Original	32.81
	Mod-original	22.42
	Approx	1.31
	Mod-approx	**1.16**
Turbulent Flow in Rough Pipe	Steady	1.00
	Original	36.87
	Mod-original	25.16
	Approx	2.76
	Mod-approx	**1.16**

5.4.2 Numerical Experiments for Transient Gas Flows

In the same pipeline as was described in the section above, gas transient experiments were tested. Dry air of 20^{o}C is used for the tests. The wavespeed is 343 m/s. Unsteady friction models based on modified-approximated weighting function simulate the numerical experiments and their results are compared with the steady friction model.

Fig. 5.8 shows the pressure variation for gas transient laminar flow at the end of pipe and at the middle of pipe. The initial flow velocity and Reynolds number are 1.107 m/s and 1,620 respectively. The unsteady friction model based on modified-approximated weighting function is incorporated into the polytropic process gas transient analysis model proposed in Chapter 3. This model does not use the energy equation for simulating the heat exchange. The heat exchange of the system is considered only by a polytropic process exponent n. If a perfect gas is assumed, at one extreme the process may be isothermal n = 1 or at the other limit it may be isentropic (reversible adiabatic), in which case n = 1.4 for air. The simulation uses 1.2 of polytropic process exponent because often an average value of 1.2 is usually used in design calculations. The simulation results are similar to water transient flows because the flow velocity is relatively slow in laminar flow condition when considering normal gas flows (fully turbulent and high-Mach number flow). In this case, the flow can be considered low-Mach number flow and slightly compressible flow. The fluid compressibility is not the dominant physical process for transient analysis. The

steady friction model shows significant discrepancies compared with the result of unsteady friction model. The unsteady friction model shows frequency-dependent attenuation (pressure wave damping) and dispersion (pressure wave phase shift).

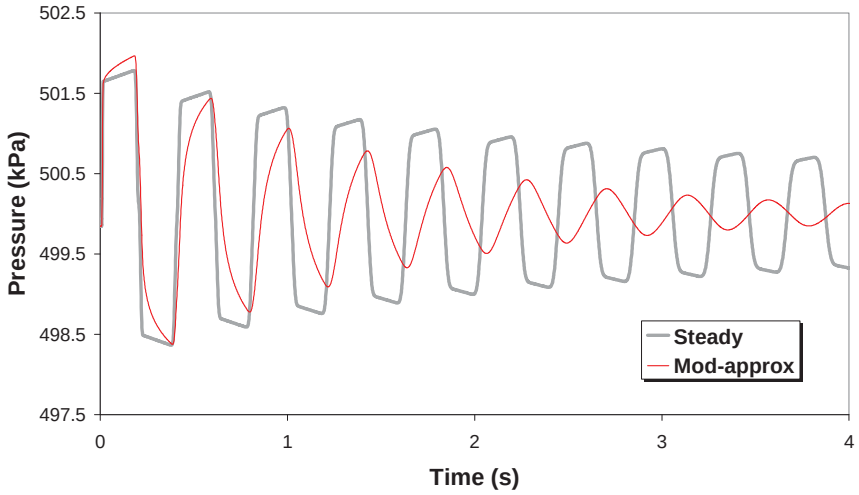

(a) Pressure Variation at the Downstream Valve

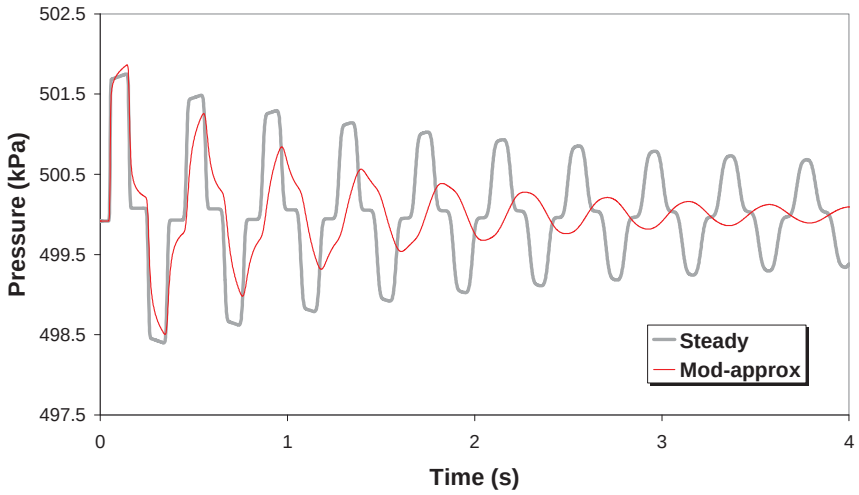

(b) Pressure Variation at the Middle of Pipe

Figure 5.8 Pressure Variation in a Gas Transient Laminar Flow

Fig. 5.9 shows the density variation for gas transient laminar flow at the end of pipe and at the middle of pipe when using the polytropic gas transient analysis model. The results are similar to the above pressure variation.

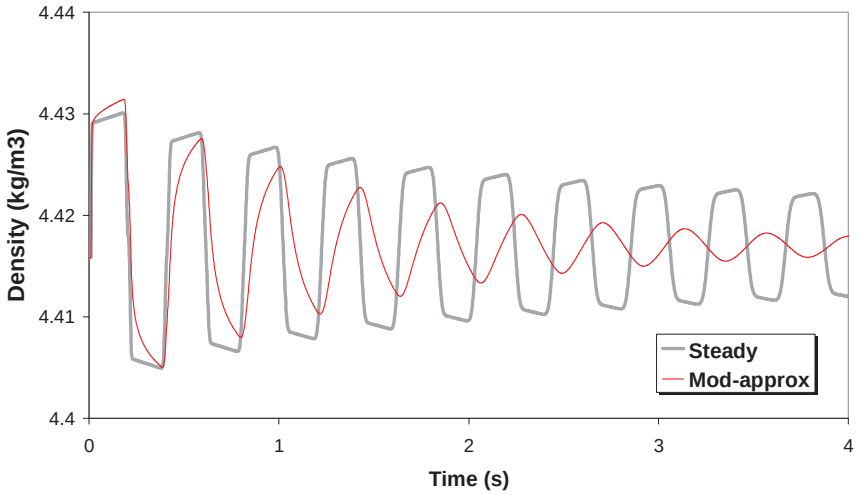

(a) Density Variation at the Downstream Valve

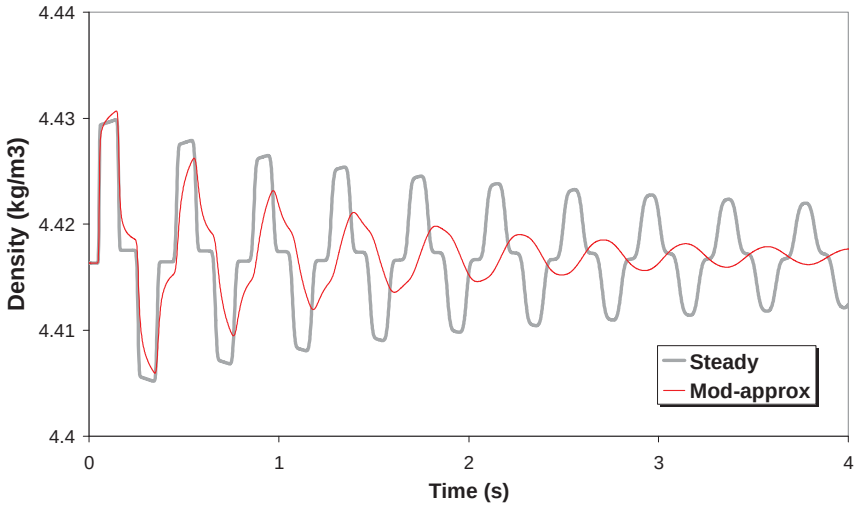

(b) Density Variation at the Middle of Pipe

Figure 5.9 Density Variation in a Gas Transient Laminar Flow

Figs. 5.10 and 5.11 show the pressure and density variation for gas transient turbulent flow at the end of pipe and at the middle of pipe. Turbulent flow is the typical situation in gas pipeline systems. The initial flow velocity and Reynolds number are 14.57 m/s and 21,330 respectively. Unlike the results of gas transient laminar flow, the results show significant line-packing effect. The storage capacity of a pipeline increases due to the relatively big change in pressure. The operation of a gas pipeline is affected by the compressibility of the gas. Line-packing is the total amount of gas contained in the pipeline that will change over time if there is an imbalance between inflow and outflow. The results of the steady friction model are similar to the results of unsteady friction model in the magnitude of pressure wave because the fluid compressibility is the dominant physical process for

transient analysis rather than frictional effect. The unsteady friction model shows slightly frequency-dependent dispersion in the phase of pressure wave.

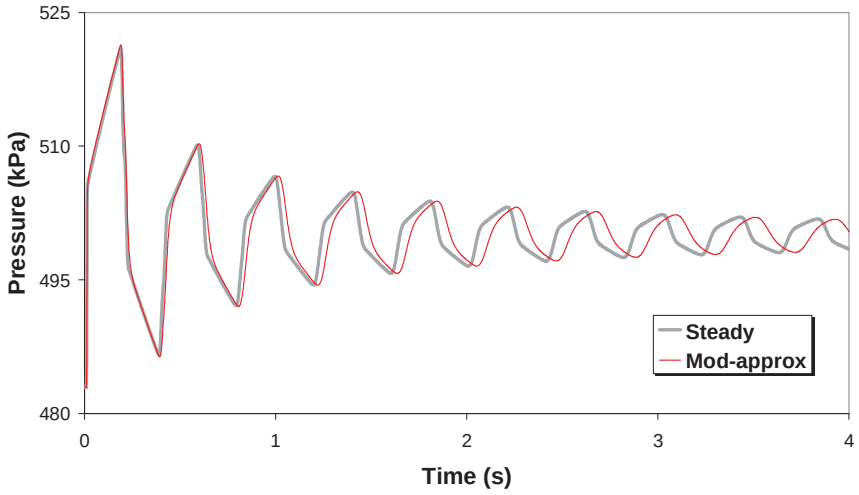

(a) Pressure Variation at the Downstream Valve

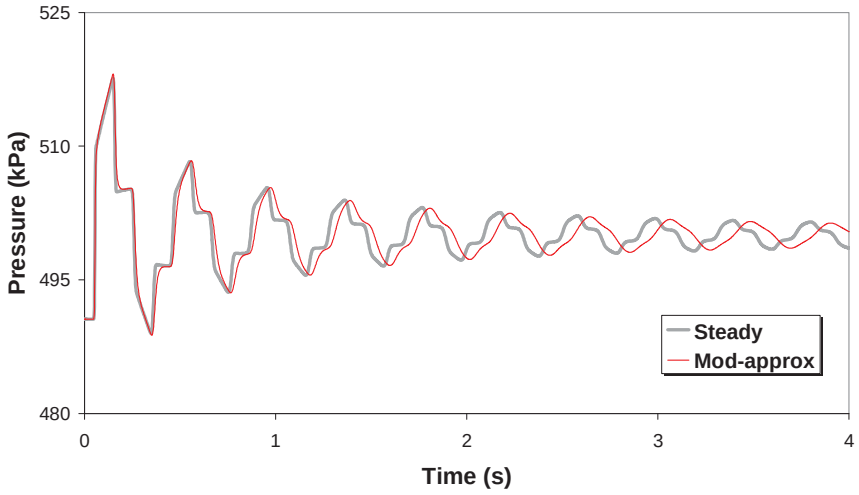

(b) Pressure Variation at the Middle of Pipe

Figure 5.10 Pressure Variation in a Gas Transient Turbulent Flow

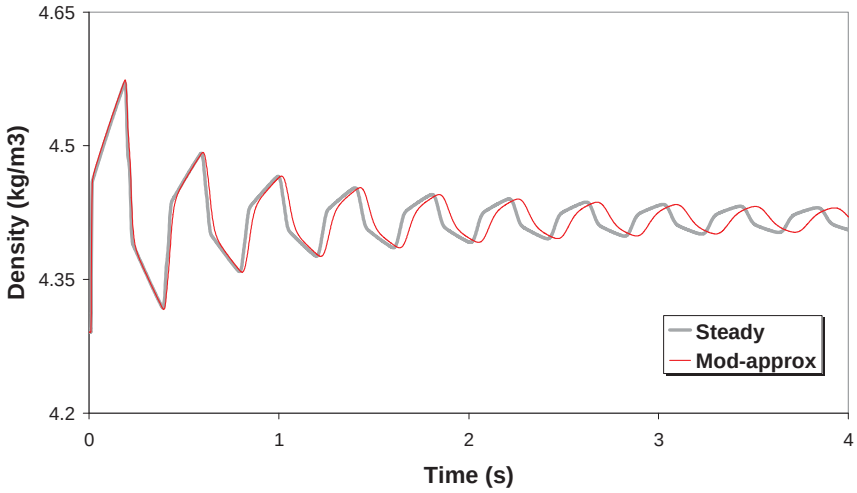

(a) Density Variation at the Downstream Valve

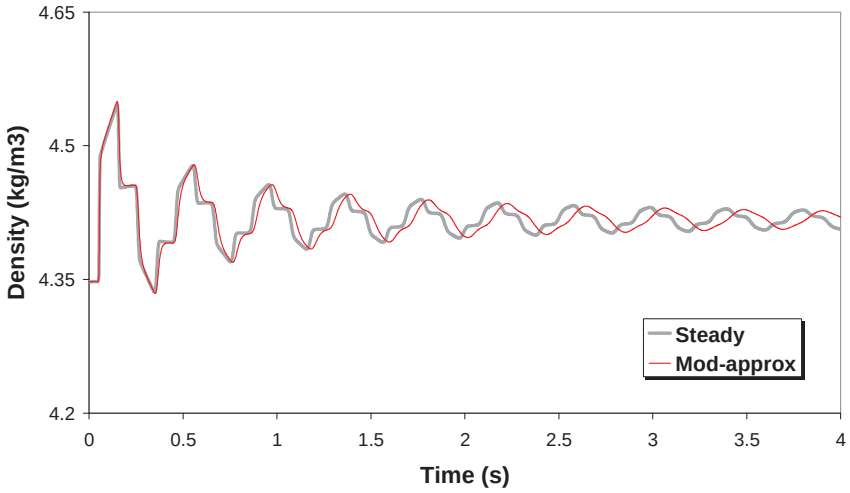

(b) Density Variation at the Middle of Pipe

Figure 5.11 Density Variation in a Gas Transient Turbulent Flow

Fig. 5.12 shows the pressure results when using different polytropic process exponents in the same gas transient turbulent flow. In the case of isothermal process, the gas in the pipe reaches thermal equilibrium with surrounding temperature. The variation of temperature due to transient event is negligible. On the other hand, the temperature variation for adiabatic process (more especially, isentropic process) affects on the wavespeed because local wavespeed is dependent on the local temperature. The wavespeed of an isentropic process is faster than that of an isothermal process. The thick gray line shows the results when the polytropic process is between isothermal and adiabatic process.

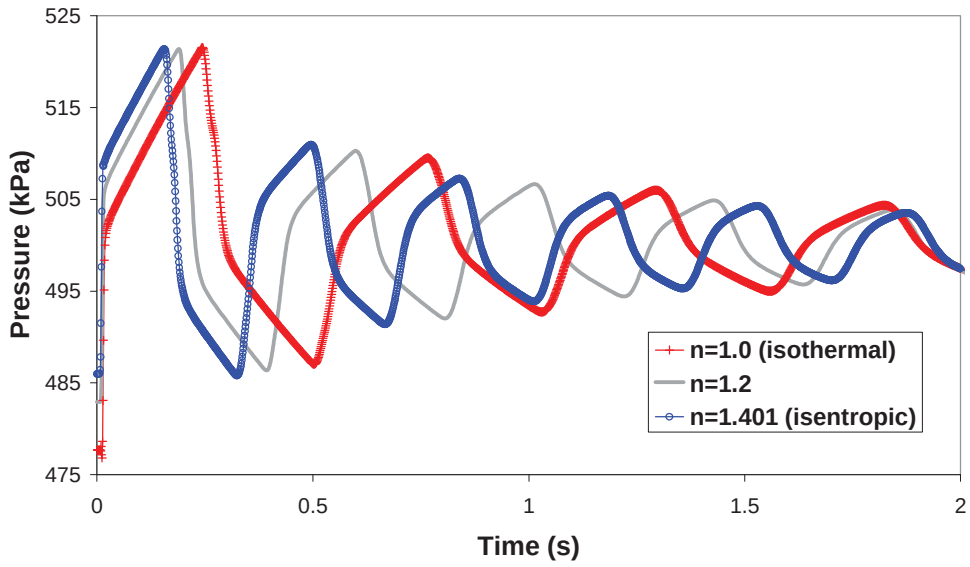

Figure 5.12 Pressure Variation under Different Polytropic Processes

Figs. 5.13 to 5.15 show the temperature variations in the same gas transient turbulent flow at the downstream end. The initial temperature of fluid and external environment is 20^{o}C. A generalized gas transient analysis model proposed in Chapter 3 is used for calculating temperature variation during transient events. This model can simulate one-dimensional gas transient problems including heat transfer across the surface due to temperature gradients (thermal conduction) and the conversion of frictional work into thermal energy. The energy equation directly calculates the variation of temperature during transients.

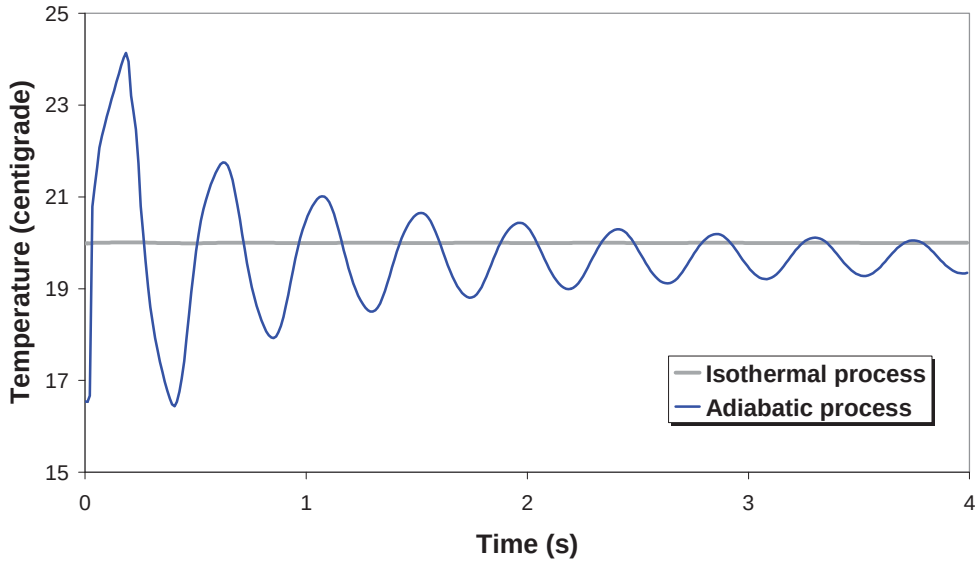

Figure 5.13 Temperature Variation in a Isothermal and Adiabatic Process

Fig. 5.13 shows the temperature variation when the gas process obeys isothermal and adiabatic process in the pipeline. The gray line is the result for isothermal process. There is no temperature change during transients because the isothermal process completely exchanges heat with the outside, which is regarded as being a heat storage unit with infinite capacity. The temperature in the pipe quickly reaches thermal equilibrium with the constant temperature of external environment, whereas the results of adiabatic process clearly shows temperature variation during transients because there is no heat exchange across the pipe wall, where the pipeline is regarded as thermal insulation. The maximum temperature difference is 7.8^{o}C.

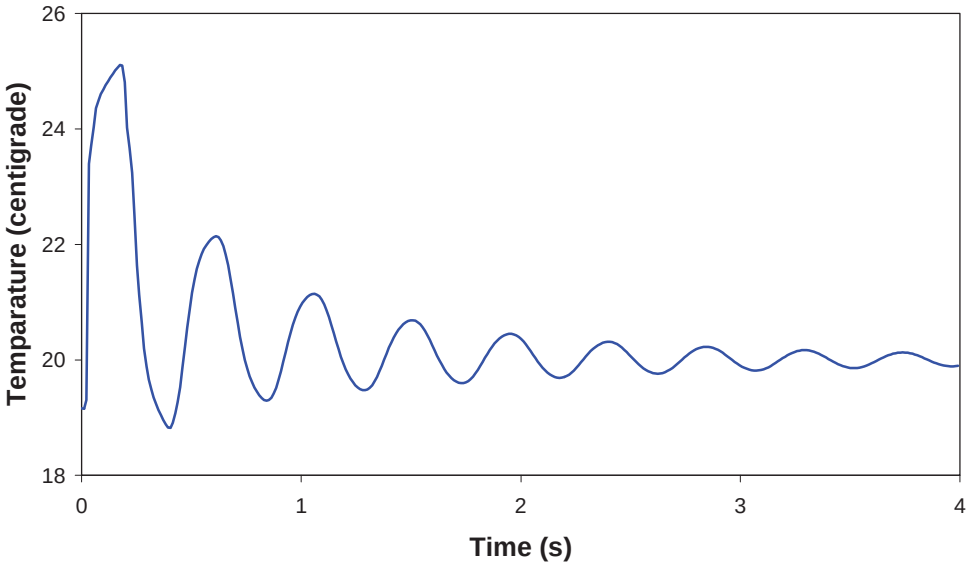

Figure 5.14 Temperature Variation in a Steel Pipeline

Figs. 5.14 and 5.15 show the temperature variation when using steel and copper pipelines. The thermal conductivities for heat flux of steel and copper are 64 *W/m·K* and 398 *W/m·K* respectively. It means that the heat conduction of copper pipeline is higher than steel pipeline and the copper pipe has more heat exchange across the pipe wall during transients. The temperature variation in the steel pipe is smaller than the temperature variation of adiabatic pipe and bigger than the temperature variation of copper pipe. The maximum temperature differences of steel and copper pipes are 6.2 and 4.9^{o}C respectively. The temperature of copper pipeline dramatically decreases from the first cycle and the

temperature variation almost reaches the constant outside temperature 20°C after 2 seconds.

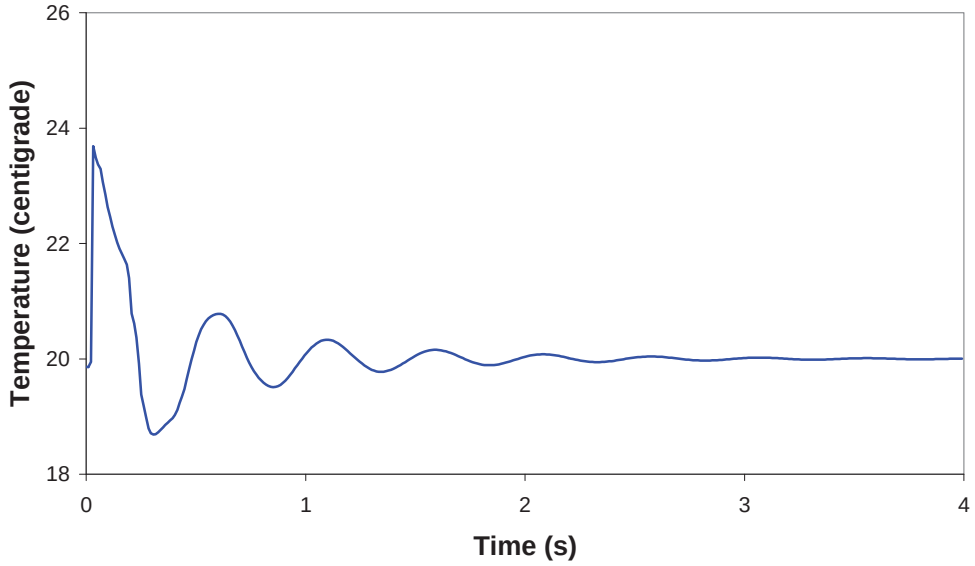

Figure 5.15 Temperature Variation in a Copper Pipeline

Although the results of fast gas transients show the temperature variations inside pipeline, they are small enough so that the fluid viscosity across the pipe is considered to be constant or linearly varied frozen viscosity for the duration of the transients. Therefore, the application of unsteady friction models based on weighting function derived by the frozen viscosity assumption is available for transient gas flows. However, the heat conduction effects by wall resistance and pressure variation are considered by a proposed polytropic process gas transient analysis model, in which the heat exchange of the system is considered by a polytropic process exponent and generalized gas transient analysis model, in which energy equation directly calculates the variation of temperature during transients.

5.5 EXPERIMENTAL VERIFICATION FOR UNSTEADY FRICTION

Laboratory experiments have been undertaken for the verification of unsteady friction models for water and gas transients of a tank-pipe-valve system. The experimental apparatus is described in Chapter 4. The layout of the pipeline system is repeated in Fig. 5.16 for clarity. The numbers of reaches used for transient simulations of a laboratory pipeline are usually 100 (0.3753 m computational space step) or 40 (0.93825 m computational space step) in this chapter as well as the following chapters.

Figure 5.16 Layout of Experimental Pipeline Apparatus

5.5.1 Experimental Verification for Transient Water Flows

Transient events are generated by a fast closing solenoid valve at the downstream end. The pipeline system can be regarded as tank-pipe-valve system. Water and surrounding temperatures are 23^{o}C. The sampling frequency of measurement data is 4 kHz. Table 5.4 shows the specified six different flow conditions used for water transient tests. The initial velocities are adjusted by the pressure conditions of the boundary tank pressurised by air compressor. These flow conditions range from laminar flow to low Reynolds number turbulent flow.

Table 5.4 Specified Six Different Flow Conditions

Flow Conditions	Tank Pressure (kPa)	Initial Velocity (m/s)	Reynolds Number (N_R)
Condition 1	117.6	0.0599	1338
Condition 2	200.0	0.0824	1827
Condition 3	297.2	0.1031	2307
Condition 4	397.4	0.1208	2672
Condition 5	502.2	0.1368	3000
Condition 6	612.1	0.1495	3326

Figs. 5.17 and 5.18 show the comparisons between measured transient data and simulation results using the unsteady friction models based on modified-approximated weighting functions for transient laminar ($N_R < 2{,}000$) and turbulent flows ($N_R > 2{,}000$) at the downstream end and the middle of pipe. Appendix C shows the measured transient data generated by fast opening events of the solenoid valve in the same test conditions. The jagged shape with high frequency sharp spikes of experimental data are caused by inertial effects of pipeline joint parts that give rise to minor loss effects during transients, although high precision straight fittings are used for the joints (see Appendix D for the details of inertial effects by joints). These effects produce flow disturbance and additional energy

losses in the magnitude of pressure wave because transients hyper-sensitively respond to the change of pipe condition.

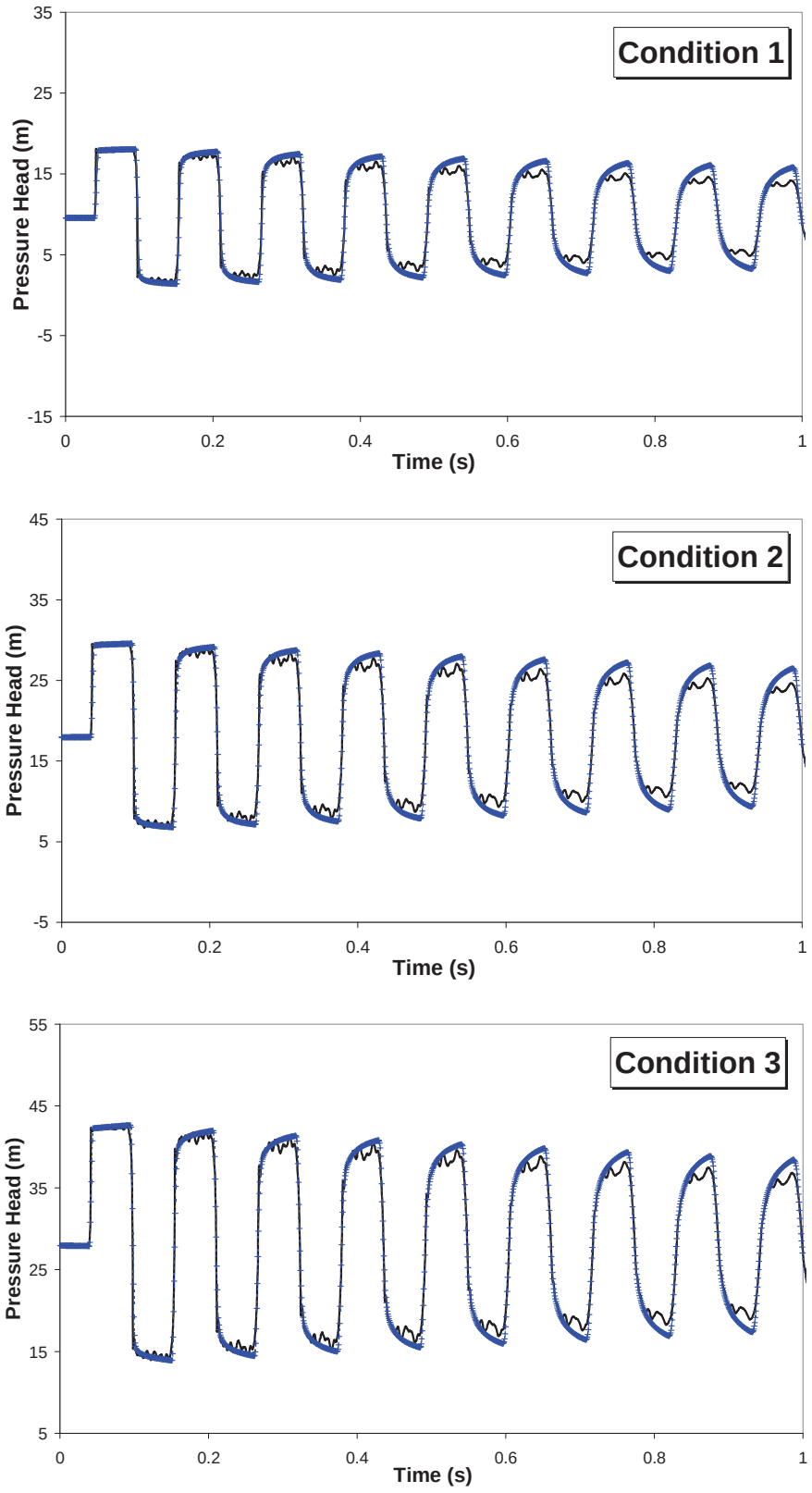

Figure 5.17 Measured Data and Simulation Results at the Downstream End

(Black line is measured data and blue line with crosses is simulation results)

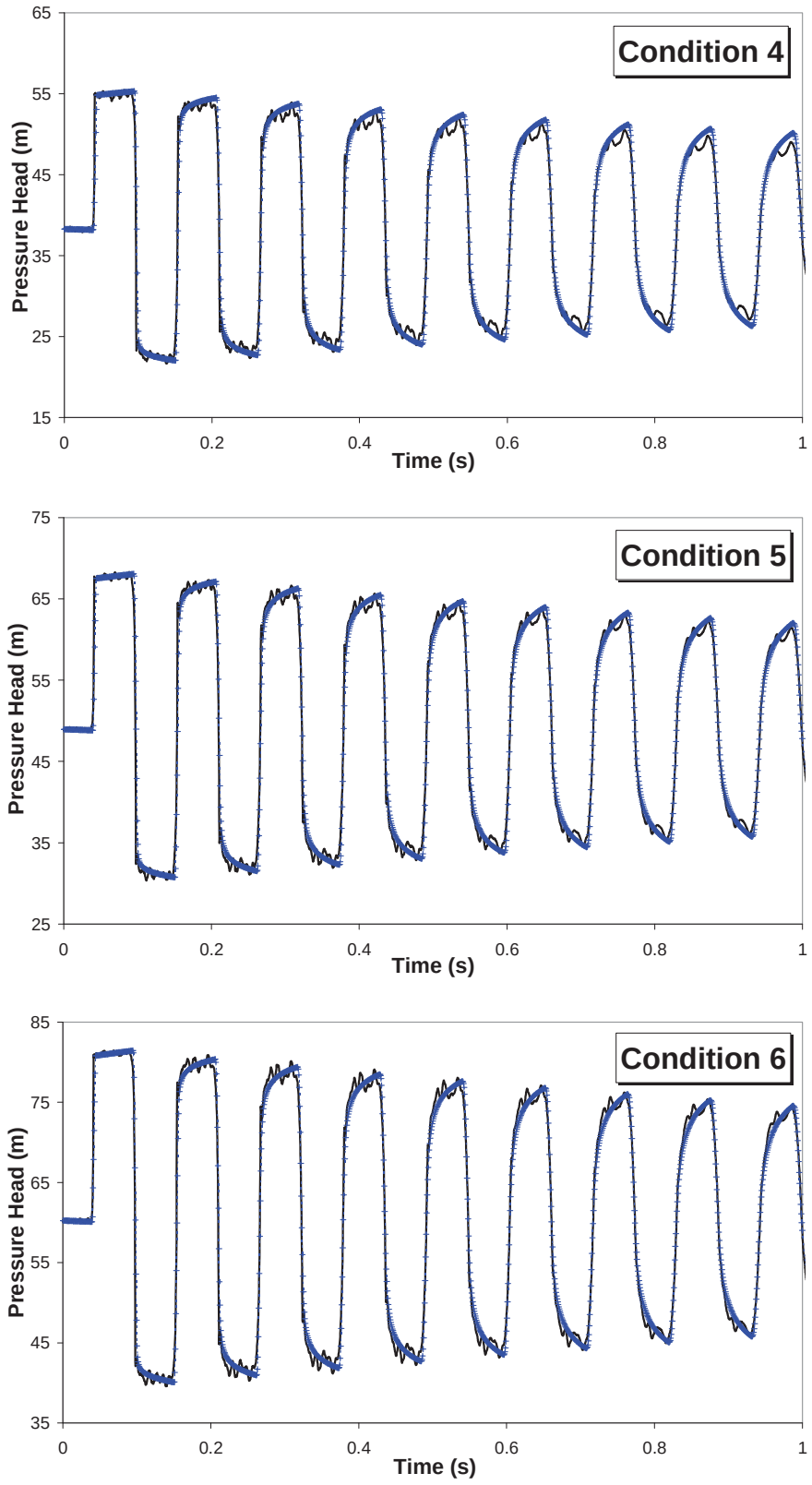

Figure 5.17 Measured Data and Simulation Results at the Downstream End (continued)

(Black line is measured data and blue line with crosses is simulation results)

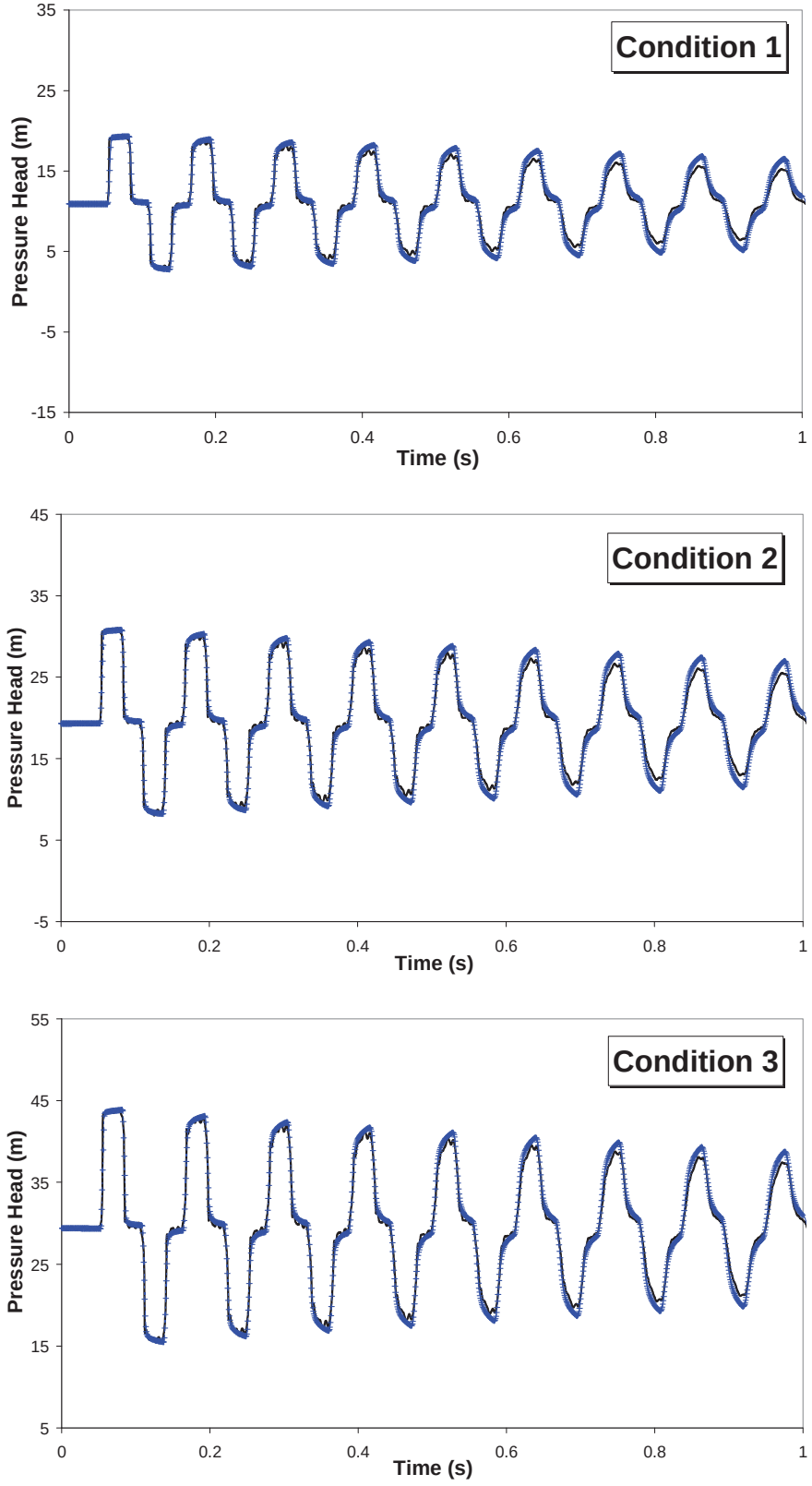

Figure 5.18 Measured Data and Simulation Results at the Middle of the Pipe

(Black line is measured data and blue line with crosses is simulation results)

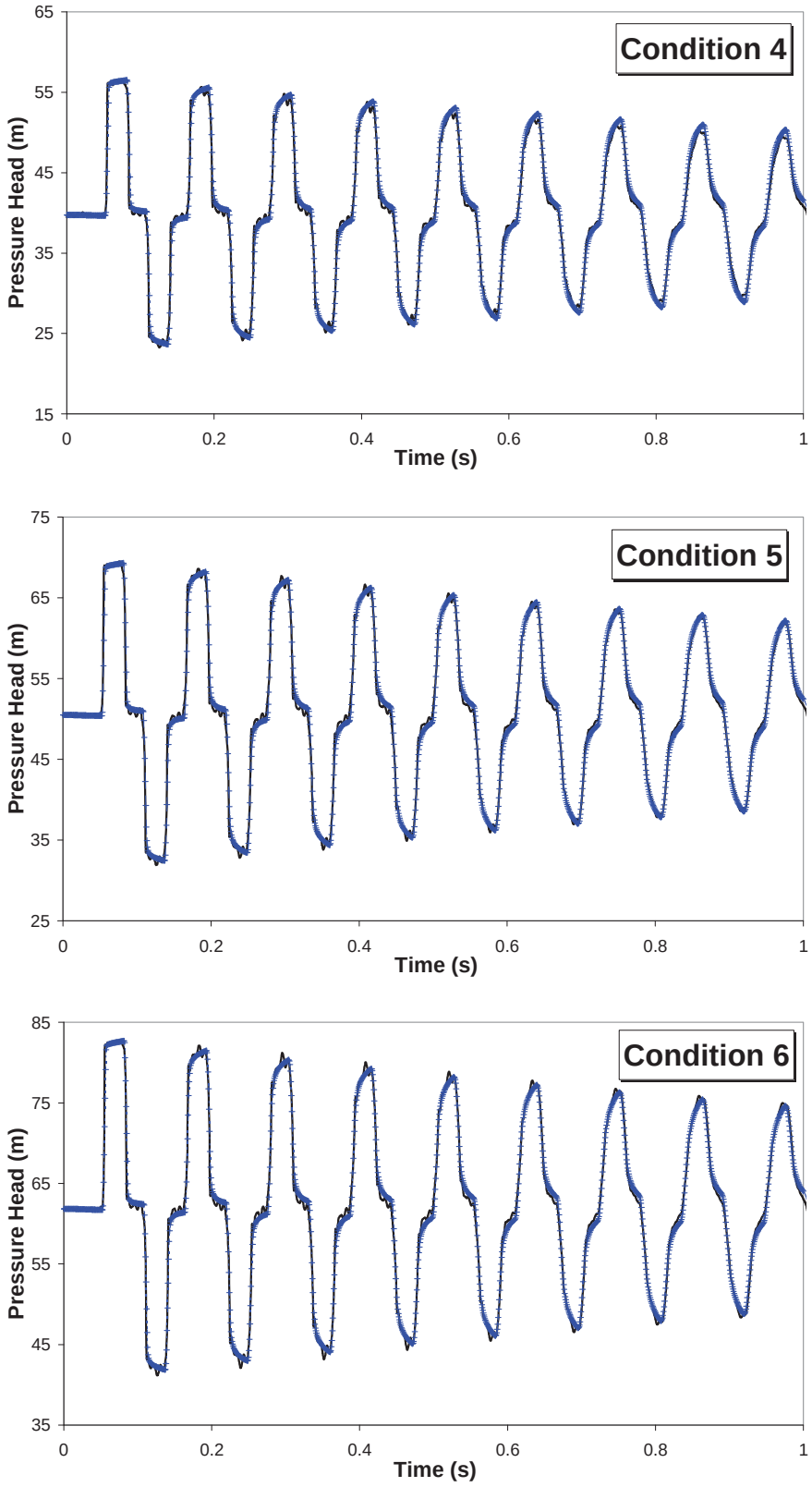

Figure 5.18 Measured Data and Simulation Results at the Middle of the Pipe (continued)

(Black line is measured data and blue line with crosses is simulation results)

The simulation results show somewhat of a discrepancy in terms of magnitude of the pressure wave for conditions 1 to 4 when compared to the measured data, and the discrepancy increases as Reynolds number decreases and simulation time gets longer. It looks as if unsteady friction model underestimates energy loss by wall shear stress during transients.

Fig. 5.19 shows the simulation results for a higher flow velocity (turbulent flow) at the end of pipe. The flow information for these flows is presented in Table 5.5. These experiments were executed by Bergant and Simpson [1994 and 1995] under initial structure condition of the same laboratory single pipeline. Transient events were generated by closing in-line valve with mechanical actuator and the valve closure time is 0.009 seconds. Pressure waves are measured at the end of pipe. Condition 8 is almost at the critical condition that would generate column separation in the pipeline system. The simulation results are similar to the results of flow condition 5 and 6. There is good agreement. If the pipeline is an ideal condition that has no joints, the simulation results are to be improved. However, real pipeline systems have numerous minor loss elements and uncertainties that create obstacles in the development of a precise transient analysis model. Generally, the unsteady friction models incorporated into conservative scheme perform well and accurately simulate the phase, magnitude and shape of the experimental data.

Table 5.5 Flow Information for Higher Velocity Flows

(Bergant and Simpson, 1994 and 1995)

Flow Conditions	Initial Velocity (m/s)	Reynolds Number (N_R)
Condition 7	0.2	3843
Condition 8	0.3	5765

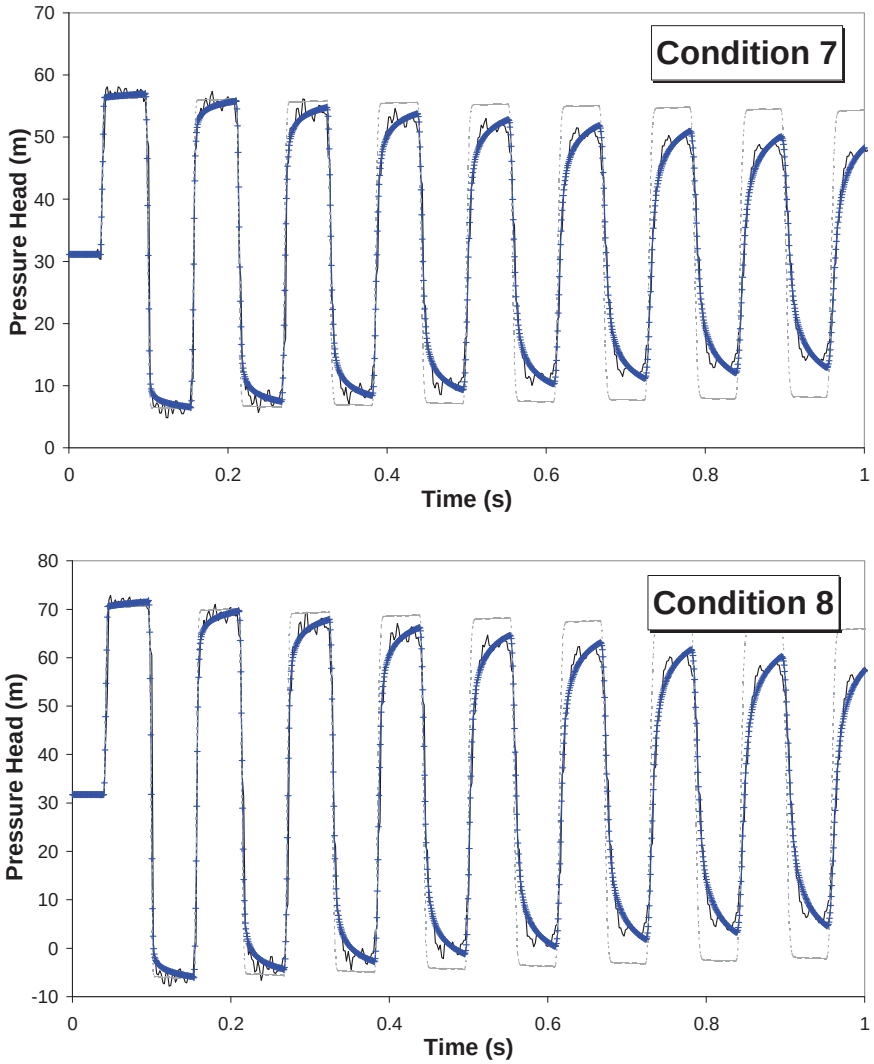

Figure 5.19 Measurement and Simulation Results for Higher Reynolds Number Flow

(Black line is measured data, broken gray line is simulation results using steady friction model, and blue line with crosses is simulation results using unsteady friction model)

5.5.2 Experimental Verification for Transient Gas Flows

Experiments for transient gas flows were conducted after draining and drying the pipeline and tanks in the same pipeline used for water transient tests. Dry air supplied by air compressor through air filters is used as the fluid medium. Transient events are generated by fast closing solenoid for condition 1 shown in Table 5.6 and flow control valve for condition 2, 3, and 4 at the downstream end. Both pressure and temperature are measured at the tank, middle of pipe, and end of pipe during transients. Table 5.6 shows the test condition for gas transients. The initial flows are adjusted by the pressure conditions of the boundary tank. The air inflow valve of compressor is closed after setting up the demand

tank pressures for each test condition. Therefore, the tank pressure changes during steady and transient tests. In the case of gas flows, it is difficult to directly measure the mass flow rate or flow velocity. This research uses the relationship of the variation of the pressure and mass flow rate in the constant tank volume to calculate the variable tank pressure and mass flow rate of gas by Eq. 4.5.

Table 5.6 Flow Conditions for Gas Transient Tests

Flow Conditions	Initial Velocity (m/s)	Tank Pressure (kPa)	Reynolds Number (N_R)	Surrounding Temperature (^oC)	Mach Number
Condition 1	8.28	479.3	12,444	15.8	0.024
Condition 2	21.98	268.9	31,134	24.5	0.064
Condition 3	38.85	211.2	55,034	24.5	0.114
Condition 4	43.73	262.5	61,952	24.5	0.128

In the relationship of Eq. 4.5, the temperature variation of tank during tests is neglected. Thus the variation of mass flow rate is a function of pressure only. A pressure transducer can easily measure the tank pressure. Fig. 5.20 shows the pressure and temperature variation during the whole transient event for condition 4 (biggest transients). The sudden pressure drop near 6 seconds represents the valve-opening event. The sudden pressure drop causes the sudden temperature drops at the end and middle of pipeline and the start of gradual temperature drop at the tank. Also the sudden pressure rise near 17 seconds due to rapid valve closure at the end of pipe causes the sudden temperature rise at the end and middle of pipeline and the start of gradual temperature rise at the tank. The pressure slightly increases to recover large pressure drop after finishing transient events (approximately from 22 seconds in Fig. 5.20a). Although Fig. 5.20 represents a clear temperature variation during transient events, the maximum temperature change is almost 1^oC that supports the use of fixed temperature in Eq. 4.5 and that is negligible for the variable of transient analysis.

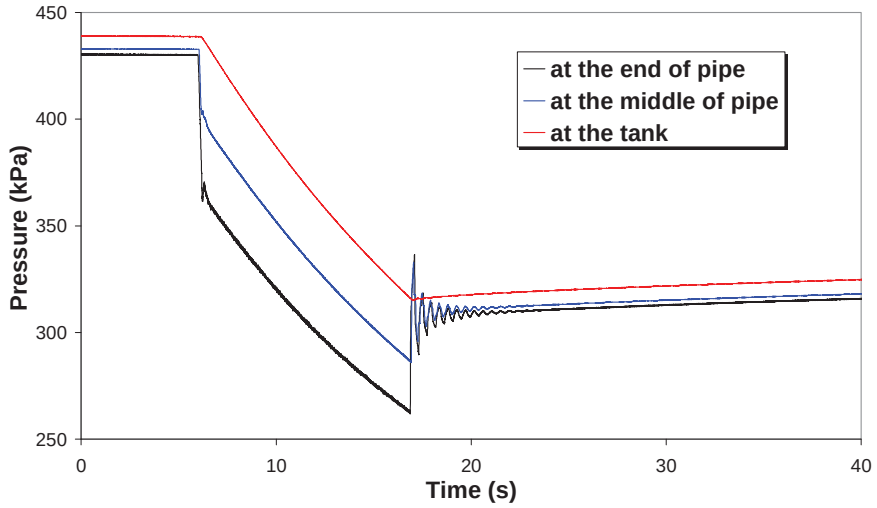

(a) Pressure Variations

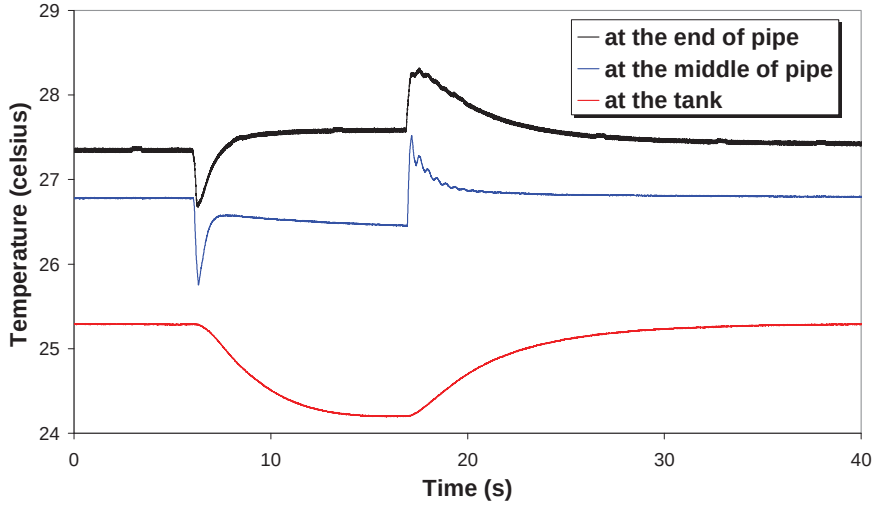

(b) Temperature Variations

Figure 5.20 Measured Pressure and Temperature during the Test for Condition 4

Figs. 5.21 and 5.22 show the measured pressure data at the end and middle of pipeline according to the above flow conditions. The pressure data are plotted at the same scale (the ranges of x-axis and y-axis are 4 seconds and 60 kPa respectively) to compare each pressure variation and pressure wave shape. The jagged shapes with high frequency sharp spikes that were caused by a mechanical problem of pipeline joint parts of measured data for water transient tests as shown in Figs. 5.17 and 5.18 almost disappear in the measured data for gas transient tests because the inertial effect of gas is less important for gas transients. Like the transients for incompressible flow, the measured data of condition 1 almost have no line-packing effect because the flow has very low Mach number and transient event is small (the maximum pressure change is almost 11 kPa). In this case, the

fluid can be regarded as slightly compressible flow and the fluid compressibility is not the dominant physical process for transient analysis. The line-packing dramatically increases as transient event increases. From the condition 2, the measured data show significant storage effect of a pipeline due to line-packing.

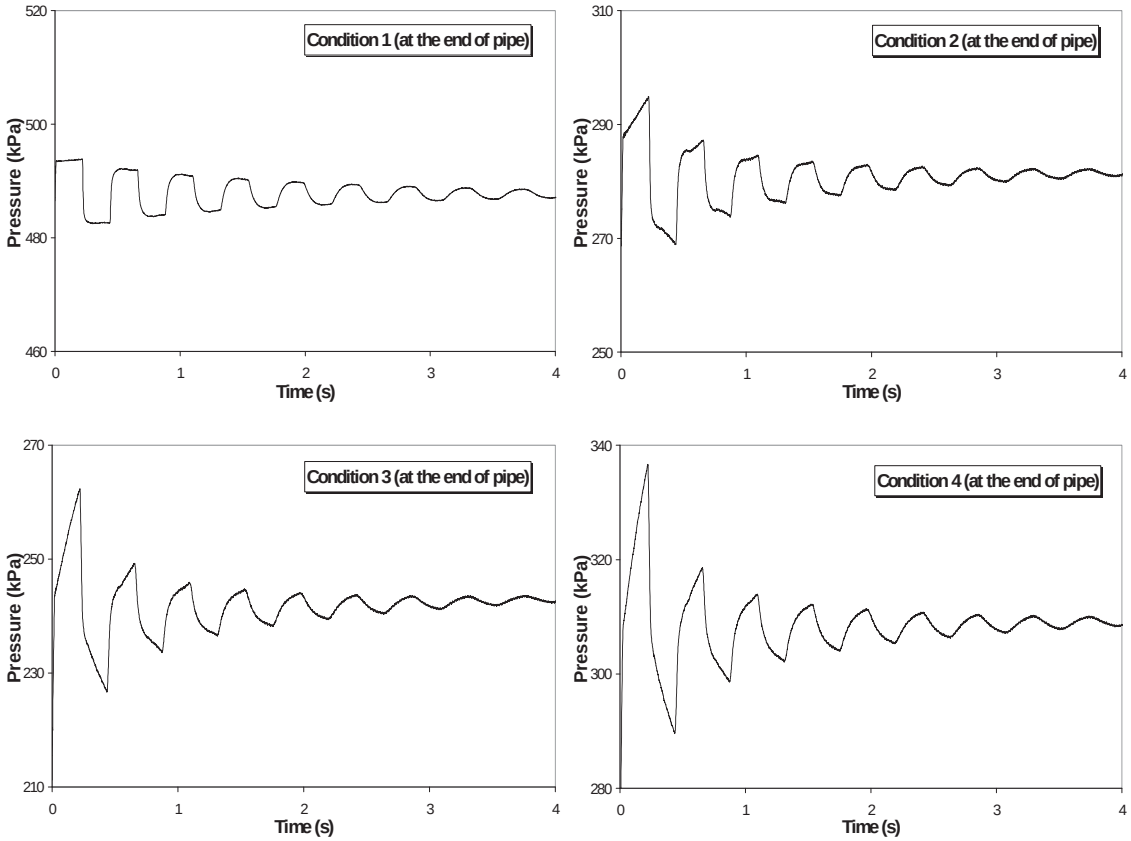

Figure 5.21 Measured Pressure Data at the End of Pipe

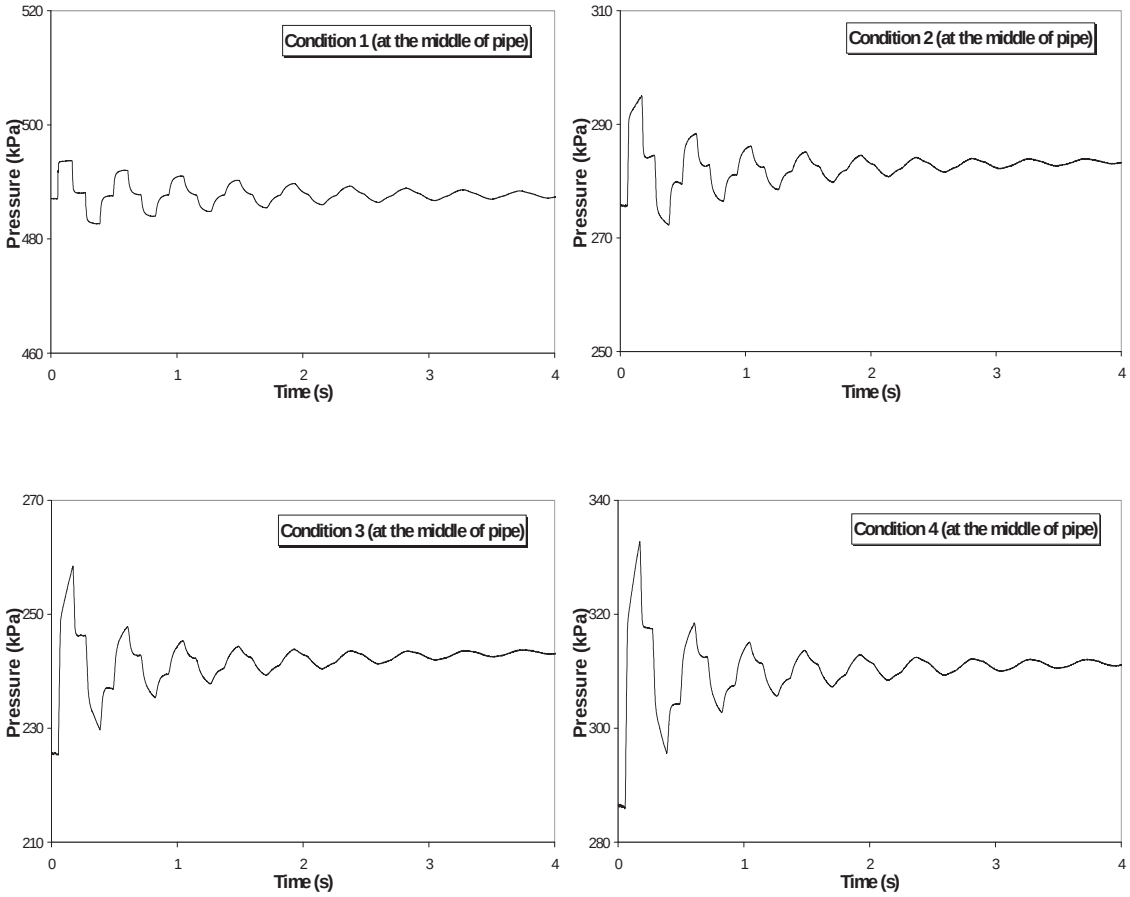

Figure 5.22 Measured Pressure Data at the Middle of Pipe

Fig. 5.23 shows the comparison between measured transient data and simulation results using the steady friction model and unsteady friction model based on the modified-approximated weighting functions for transient turbulent flow at the downstream end. The polytropic process gas transient analysis model is used for gas transient analysis because the temperature variation is small during transient events as shown in Fig. 5.20. The polytropic process exponent *n*, which considers heat exchange of the system, is decided by comparison between measured data and simulation results. The calibrated polytropic process exponent ranges from 1.15 to 1.18 depending on the test condition. These values represent that the pipeline system has somewhat rapid heat exchange process because copper (pipeline material) has a high thermal conductivity. Like the results of numerical experiments as shown in Fig. 5.10, the results of steady friction model are similar to the results of unsteady friction model in the magnitude of pressure wave and the results of unsteady friction model show slightly frequency-dependent dispersion in the phase of pressure wave. The impact of unsteady friction, very important in water transients, appears to be less important in the gas transients. The compressibility of gas may be more

dominant for transient damping effect. Although the models can predict the whole transient traces, the simulation results of models overestimate the line-packing. These errors may come from the characteristics of compressibility. The Mach numbers of flow conditions for gas transient tests are smaller than that of compressible subsonic flow (Mach number > 0.3). To some degree, the gas flows for experiments may still have the property of incompressible flow. Therefore, the tested flows do not show complete storage capacity of a pipeline due to an increase in pressure, especially for the initial pressure rises during transient events. After the third pressure wave cycle, there is good agreement between measured data and simulation results because the effect of line-packing decreases.

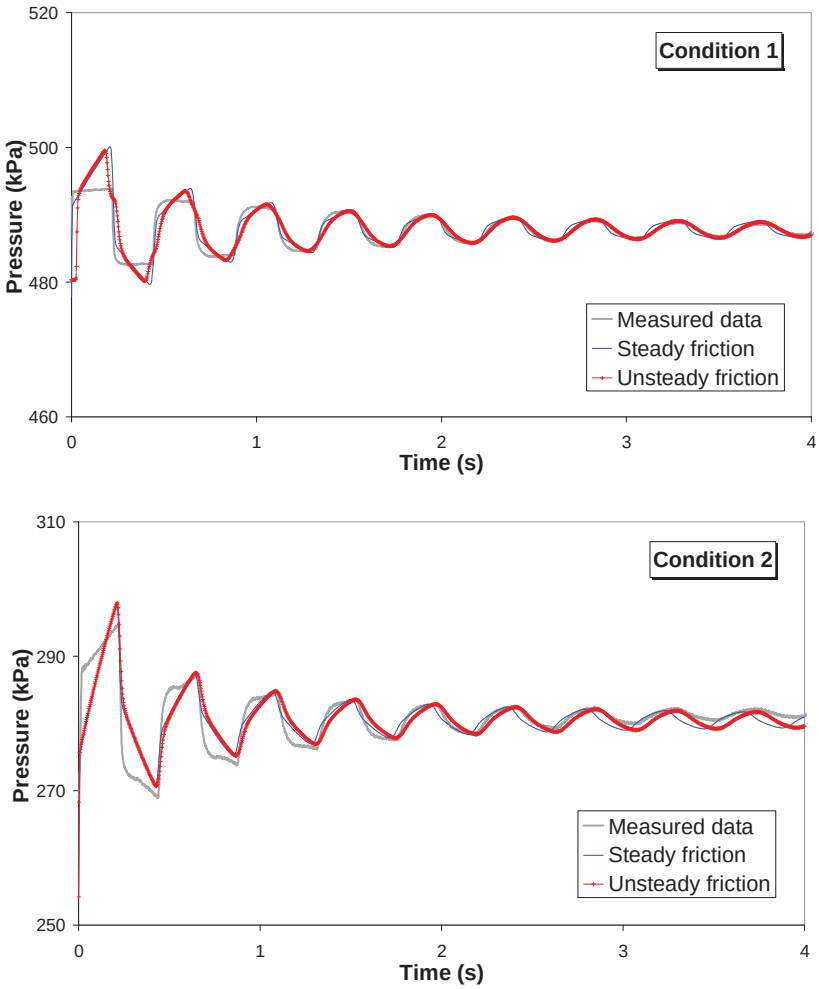

Figure 5.23 Simulation Results for Gas Transients

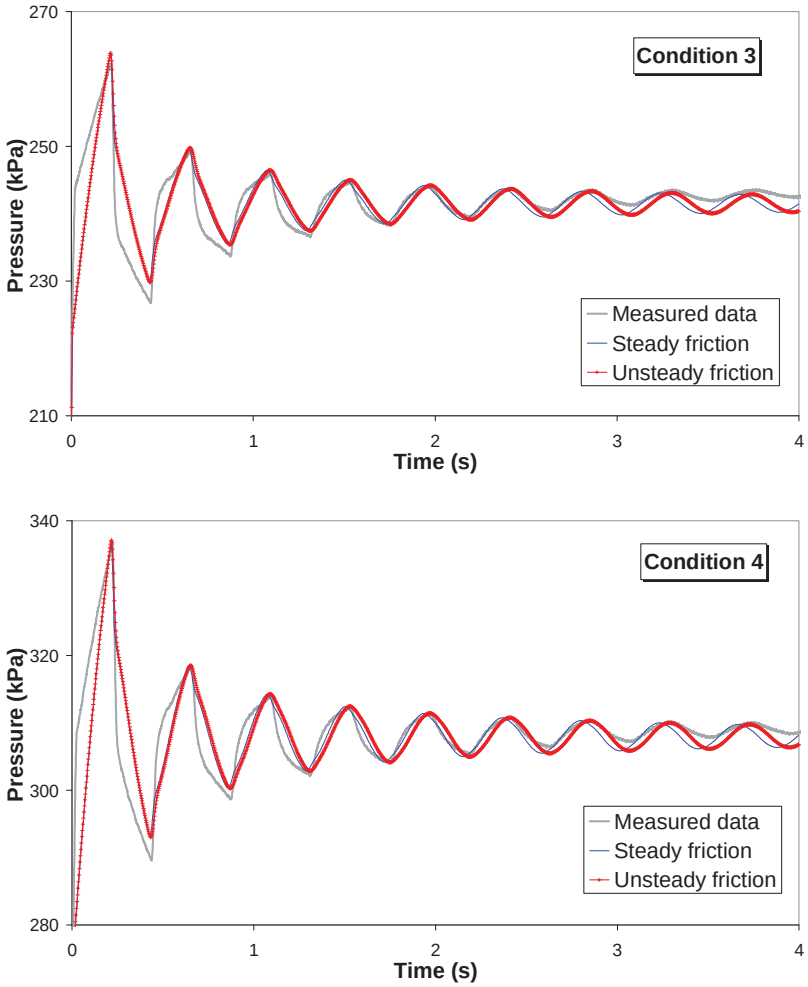

Figure 5.23 Simulation Results for Gas Transients (continued)

5.6 SUMMARY AND CONCLUSIONS

Understanding the unsteady hydraulic resistance behaviour caused by pipe wall shear stress is of great importance for the dynamic calculation in system design and assessment. This is especially true for the transient analysis beyond the first pressure wave cycle. Various unsteady friction models based on convolution weighting functions have been incorporated and modified in the conservative solution scheme for both transient laminar and turbulent flows and both water and gas transients. Each of the simulation results using four different unsteady friction models, including the original weighting function model, approximated weighting function model, and their modified models, for the conservative scheme shows good agreement. Also, the modified model effectively decreases the computation time.

Unsteady friction models originally developed for water transient flow have been applied to gas transient flows to verify their effectiveness for compressible flows. The assumptions involved in developing weighting function type unsteady friction models are that (i) the convective acceleration terms are negligible, (ii) the incompressible continuity equation is used, and therefore the influence of mass storage on velocity profile is negligible, and (iii) the temperature variations are small enough so that the fluid viscosity across the pipe is considered to be constant or linearly varied viscosity for the duration of the transients. In systems with a high-Mach-number compressible flow with a relatively high speed flow and low wavespeed, neglecting the convective terms may result in a loss of accuracy of the simulation results. However, the convective terms become very small near the pipe wall because the flow velocity is very low when applying the no-slip boundary condition. Also, these terms are fully considered in the basic equations of the conservative scheme. In the same manner, the compressibility near the pipe wall is also relatively small because the flow becomes low-Mach-number compressible flow. The unsteady friction can be developed using the incompressible continuity equation.

Gas flow situations may be divided into two categories for analysis purposes, slow and fast transients. For the case of slow transients, the gas in the pipe has sufficient time to reach thermal equilibrium with constant surrounding temperature. Similarly, for the case of fast transients, pressure changes occur instantaneously. There is no time for heat transfer to take place between the gas in the pipe and the surroundings. Therefore, the temperature variation is small enough so that the fluid viscosity across the pipe can be considered to be constant or linearly varied viscosity for the duration of the transients. However, the flow viscosity depends on local temperature. For many dynamic gas applications, the temperature profile of gas is a function of pipeline distance with local heat source or sink (non-isothermal and non-adiabatic flow). This heat exchange is directly calculated by the energy equation in the conservative scheme.

The measured data of gas transient turbulent flow show a significant line-packing effect because the storage capacity of a pipeline increases due to the increase in pressure. The fluid compressibility is the dominant physical process for transient analysis rather than frictional effect. As a result, the simulation results for the steady friction model are similar to the results of the unsteady friction model in terms of the magnitude of pressure wave. The unsteady friction model shows slight frequency-dependent dispersion in terms of the

phase of pressure wave. The impact of unsteady friction, which is very important in water transients, has been shown to be less important in the turbulent gas transients. On the other hand, the measured data for gas transient in the laminar flow region are similar to the results of incompressible flow because the flow velocity is very slow when considered to normal gas flows that are fully turbulent and high-Mach number flow. In this laminar case, the flow can be considered as slightly compressible flow with a low-Mach number. The energy loss by wall friction is the dominant physical process for transient analysis rather than the fluid compressibility.

Although the gas transient models including an unsteady friction term can reasonably accurately predict the whole transient traces, the simulation results of models overestimate the line-packing. These errors may come from the characteristics of compressibility. The Mach numbers of flow conditions for gas transient tests are smaller than that of compressible subsonic flow. To some degree, the gas flows for experiments may still have the property of incompressible flow. Therefore, the tested flows do not show complete storage capacity of a pipeline due to an increase in pressure, especially for the initial pressure rises during transient events.